

Unravelling the functional interconnections among the mitochondrial uniporter complex components



Dissertation

Fakultät für Biologie Ludwig-Maximilians-Universität München

Valerie Goh

München, 2020

1. Gutachter: Prof. Barbara Conradt
2. Gutachter: Prof. Thomas Nägele
Tag der Einreichung: 24.08.2020
Tag der mündlichen Prüfung: 03.02.2021

Eidesstattliche Versicherung

Ich versichere hiermit an Eides statt, dass die vorgelegte Dissertation von mir selbständig und ohne unerlaubte Hilfe angefertigt ist.

Hiermit erkläre ich dass die Dissertation nicht ganz oder in wesentlichen Teilen einer anderen Prüfungskommission vorgelegt worden ist.

München, den 30.07.2020

Valerie Goh

Table of Contents

Abbreviations	1
List of publications	2
Summary	4
1. Introduction	6
1.1. Mitochondria	6
1.2. Calcium signalling	7
1.3. Mitochondrial calcium signalling.....	9
1.4. Physiological roles of mitochondrial calcium handling.....	11
1.5. Mitochondrial calcium influx and efflux machineries.....	13
1.5.1 <i>Molecular components of mitochondrial calcium efflux</i>	13
1.5.2 <i>Molecular components of mitochondrial calcium influx</i>	14
1.5.3 <i>Structures of mitochondrial calcium influx components</i>	16
1.6. Pathophysiology of mitochondrial calcium dysregulation	17
2. Research aims	21
3. Publications	24
Publication I	24
Publication II	48
4. Discussion	79
4.1. The functional interaction between MCU and MICU1	79
4.2. The uniporter evolutionary history	82
References	86
Contributions	100
Acknowledgement.....	101
Curriculum vitae	102

Abbreviations

ATP	adenosine triphosphate
CaM	Calmodulin
CCD	Coiled coil domain
CRAC	Ca ²⁺ release-activated Ca ²⁺ channel
CypD	cyclophilin D
cyt-Ca ²⁺	cytosolic Ca ²⁺
DN	dominant-negative
ER/SR	endoplasmic/sacroplasmic reticulum
ETC	electron transport chain
FADH2	flavin adenine dinucleotide
HCX	H ⁺ /Ca ²⁺ exchanger
IMM	inner mitochondrial membrane
Ins(1,4,5)P ₃ R	inositol 1,4,5-trisphosphate receptors
KO	knockout
LETM1	leucine zipper EF hand containing transmembrane protein 1
LHD	linker-helix domain
MCUC	Mitochondrial Calcium Uniporter Channel
MCU	mitochondrial calcium uniporter protein
MCUP	fungal-specific MCU paralog
MICU1	mitochondrial Ca ²⁺ uptake 1
mt-Ca ²⁺	mitochondrial Ca ²⁺
NAC	N-acetyl-cysteine
NADH	Nicotinamide adenine dinucleotide
NCX	Na ⁺ /Ca ²⁺ exchanger
NTD	N-terminal domain
OXPHOS	oxidative phosphorylation
PM	plasma membrane
PMCA	PM Ca ²⁺ ATPase
PTP	permeability transition pore
ROS	reactive oxygen species
RNAi	RNA interference
RuRed	ruthenium red
RyR	ryanodine receptors
SERCA	ER/SR Ca ²⁺ ATPases
TCA	tricarboxylic acid
TMDs	transmembrane domains
TRPC	transient receptor potential channels
VDAC	Voltage-dependent anion channel
WT	wild-type

List of publications

Publication I

Jennifer Wettmarshausen*, **Valerie Goh***, Kai-Ting Huang, Daniela M. Arduino, Utkarsh Tripathi, Anja Leimpek, Yiming Cheng, Alexandros A. Pittis, Toni Gabaldón, Dejana Mokranjac, György Hajnóczky, and Fabiana Perocchi.

MICU1 Confers Protection from MCU-Dependent Manganese Toxicity.

(2018) **Cell Reports**, 25, 1425-1435.

*equal author contributions

Abstract

The mitochondrial calcium uniporter is a highly selective ion channel composed of species- and tissue-specific subunits. However, the functional role of each component still remains unclear. Here, we establish a synthetic biology approach to dissect the interdependence between the pore-forming subunit MCU and the calcium-sensing regulator MICU1. Correlated evolutionary patterns across 247 eukaryotes indicate that their co-occurrence may have conferred a positive fitness advantage. We find that, while the heterologous reconstitution of MCU and EMRE in vivo in yeast enhances manganese stress, this is prevented by co-expression of MICU1. Accordingly, MICU1 deletion sensitizes human cells to manganese-dependent cell death by disinhibiting MCU-mediated manganese uptake. As a result, manganese overload increases oxidative stress, which can be effectively prevented by NAC treatment. Our study identifies a critical contribution of MICU1 to the uniporter selectivity, with important implications for patients with MICU1 deficiency, as well as neurological disorders arising upon chronic manganese exposure.

Publication II

Alexandros A. Pittis*, **Valerie Goh***, Alberto Cebrian-Serrano, Jennifer Wettmarshausen, Fabiana Perocchi & Toni Gabaldón.

Discovery of EMRE in fungi resolves the true evolutionary history of the mitochondrial calcium uniporter.

(2020), **Nature communications**, 11, 4031.

*equal author contributions

Abstract

Calcium (Ca^{2+}) influx into mitochondria occurs through a Ca^{2+} -selective uniporter channel, which regulates essential cellular processes in eukaryotic organisms. Previous evolutionary analyses of its pore-forming subunits MCU and EMRE, and gatekeeper MICU1, pinpointed an evolutionary paradox: the presence of MCU homologs in fungal species devoid of any other uniporter components and of mt- Ca^{2+} uptake. Here, we trace the mt- Ca^{2+} uniporter evolution across 1,156 fully-sequenced eukaryotes and show that animal and fungal MCUs represent two distinct paralogous subfamilies originating from an ancestral duplication. Accordingly, we find EMRE orthologs outside Holoza and uncover the existence of an animal-like uniporter within chytrid fungi, which enables mt- Ca^{2+} uptake when reconstituted in vivo in the yeast *Saccharomyces cerevisiae*. Our study represents the most comprehensive phylogenomic analysis of the mt- Ca^{2+} uptake system and demonstrates that MCU, EMRE, and MICU formed the core of the ancestral opisthokont uniporter, with major implications for comparative structural and functional studies.

Summary

Mitochondrial calcium (mt- Ca^{2+}) uptake is central for the buffering of intracellular Ca^{2+} signals to regulate several cellular processes. This uptake activity is mainly achieved through a highly selective Ca^{2+} uniporter located at the inner mitochondrial membrane that consists of species- and tissue-specific subunits. While the functional roles and physiological implications of these subunits on the uniporter activity have been investigated in mammalian systems, the different modulation of the uniporter in these model systems, such as the level of gene silencing, have hindered the interpretations of these results. Hence, the functional role of each uniporter component still remained unclear.

To dissect the functional contribution of the uniporter pore-forming subunit MCU and its Ca^{2+} -sensing regulator MICU1, a testbed using yeast as the model system was established due to its absence of detectable MCU homolog and endogenous mt- Ca^{2+} uptake activity. The heterologous expression of MCU and its essential subunit EMRE in yeast reconstituted *in vivo* mt- Ca^{2+} uptake that was augmented by the co-expression of MICU1. As there was a tight co-evolution of MCU and MICU1, the cellular advantage provided by the interaction of MCU and MICU1 was investigated through biological conditions that would benefit the yeast cellular fitness. Among all the tested conditions, manganese (Mn^{2+}) treatment was found to be lethal to yeast cells expressing MCU and EMRE that was prevented by the co-expression of MICU1. Similarly, mammalian cells that lack MICU1 were susceptible to Mn^{2+} -induced cell death, due to the uptake of Mn^{2+} through the unregulated MCU pore. The resultant accumulation of Mn^{2+} in these cells led to an increase in oxidative stress that was circumvented by an antioxidant, N-acetylcysteine. Altogether, the unravelled role of MICU1 as a Ca^{2+} selectivity gatekeeper for the uniporter provides crucial implications for MICU1-deficient patients.

While preliminary evolutionary analyses of MCU and MICU1 suggested an ancient eukaryotic origin of mt- Ca^{2+} uptake, EMRE was instead discovered as a metazoan-specific protein. The detection of MCU homologs as the sole uniporter subunit within fungi, without any detectable mt- Ca^{2+} uptake activity, further indicated a discrepancy between the suggested ancient eukaryotic origin of mt- Ca^{2+} uptake and the phylogenetic profile of MCU, MICU1 and EMRE. To clarify the evolutionary origin of mt- Ca^{2+} uptake activity in eukaryotes, the evolutionary patterns and distributions of MCU, MICU1 and EMRE were investigated using a comprehensive phylogenomic analysis coupled with experimental validation in yeast. Two distinct paralogous MCU subfamilies, animal-like and fungal-specific MCU paralog (MCUP) proteins, were found to originate from an ancestral duplication. While most fungi retained only the fungal-specific MCU paralog, three chytrid fungi were found to contain both fungal-specific and animal-like MCU paralogs, together with MICU and EMRE. The first identification of non-

animal EMRE orthologs and the complete animal-like uniporter complex, consisting of animal-like MCU, MICU1, and EMRE, within chytrid fungi had re-set the origin of mitochondrial Ca^{2+} uniporter to an opisthokont origin. Together with experimental confirmation of the ability to reconstitute mt- Ca^{2+} through animal-like MCUs in the presence of their respective EMRE, but not MCUPs, resolved the initial evolutionary paradox. Overall, the orthologous uniporter complex in fungi provides relevant targets for future comparative structural and functional studies to identify crucial MCU-EMRE regions to understand their functional interconnection.

Altogether, both studies emphasize that the importance of an accurate phylogenetic analysis to understand the shared evolutionary history of the uniporter subunits, revealing additional role of its regulatory subunit and uncovers closely-related orthologs. Hence, these orthologs provides additional information for future structural and functional studies to better understand the regulation of the uniporter and provide insights for mt- Ca^{2+} related diseases.

Introduction

1.1. Mitochondria

Mitochondria, the double membrane bound organelles present in almost all eukaryotic cells, are commonly known as cellular powerhouses that generate energy via the process of oxidative phosphorylation (OXPHOS) (Spinelli and Haigis, 2018). Sugars, fatty acids and amino acids are catabolized in the mitochondrial matrix through the tricarboxylic acid (TCA) cycle that generates reducing cofactors such as nicotinamide adenine dinucleotide (NADH) and flavin adenine dinucleotide (FADH₂). The transfer of electrons from these cofactors into the electron transport chain (ETC) at the inner mitochondrial membrane (IMM), together with oxygen, pumps protons (H⁺) from the matrix into the intermembrane space, generating a membrane potential difference for the synthesis of adenosine triphosphate (ATP) (Figure 1.1A).

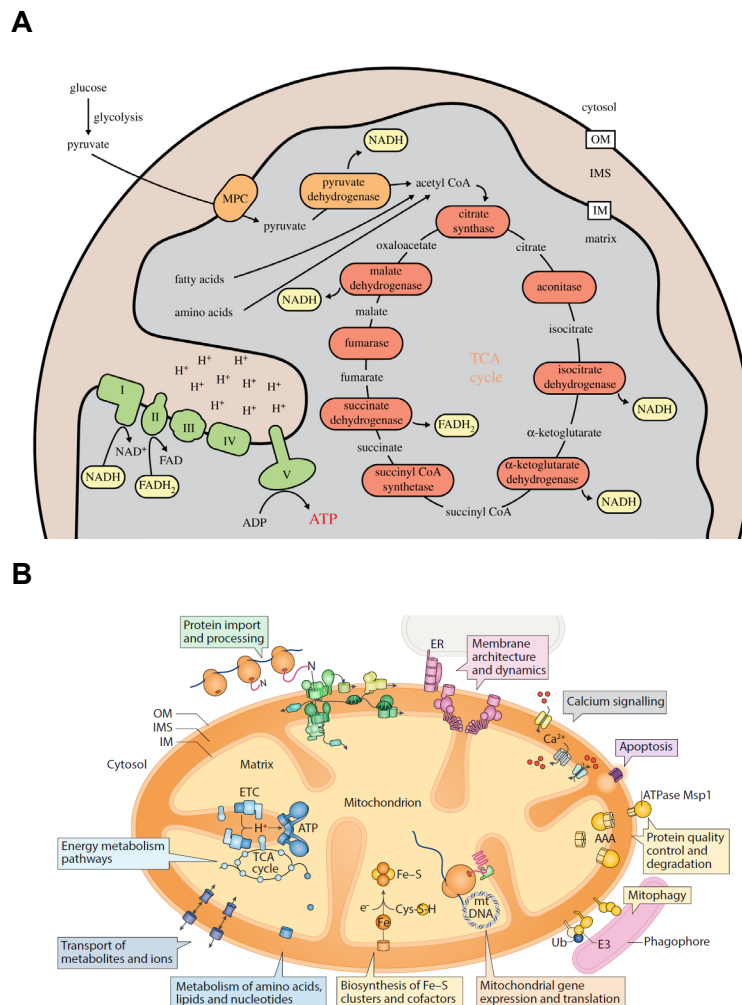


Figure 1.1. Mitochondrial metabolism. (A) Mitochondrial bioenergetics. Adapted from Anderson *et al.* (2019). (B) Overview of mitochondrial function. Adapted from Pfanner *et al.* (2019).

Besides energy production, mitochondria are the centre of multiple processes that are fundamental for the maintenance of normal cellular function, including the synthesis of phospholipids and heme, the regulation of calcium (Ca^{2+}) homeostasis and cell death (Pfanner *et al.*, 2019) (Figure 1.1B). These pleiotropic roles of mitochondria are reflected in the size of their proteome, consisting of 1500 proteins in humans (Lopez *et al.*, 2000; Pagliarini *et al.*, 2008) and 1000 proteins in unicellular model organisms, such as yeast (Morgenstern *et al.*, 2017). Of these proteins, over 99% are encoded in the nuclear genome, translated in the cytosol, targeted and imported into mitochondria. Instead, only 13 proteins, together with two ribosomal RNAs and 22 transfer RNAs that are necessary for their translation, are still synthesised in loco from the mitochondrial DNA (Anderson *et al.*, 1981). As the latter resembles the genome from an ancestral, aerobic proteobacterium, the origin of the mitochondrial organelle is uniquely descendant from endosymbiosis (Anderson *et al.*, 1981). Owing to the dual genetic origins, a robust coordination between nuclear and mitochondrial gene expression is necessary for the proper assembly and function of proteins required for mitochondrial biogenesis (Suomalainen and Battersby, 2018). Mutations in any of these nuclear or mitochondrial genes can therefore lead to mitochondrial dysfunction that has been implicated in a wide range of human diseases, from metabolic syndrome-related disorders (e.g., diabetes and obesity) to neurodegenerative diseases (e.g., Parkinson's and Alzheimer's diseases) (Figure 1.2).

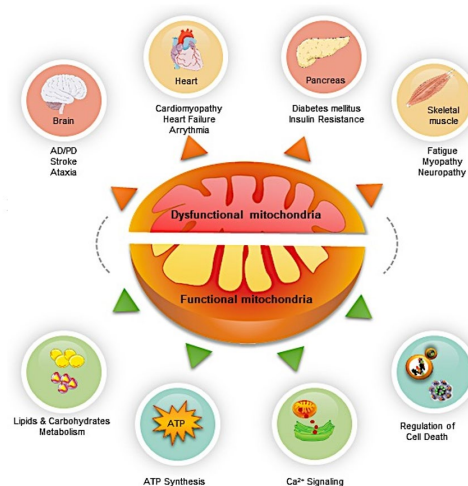


Figure 1.2. Mitochondria in health and diseases. The role of mitochondria in health and diseases. The model is based on Mammucari *et al.* (2017).

1.2. Calcium signalling

Each cell is constantly engaged in a bi-directional communication with its intra- and extracellular environment to tune cellular functions for specific demands (Berridge *et al.*, 1999,

2003). This transmission of signals occurs mainly by sensing and decoding Ca^{2+} -mediated signal transduction events (Berridge *et al.*, 2003). Ca^{2+} ions are fundamental for regulating diverse processes from transcription, differentiation, metabolism, proliferation to cell death (Berridge *et al.*, 2000). The role of Ca^{2+} in controlling physiological events initially emerged from the observation by Ringer (1883) that the addition of Ca^{2+} to the perfusion buffer of isolated hearts triggered their contraction. With technical development and advancement in monitoring cellular Ca^{2+} changes, cytosolic Ca^{2+} (cyt- Ca^{2+}) signals have been shown to appear either as Ca^{2+} spikes or repetitive oscillations, with different spatial and temporal properties (Bagur and Hajnóczky, 2017; Berridge and Galione, 1988; Clapham, 2007). During synaptic transmission and muscle (skeletal and cardiac) cell contractions, for example, Ca^{2+} triggers a rapid cellular response, within milliseconds (Boulware and Marchant, 2008) (Figure 1.3A). Instead, prolonged Ca^{2+} signals, over the range from minutes to hours, are required to drive cellular processes such as transcription and proliferation. These Ca^{2+} signals originate from the coordinated regulation of Ca^{2+} entry from the extracellular medium ($\sim 1 \text{ mM } \text{Ca}^{2+}$) through the plasma membrane (PM) and Ca^{2+} release from intracellular stores like the endoplasmic/sarcoplasmic reticulum (ER/SR, $> 500 \mu\text{M } \text{Ca}^{2+}$) (Pozzan *et al.*, 1994; Rizzuto and Pozzan, 2006) in response to external and internal stimuli (membrane depolarization, noxious stimuli, intracellular messengers, etc). Intracellular Ca^{2+} signals are mediated by PM and ER/SR Ca^{2+} channels, such as the transient receptor potential channels (TRPC) and Ca^{2+} release-activated Ca^{2+} channel (CRAC), and the inositol 1,4,5-trisphosphate receptors (Ins(1,4,5) P_3R) and ryanodine receptors (RyR), respectively (Figure 1.3B) (Giorgi *et al.*, 2018). In turn, Ca^{2+} pumps and exchangers at both cellular sites, such as the PM Ca^{2+} ATPase (PMCA) and ER/SR Ca^{2+} ATPases (SERCA), are responsible for returning cyt- Ca^{2+} level to basal.

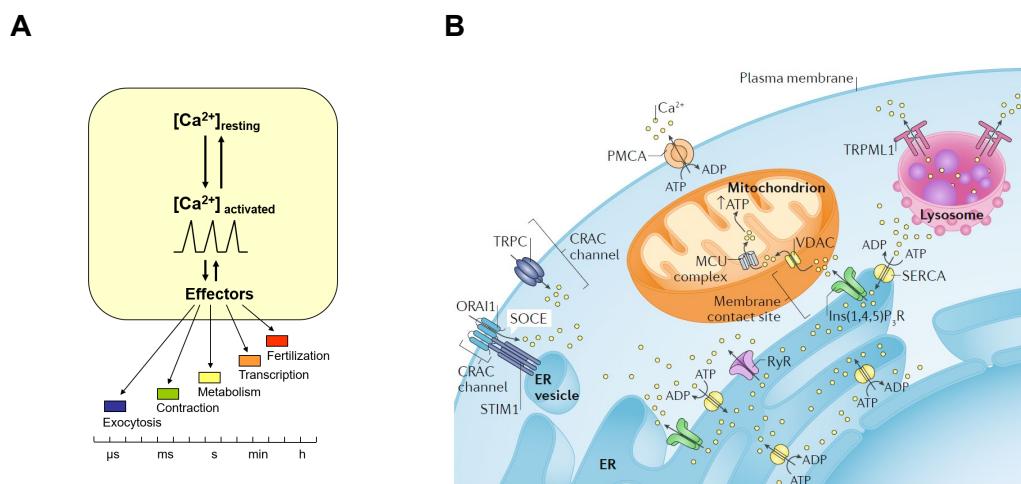


Figure 1.3. Ca^{2+} signalling. (A) Dynamics of Ca^{2+} signalling. Adapted from Berridge *et al.* (2003). (B) Intracellular Ca^{2+} signalling. From Giorgi *et al.* (2018).

Interestingly, cellular processes that are regulated by Ca^{2+} signalling varies among cells and organisms (bacteria, plants, fungi and animals) (Berridge *et al.*, 2003; Clapham, 2007; Kudla *et al.*, 2010; Norris *et al.*, 1996; Zelter *et al.*, 2004). This interspecies diversity in Ca^{2+} signalling suggests that specific sets of proteins are evolutionarily selected to meet the physiological demands of each organism (Cai and Clapham, 2012). As an example, fungi have been shown to lack Ca^{2+} signalling at the mitochondria, which is instead essential in all vertebrates (Figure 1.4).

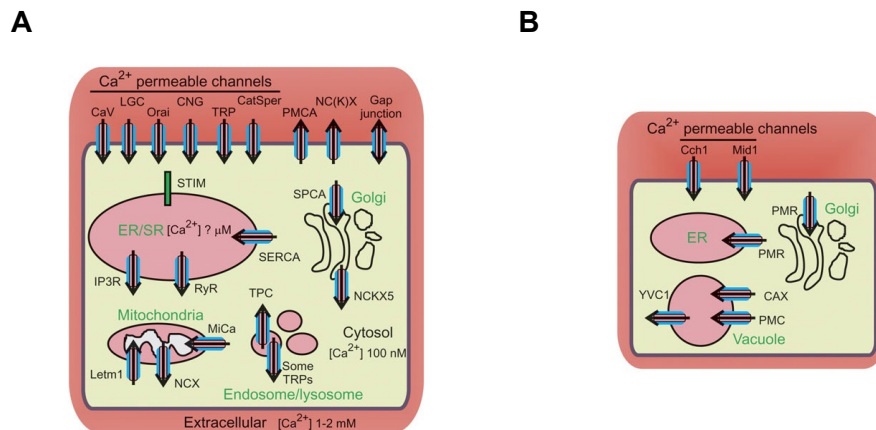


Figure 1.4 Schematic representation of Ca^{2+} signalling machineries. Ca^{2+} signalling machineries in animals (A) and fungi (B). From Cai & Clapham (2012).

1.3. Mitochondrial calcium signaling

Mitochondria are involved in the regulation and decoding of cellular Ca^{2+} dynamics through their ability to take up and release Ca^{2+} ions (Berridge *et al.*, 2000). With the development of the chemiosmotic theory, it became clear that the driving force for mitochondrial Ca^{2+} (mt- Ca^{2+}) transport is the negative membrane potential generated across the IMM by H^+ extrusion through the ETC (Rottenberg and Scarpa, 1974). The uptake of Ca^{2+} by mitochondria has been documented over 50 years ago when isolated mitochondria from mouse and rat organs were shown to buffer more than 20 mM of Ca^{2+} in the presence of respiratory substrates and phosphate (DeLuca & Engstrom, 1961; Vasington & Murphy, 1962). Instead, the release of mt- Ca^{2+} was found to be coupled with the entry of other ions, such as sodium (Na^+) and H^+ (Carafoli *et al.*, 1974; Crompton *et al.*, 1976) (Figure 1.5).

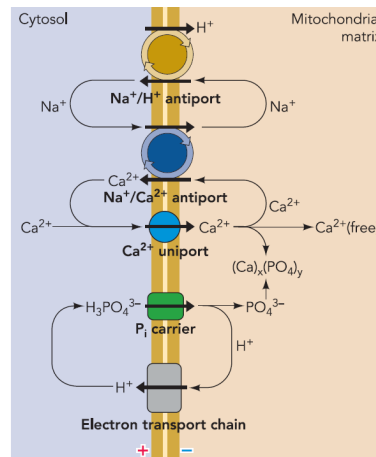


Figure 1.5. Ca^{2+} cycling between cytosolic and mitochondrial matrix space. The uptake and extrusion of Ca^{2+} is coupled to H^+ and Na^+ cycling, maintained by the ETC in mitochondria. From Szabadkai & Duchen (2008).

Ca^{2+} has been speculated to be transported across the IMM via a uniporter mechanism that follows the Ca^{2+} gradient between the cytosol and mitochondrial matrix and is driven by mitochondrial membrane potential (Drahota *et al.*, 1965). However, it was not until the year 2004 when electrophysiological measurements of Ca^{2+} currents across the IMM confirmed the existence of a high conductance and Ca^{2+} selective mitochondrial channel, that is referred as the Mitochondrial Calcium Uniporter Channel (MCUC) in this thesis (Kirichok *et al.*, 2004). In addition, MCUC was shown to be selectively inhibited by nanomolar concentrations of ruthenium red (RuRed) (Vasington *et al.*, 1972) and its derivative Ru360 (Matlib *et al.*, 1998; Ying *et al.*, 1991). However, given the low affinity of MCUC for Ca^{2+} , the shuttling of mt- Ca^{2+} as a physiologically relevant mitochondrial function, even at low peripheral cyt- Ca^{2+} levels during cellular stimulation, has been questioned for a long time (Carafoli and Crompton, 1978; Denton and McCormack, 1990; McCormack *et al.*, 1990; Spät *et al.*, 2008).

This initial discrepancy has been reconciled by several studies that have demonstrated the existence of Ca^{2+} hot spots around the mitochondrial surfaces that are in close proximity to Ca^{2+} release sites like the channels at the ER (Csordás *et al.*, 1999; Mannella *et al.*, 1998; Rizzuto *et al.*, 1998) or PM (Frieden *et al.*, 2005; Glitsch *et al.*, 2002; Westermann, 2015). Indeed, the close contacts between the mitochondria and ER membranes (within 10 nm to 60 nm) in live cells, demonstrated by electron micrographs, have confirmed that mitochondria are able to position strategically to activate MCUC and ensure efficient mt- Ca^{2+} buffering, shaping cyt- Ca^{2+} signals (Rizzuto *et al.*, 1998) (Figure 1.6). For example, in hepatocytes, cellular stimulation by an $\text{Ins}(1,4,5)\text{P}_3$ -dependent hormone triggers cyt- Ca^{2+} spikes that are efficiently transmitted into the mitochondrial matrix, in phase with the transient activation of Ca^{2+} -

sensitive mitochondrial enzymes (Hajnóczky *et al.*, 1995; Robb-Gaspers *et al.*, 1998). In addition, these cyt-Ca^{2+} oscillations are dependent on the mitochondrial membrane potential, shown in the sperm-induced activation of mouse oocytes (Wang *et al.*, 2018). As mitochondria are able to sense and halt its motility at these Ca^{2+} hot-spots, this facilitates the transfer of Ca^{2+} from the ER to the mitochondria (Liu and Hajnóczky, 2009; Yi *et al.*, 2004). In turn, the sequestration of mt-Ca^{2+} provides a regulatory feedback mechanism that can be activatory, inhibitory or biphasic to the respective Ca^{2+} channels (Hajnóczky *et al.*, 1999).

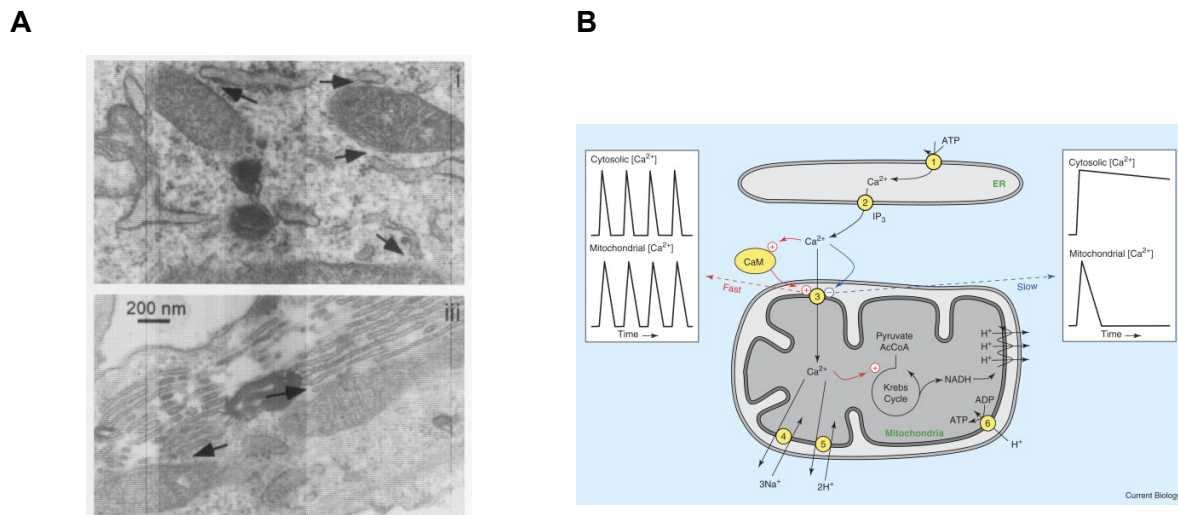


Figure 1.6. ER-mitochondria micro-domains. (A) Electron micrographs of intact H9c2 myotubes. Arrows indicate the close junctions between ER and mitochondria. Adapted from Pacher *et al.* (2000). (B) Regulation of mt-Ca^{2+} . The close contacts between ER Ca^{2+} release sites and mitochondria facilitates mt-Ca^{2+} uptake. Calmodulin (CaM) mediates the fast activation of the uniporter and enhances mt-Ca^{2+} accumulation that closely follow the changes in cyt-Ca^{2+} oscillations (left inset). A prolonged rise in cyt-Ca^{2+} then slowly inactivates the uniporter to limit mt-Ca^{2+} uptake (right inset). (1) SERCA; (2) $\text{Ins}(1,4,5)\text{P}_3\text{R}$; (3) MCUC; (4) $\text{Ca}^{2+}/\text{Na}^{+}$ exchanger; (5) $\text{Ca}^{2+}/\text{H}^{+}$ exchanger; (6) ATP synthetase. From Putney & Thomas (2006).

1.4. Physiological roles of mitochondrial calcium handling

Since the discovery of mt-Ca^{2+} uptake, several roles for Ca^{2+} in mitochondria have been suggested. The increase of mt-Ca^{2+} level has been shown to stimulate aerobic metabolism via the activation of three rate-limiting enzymes of the TCA cycle (pyruvate, α -ketoglutarate, and isocitrate dehydrogenase) (Denton and McCormack, 1980; Hajnóczky *et al.*, 1995; McCormack *et al.*, 1990) (Figure 1.7). This augments the production of NADH, promoting the transfer of electrons through the respiratory chain and up-regulating ATP production to meet the increased energy demand in signalling cells (Denton and McCormack, 1985). Similarly,

cyt- Ca^{2+} rise stimulates aspartate/glutamate exchangers at the IMM, which provide mitochondria with metabolites for ATP synthesis (Lasorsa *et al.*, 2003).

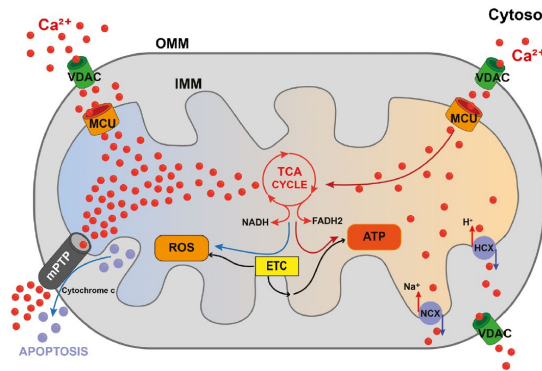


Figure 1.7. Regulation of mt- Ca^{2+} homeostasis. The influx and efflux mechanism regulates mt- Ca^{2+} homeostasis that have an impact on oxidative metabolism, ROS generation, and PTP opening. While mt- Ca^{2+} uptake via the uniporter, MCU, stimulates TCA cycle and ATP production, mt- Ca^{2+} overload causes the opening of mitochondrial PTP and cell death. NCX, $\text{Na}^+/\text{Ca}^{2+}$ exchanger; HCX, $\text{H}^+/\text{Ca}^{2+}$ exchanger. From Mammucari *et al.* (2018).

Apart from regulating mitochondrial metabolism, mt- Ca^{2+} has been associated with necrotic and apoptotic cell death (Duchen, 2000; Kruman and Mattson, 1999; Zong and Thompson, 2006). Prolonged high levels of cyt- Ca^{2+} can cause an overload of mt- Ca^{2+} . Together with an increase in reactive oxygen species (ROS), the mitochondrial permeability transition pore (PTP) changes to an open state (Bernardi, 1999; Bonora and Pinton, 2014) (Figure 1.7). The subsequent collapse of the mitochondrial membrane potential, followed by the depletion of ATP production, ion homeostasis and cell integrity, results in the eventual necrotic cell death. Consistently, this phenomenon has been shown to be prevented by an immunosuppressant, cyclosporine A that binds to the mitochondrial matrix protein cyclophilin D (CypD) (Schinzel *et al.*, 2005). Indeed, the knockout of CypD diminished the necrotic damage in the heart during ischaemia and reperfusion injury (Nakagawa *et al.*, 2005). The opening of PTP has not only been hypothesized to cause necrosis, but also apoptosis. Mitochondrial swelling upon PTP opening can release mitochondrial proapoptotic factors, such as cytochrome C (Kantrow and Piantadosi, 1997) and endonuclease G (Davies *et al.*, 2003), inducing apoptotic cell death. An anti-apoptotic oncogene *bcl-2* that localizes on the ER and mitochondrial membranes regulates intracellular Ca^{2+} homeostasis by reducing Ca^{2+} leak from the ER to mitochondria, protecting cells against mt- Ca^{2+} overload and apoptosis (Palmer *et al.*, 2004; Pinton *et al.*, 2000, 2001). Lastly, a study of the inhibitory effect on AMP-activated protein kinase activity exerted by mt- Ca^{2+} suggests a possible role of mt- Ca^{2+} in an autophagic rescue (Cárdenas *et al.*, 2010).

1.5. Mitochondrial calcium influx and efflux machineries

The roles of Ca^{2+} signalling in mitochondria and the biophysical properties of the uniporter have been comprehensively studied and established since the first discovery of Ca^{2+} uptake by the organelle. However, the molecular identity of the channels and transporters responsible for mt- Ca^{2+} handling have remained a mystery until very recently.

1.5.1 Molecular components of mitochondrial calcium efflux

Two mt- Ca^{2+} efflux systems, the mitochondrial $\text{Na}^+/\text{Ca}^{2+}$ and $\text{H}^+/\text{Ca}^{2+}$ exchangers, have been proposed to mediate Ca^{2+} extrusion from the mitochondrial matrix (Figure 1.8). In 2010, NCLX, belonging to the $\text{Na}^+/\text{Ca}^{2+}$ exchanger family, was characterized as the *bona fide* mt- Ca^{2+} exchanger, localized to the IMM in several tissues and able to catalyse Na^+ - and also Li^+ -dependent Ca^{2+} transport (Palty *et al.*, 2004, 2010). In addition, NCLX has been shown to be inhibited by a $\text{Na}^+/\text{Ca}^{2+}$ antiporter inhibitor, CGP-37157, and its knockdown alters mt- Ca^{2+} efflux, corroborating the role of NCLX as the mitochondrial $\text{Na}^+/\text{Ca}^{2+}$ antiporter.

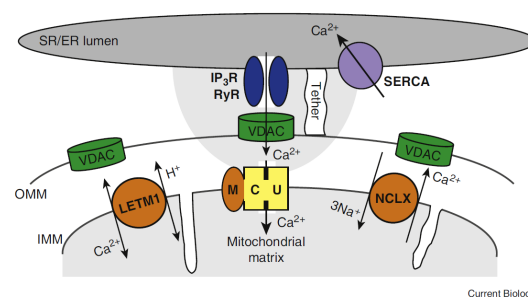


Figure 1.8. Molecular aspects of mitochondrial transport. From Hajnóczky & Csordás (2010).

Although the role of NCLX in mt- Ca^{2+} efflux has been widely accepted, the identification of the leucine zipper EF hand containing transmembrane protein 1 (LETM1) as the mitochondrial $\text{H}^+/\text{Ca}^{2+}$ exchanger has been controversial. LETM1 was first reported as a specific mitochondrial $\text{H}^+/\text{Ca}^{2+}$ exchanger from a genome-wide RNA interference (RNAi) screen in *Drosophila* cells (Jiang *et al.*, 2009). In both *Drosophila* and HeLa cells, LETM1 was reported to import mt- Ca^{2+} at low cyt- Ca^{2+} concentrations, paralleled with an export of H^+ , which was reversed at high cyt- Ca^{2+} levels. However, this import of Ca^{2+} into the mitochondria was shown to be inhibited by RuRed and CGP-37157, questioning its role in mt- Ca^{2+} efflux. Indeed, a previous study performed by Nowikovsky *et al.* (2004) has shown that LETM1 is a mitochondrial K^+/H^+ exchanger. While Tsai *et al.* (2014) has partially clarified that LETM1 is

unable to mediate the RuRed-sensitive mt- Ca^{2+} uptake, the role of LETM1 as a mitochondrial K^+/H^+ exchanger was not addressed. Due to these conflicting results (Doonan *et al.*, 2014; Jiang *et al.*, 2009; Nowikovsky *et al.*, 2004; Shao *et al.*, 2016), additional experimental evidence are required to reaffirm the functional role of LETM1.

1.5.2 Molecular components of mitochondrial calcium influx

The molecular components of MCUC have remained unknown for decades since the first observation of mt- Ca^{2+} uptake and buffering by DeLuca & Engstrom (1961) and Vasington & Murphy (1962). Common approaches for direct ion channel identification could not be undertaken as inhibitors for MCUC, such as RuRed, lack specificity (Stimers and Byerly, 1982). Yeast genetics could also not be employed due to the absence of mt- Ca^{2+} uptake activity (Carafoli and Lehninger, 1971). In light of the completed mammalian mitochondrial protein inventory, MitoCarta (Pagliarini *et al.*, 2008), an unbiased search was performed on the basis of the phylogenetic appearance of RuRed-sensitive Ca^{2+} uptake in vertebrates and kinetoplastids, such as the genus *Trypanosoma*, but not in yeast; mitochondrial localization with at least two transmembrane domains (TMDs); and tissue distribution (Perocchi *et al.*, 2010). From this analysis, 18 candidate genes were selected for RNAi screen, identifying a 54 kDa protein termed mitochondrial Ca^{2+} uptake 1 (MICU1) as the founding member of MCUC.

MICU1 is a calcium-binding protein containing two evolutionary EF-hand domains and located in the IMS (Perocchi *et al.*, 2010). The loss of MICU1 impairs mt- Ca^{2+} uptake, without disrupting the mitochondrial respiration and membrane potential, and reduces metabolic coupling between cyt- Ca^{2+} transients and energy metabolism. Although MICU1 has been shown to affect mt- Ca^{2+} uptake, the presence of only one TMD suggested a role as a regulatory rather than a pore-forming subunit of the uniporter. Subsequent studies defined the role of MICU1 as the 'gatekeeper' of MCUC that is responsible for setting the threshold of extra-mitochondrial Ca^{2+} concentration at which the uniporter is activated (Csordás *et al.*, 2013; Mallilankaraman *et al.*, 2012) (Figure 1.9).

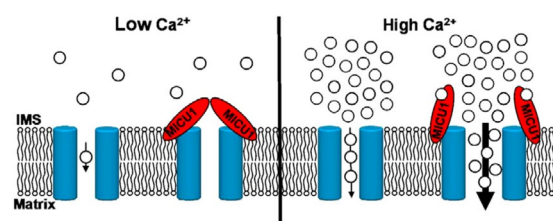


Figure 1.9. Graphical representation of the modulation of MCUC by MICU1. From Csordás *et al.* (2013).

Shortly after the discovery of MICU1, an integrative genomics approach based on evolutionary co-occurrence and co-expression with MICU1 together with physiological, biochemical and pharmacological analyses, identified a 40 kDa unstudied protein, CCDC109A, as the pore-forming subunit of MCUC (Baughman *et al.*, 2011; De Stefani *et al.*, 2011). This protein was then re-named as the mitochondrial calcium uniporter protein (MCU). First, the silencing of MCU inhibited mt- Ca^{2+} uptake in cultured cells and purified mouse liver mitochondria, whereas MCU overexpression in cells enhanced the RuRed-sensitive mt- Ca^{2+} uptake (Baughman *et al.*, 2011). Next, MCU formed oligomers and spanned the IMM via two transmembrane helices that are separated by a highly conserved linker, which consists of a DXXE motif (Baughman *et al.*, 2011; De Stefani *et al.*, 2011). Mutations on key acidic residues (E257A, D261A and E264A) near and within the DXXE motif, which may interact with Ca^{2+} , were shown to abolish mt- Ca^{2+} uptake activity, whereas a point mutation on the residue S259A conferred resistance to an analog of RuRed, Ru360 (Baughman *et al.*, 2011). Moreover, voltage-clamping of mitoplasts also confirmed that the loss of MCU leads to the loss of Ca^{2+} current (Chaudhuri *et al.*, 2013), further supporting the role of MCU as the pore-forming subunit of the uniporter. Finally, MCU and MICU1 were known to interact and run on the BN-PAGE as a large macromolecular complex of about 450 kDa (Baughman *et al.*, 2011) that includes several additional components discovered after the year 2011 (Plovanich *et al.*, 2013; Raffaello *et al.*, 2013; Sancak *et al.*, 2013) (Figure 1.10).

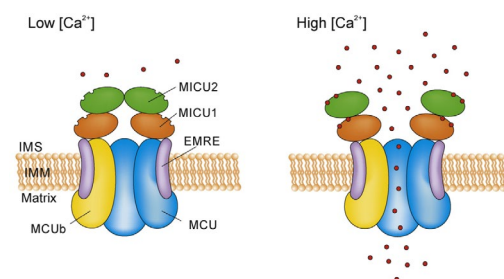


Figure 1.10. MCUC comprises pore-forming and regulatory proteins. From Mammucari *et al.* (2016).

MCUb was discovered in the year 2013 as a 33 kDa MCU paralog, originating from gene duplication (Raffaello *et al.*, 2013). However, MCUb and MCU sequences differ in the DXXE motif that is critical for ion permeation, which is suggested to provide a mechanistic basis to its dominant negative effect on the MCU-mediated Ca^{2+} uptake. Soon after, MICU2 and MICU3 were found as MICU1 paralogs (Plovanich *et al.*, 2013). While MICU1 is widely expressed in all tissues, MICU2 and MICU3 are mainly expressed in visceral organs and the central nervous system, respectively, suggesting a tissue-specific variation in the uniporter

composition. A knockout of either MICU1 or MICU2 in cells has been shown to result in an uptake of mt- Ca^{2+} at a lower threshold of Ca^{2+} (Kamer and Mootha, 2014). There is now consensus that MICU1 acts as a gatekeeper of the uniporter, inhibiting the channel at baseline cyt- Ca^{2+} levels (Mallilankaraman *et al.*, 2012; Yamamoto *et al.*, 2016), while MICU2 requires the presence of MICU1 for stability to set the Ca^{2+} threshold for the uniporter activity (Kamer and Mootha, 2014; Patron *et al.*, 2014). Recently, MICU3 has been found to form a dimer with MICU1 to act as an enhancer of MCU-dependent mt- Ca^{2+} uptake (Patron *et al.*, 2019). The silencing of MICU3 in primary cortical neurons was shown to impair Ca^{2+} signals elicited by synaptic activity, further suggesting a specific role in the regulation of neuronal functions.

Another subunit, the essential regulator EMRE, was characterized using affinity purification and quantitative proteomics by Sancak *et al.* (2013). EMRE, a 10 kDa transmembrane protein, was shown to be an essential component of the uniporter that interacts with MICU1 and MCU via its C-terminal domain at the poly-aspartate tail (EDDDDDD) and Gxxx[G/A/S] motif, respectively (Sancak *et al.*, 2013; Tsai *et al.*, 2016). Although EMRE was found to be a metazoan innovation, which did not evolve together with MCU and MICU1, its removal led to the complete loss of mt- Ca^{2+} uptake. In addition, EMRE loss-of-function was shown to disrupt the interaction of MICU1, and hence MICU2, with MCU.

1.5.3 Structures of mitochondrial calcium influx components

Several structural analyses of MCUC have attempted to decipher its oligomeric structure and functional roles upon Ca^{2+} stimulation (Baradaran *et al.*, 2018; Cao *et al.*, 2017; Fan *et al.*, 2018; Nguyen *et al.*, 2018; Oxenoid *et al.*, 2016; Wang *et al.*, 2019; Yoo *et al.*, 2018). These studies have revealed the architectural arrangement of MCU from different organisms, including *Caenorhabditis elegans*, zebrafish, fungi, and human, and also confirmed that the DXXE motif forms the selectivity filter of the channel. Human MCU has been shown to assemble as a tetramer, whereby each subunit consists of a N-terminal domain, linker-helix domain, coiled-coil domain and a TMD (Wang *et al.*, 2019) (Figure 1.11A). While fungal MCU also assembles as a tetramer, each subunit lacks the linker helix domain (Yoo *et al.*, 2018) (Figure 1.11B). Hence, interspecies structural studies provide a comparative framework for interpreting and further dissecting the function-structure relationships between components of the uniporter.

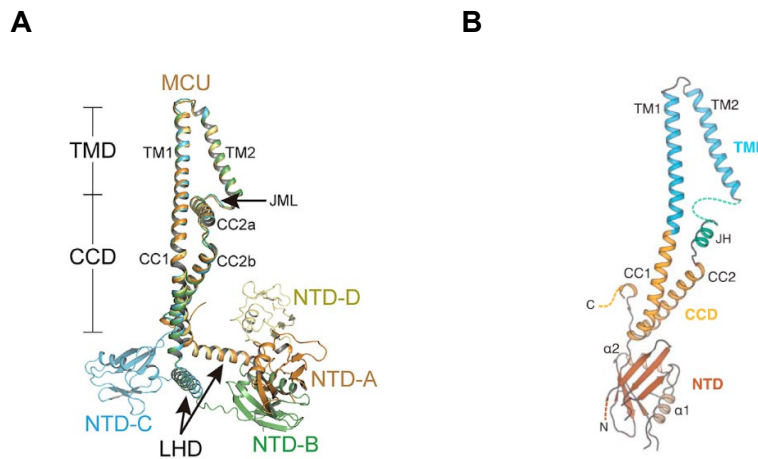


Figure 1.11. Structural alignment and domain of MCU. MCU structure from human (A) and fungi (B). NTD, N-terminal domain; LDH, linker-helix domain; CCD, coiled-coil domain; TMD, transmembrane domain. From Wang *et al.* (2019) and Yoo *et al.* (2018), respectively.

The structure of human EMRE has been recently described, consisting of a transmembrane helix connected to an N-terminal β -hairpin via an extended linker (Wang *et al.*, 2019) (Figure 1.12A). It is this extended linker on EMRE that has been shown to be crucial for the regulation of MCU conductivity. In addition, EMRE has been suggested to maintain an open MCU conformation for mt- Ca^{2+} uptake (Figure 1.12B), further confirming the importance of EMRE in the functionality of MCU.

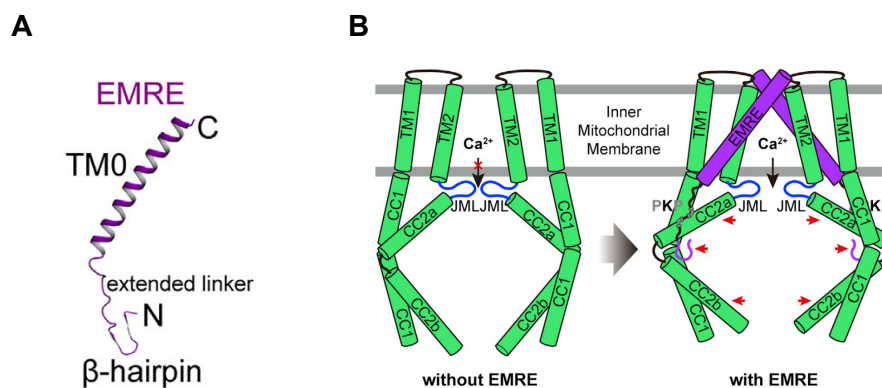


Figure 1.12. Structural domains of EMRE. Structure of human EMRE (A) and the proposed model of EMRE-regulated MCU conductivity (B). From Wang *et al.* (2019).

1.6. Pathophysiology of mitochondrial calcium dysregulation

Several studies have elucidated the regulatory role of mt- Ca^{2+} homeostasis on cell fate and function in different tissues and animal models, confirming that its deregulation is associated to various pathophysiological processes, such as diabetes, cardiovascular pathologies,

inflammation and neurodegeneration (Mammucari *et al.*, 2017) (Figure 1.13). For instance, pancreatic β -cells are responsible for the synthesis and secretion of insulin for glucose metabolism (Schuit *et al.*, 1988). The uptake of glucose stimulates oxidative metabolism and ATP synthesis that in turn closes ATP-sensitive potassium channels on the PM. The resultant depolarization of the PM stimulates Ca^{2+} influx via the PM voltage-gated Ca^{2+} channels that is relayed into the closely associated mitochondria, triggering, amplifying and sustaining the glucose-dependent insulin secretion process (Kennedy *et al.*, 1996; Wiederkehr *et al.*, 2011). A defect in mt- Ca^{2+} homeostasis in β -cells has been shown to decrease cytosolic ATP levels, impairing insulin secretion that is associated to the onset of type-2 diabetes (Alam *et al.*, 2012). Similarly, during an excitation-contraction coupling event in cardiomyocytes, the influx of Ca^{2+} through the L-type Ca^{2+} channels at the PM triggers the release of Ca^{2+} from the SR via RyRs and binds troponin C, inducing contraction (Kohlhaas *et al.*, 2017; Murgia *et al.*, 2009). As ATP is constantly hydrolysed to meet the energy demand required for this process, the depolarization-induced mt- Ca^{2+} uptake regenerates reducing cofactors for the ETC and maintains cellular antioxidant capacity. A decrease in mt- Ca^{2+} accumulation and a consequent decrease in NADH oxidation and mitochondrial respiration, was shown to impair fight-or-flight responses in the heart (Kwong *et al.*, 2015; Liu and Rourke, 2008; Luongo *et al.*, 2015; Wu *et al.*, 2015).

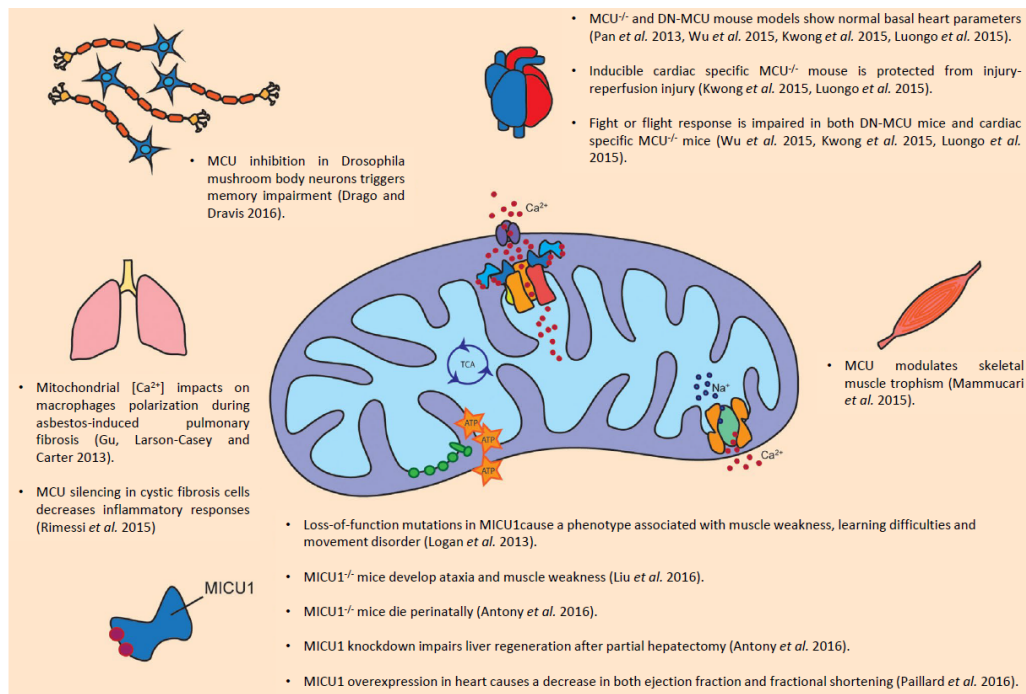


Figure 1.13 Pathophysiological roles of MCUC. The effects of MCU activity modulation in organs and tissues, both in animal models as well as in patients. From Mammucari *et al.* (2017).

MCU has been shown to regulate the buffering of cyt-Ca^{2+} during contraction of neonatal cardiomyocytes *ex vivo*, whereby the silencing or over-expression of MCU led to an increase or decrease in cyt-Ca^{2+} , respectively (Drago *et al.*, 2012). The manipulation of mt-Ca^{2+} accumulation in mice by constitutive MCU knockout (KO) on an outbreed CD1 background, inducible MCU deletion at adulthood, or the expression of a dominant-negative (DN) MCU mutant have been shown to result in a complete loss of mt-Ca^{2+} accumulation (Holmström *et al.*, 2015; Kwong *et al.*, 2015; Luongo *et al.*, 2015; Wu *et al.*, 2015). However, these mouse models consistently showed normal basal cardiac function and heart morphology. Instead, they were irresponsive to an acute increase in workload via β -adrenergic receptor stimulation demonstrated by their cellular inability to activate mitochondrial dehydrogenases, decreasing energy production and impairing physiological fight-or-flight heart rate acceleration (Luongo *et al.*, 2015; Wu *et al.*, 2015). Apart from the heart, skeletal muscles were also shown to be highly affected in MCU-KO mice, displaying a decrease in exercise capacity and muscle strength (Pan *et al.*, 2013). In addition, the postnatal overexpression or silencing of MCU in skeletal muscles resulted in muscle hypertrophy or atrophy, respectively (Mammucari *et al.*, 2015). Moreover, the ablation of MCU in C57BL/6J resulted in embryonic lethality (Murphy *et al.*, 2014), proving the importance of mt-Ca^{2+} uptake for life. So far, no pathogenic human MCU mutations have been described, possibly due to the low survival rate given that MCU has a pLI (a score indicating the probability that a gene ($\text{pLI} \geq 0.9$) is intolerant to a loss-of-function mutation) of 0.83 (<https://gnomad.broadinstitute.org>).

MICU1-KO mice have been reported to be perinatally lethal, without any major observable anatomical deficiencies, but are under-developed, displaying muscle weakness, ataxia and biochemical abnormalities (Antony *et al.*, 2016; Debattisti *et al.*, 2019; Liu *et al.*, 2016). These phenotypes were shown to improve with age, possibly due to an age-dependent remodelling of the uniporter, limiting the activity of the uniporter (Liu *et al.*, 2016). The knockdown of MICU1 in mouse liver tissues not only demonstrated a lowered threshold and cooperativity of Ca^{2+} -dependent activation of mt-Ca^{2+} uptake, but also showed an impairment in tissue regeneration upon stress (Antony *et al.*, 2016). Instead, an overexpression of MICU1 in heart tissues displayed a higher mt-Ca^{2+} uptake threshold that resulted in contractile dysfunction (Paillard *et al.*, 2017). While MICU2-KO mice are compatible with life and development, they presented abnormalities in cardiac relaxation and developed lethal abdominal aortic aneurysm (Bick *et al.*, 2017). Human subjects with loss-of-function mutations in MICU1 exhibited a range of severe symptoms characterized by muscle weakness, episodes of fatigue and lethargy, elevated creatine kinase activity, and neurological features including ataxia and chorea (Lewis-Smith *et al.*, 2016; Logan *et al.*, 2014; Musa *et al.*, 2019). Fibroblasts obtained from these patients also showed higher basal mt-Ca^{2+} levels, similar to that observed in MICU1-KO

HEK cells and young MICU1-KO mouse model (Kamer and Mootha, 2014; Liu *et al.*, 2016). Patients with mutated MICU2 have also been described, displaying encephalopathy and severe cognitive impairment without signs of myopathy (Shamseldin *et al.*, 2017). Overall, these findings support the crucial role of mt-Ca²⁺ homeostasis in organ physiology and qualify MCUC as potential players in pathophysiology.

Research aims

Research aim 1: To investigate the functional interconnection between MCU and MICU1 and its implication in human disorders

So far, several studies have investigated the physiological roles of each uniporter subunit in the regulation of mt-Ca²⁺ homeostasis and Ca²⁺ signalling. The general consensus is that owing to the large dynamic range of cyt-Ca²⁺ level, the uniporter must enable the uptake of cyt-Ca²⁺ into the mitochondrial matrix upon stimulation, while at the same time limit its entry at rest to prevent futile Ca²⁺ cycling as well as mt-Ca²⁺ overload (Duchen, 2000; Hajnóczky *et al.*, 1999). This is achieved by the coordinated action of the highly Ca²⁺ selective MCU pore and MICU1/MICU2 or MICU3-dependent gating and cooperative channel activation (Arduino *et al.*, 2017; Baughman *et al.*, 2011; Chaudhuri *et al.*, 2013; Csordás *et al.*, 2013; Kamer *et al.*, 2017; Mallilankaraman *et al.*, 2012; Patron *et al.*, 2014, 2019). As mammalian systems have been mostly employed to dissect the respective functional and mechanistic roles of each subunit in the regulation of the uniporter activity, the interpretation of these results is hampered by the differences in gene silencing approaches (Csordás *et al.*, 2013; Mallilankaraman *et al.*, 2012), compensatory remodelling of protein expression (Liu *et al.*, 2016; Paillard *et al.*, 2017), and tissue-specific MCUC composition and stoichiometry (Murgia and Rizzuto, 2015; Vecellio Reane *et al.*, 2016).

The baker's yeast, *Saccharomyces cerevisiae*, is an optimal system to decipher the functional contribution of each subunit of the human MCUC. Yeast mitochondria are completely devoid of MCU homologs (Bick *et al.*, 2012; Cheng and Perocchi, 2015), showing no detectable mt-Ca²⁺ uptake activity (Arduino *et al.*, 2017; Carafoli and Lehninger, 1971; Kovačs-Bogdán *et al.*, 2014; Yamamoto *et al.*, 2016). In addition, yeast allows ease expression and targeting of human mitochondrial proteins. Moreover, previous studies have demonstrated that the co-expression of human MCU and EMRE subunits is sufficient to reconstitute mt-Ca²⁺ uptake activity in isolated yeast mitochondria (Arduino *et al.*, 2017; Kovačs-Bogdán *et al.*, 2014; Yamamoto *et al.*, 2016).

The study described in part 1 of this thesis aims to establish a yeast-based heterologous system to investigate the functional interconnection between MCU and MICU1 *in vivo*. This allowed the screening for stress conditions whereby the presence of MICU1 would confer yeast strains with a reconstituted mt-Ca²⁺ activity a fitness advantage. A protective role of MICU1 against MCU-dependent manganese (Mn²⁺) toxicity was identified. Consistently, silencing of MICU1 in human HEK-293 cells led to Mn²⁺ leak into the mitochondrial matrix. Mn²⁺ uptake was genetically and chemically prevented by the re-introduction of wild-type (WT)

MICU1 and by RuRed, respectively. As a consequence, MICU1-KO greatly sensitized cells to Mn^{2+} -induced cell death, which was triggered by an increase in oxidative stress and prevented by N-acetyl-cysteine (NAC) treatment. Altogether, the findings presented here highlight a previously unknown function of MICU1 in the regulation of the uniporter ion selectivity, with important implications for both MICU1 and Mn^{2+} -related human disorders.

Research Aim 2: To reconstruct the evolutionary origin of mt- Ca^{2+} uptake and identify novel molecular targets for comparative MCUC structural and functional studies

Comparative genomics analyses have been instrumental in the molecular identification of MCUC (Baughman *et al.*, 2011; Perocchi *et al.*, 2010; Plovanich *et al.*, 2013; Raffaello *et al.*, 2013; Sancak *et al.*, 2013). While MCU and MICU1 were shown to have a correlated evolutionary history across over a hundred sequenced eukaryotic organisms (Baughman *et al.*, 2011; Bick *et al.*, 2012), EMRE was suggested to be an animal-specific MCU interactor due to the lack of EMRE homolog outside the metazoan lineage (Sancak *et al.*, 2013). Consistently, an amoeba, *Dictyostelium discoideum*, which had diverged before the origin of opisthokont (fungi and metazoan lineages), expresses both MCU and MICU1 orthologs that form a functional uniporter in the absence of EMRE (Kovács-Bogdán *et al.*, 2014). The differences in the evolutionary history of MCU, EMRE and MICU1 hinted a diversified MCUC composition and regulation in different phylogenetic clades. For instance, in the fungal clade, Basidiomycota and Ascomycota (e.g., *Neurospora crassa* and *Aspergillus fumigatus*) have been identified to contain MCU as the sole component of the MCUC (Bick *et al.*, 2012), suggesting that fungal MCU homologs are self-sufficient to regulate the uptake of mt- Ca^{2+} . Although several structural studies have used these Ascomycota MCUs to associate their structure to the uniporter function (Baradaran *et al.*, 2018; Fan *et al.*, 2018; Nguyen *et al.*, 2018; Yoo *et al.*, 2018), *N. crassa* and *A. fumigatus* have been previously shown to lack mt- Ca^{2+} uptake activity (Carafoli and Lehninger, 1971; Gonçalves *et al.*, 2015). In addition, the expression of their MCU homologs were incapable of reconstituting mt- Ca^{2+} uptake in HeLa and yeast cells (Baradaran *et al.*, 2018; Wettmarshausen *et al.*, 2018). Altogether, there is a discrepancy between the suggested ancient eukaryotic origin of mt- Ca^{2+} uptake and the phylogenetic profile of MCU, MICU1 and EMRE.

In collaboration with Dr. Alexandros A. Pittis (University of British Columbia) and Prof. Toni Gabaldón (Universitat Pompeu Fabra), the study described in part 2 of this thesis aims to perform a precise and detailed phylogenetic profiling and analysis to clarify the evolutionary origin of mt- Ca^{2+} uptake activity in eukaryotes. A gene duplication at the common ancestor of opisthokont was identified, giving rise to two MCU paralogous clades (animal-like and fungal-specific). Within the animal-like MCU clade, animal-like MCU, MICU and EMRE displayed a

strong co-evolutionary pattern across opisthokonts. While most fungi retained only the fungal-specific MCU paralog, three early-diverging fungi were found to contain both fungal-specific and animal-like MCU paralogs, together with MICU and EMRE. Heterologous expression of EMRE with animal-like MCU, but not fungal-specific paralog, from these fungal species reconstituted mt-Ca²⁺ uptake in HeLa and yeast cells. Altogether, these findings demonstrate that animal-like MCU, EMRE, and MICU represent the minimal core components of the ancestral opisthokont uniporter, providing key targets for future comparative structural and functional studies to understand the molecular basis of functional interactions within the uniporter complex.

Publication I

Jennifer Wettmarshausen*, **Valerie Goh***, Kai-Ting Huang, Daniela M. Arduino, Utkarsh Tripathi, Anja Leimpek, Yiming Cheng, Alexandros A. Pittis, Toni Gabaldón, Dejana Mokranjac, György Hajnóczky, and Fabiana Perocchi, 2018. **MICU1 Confers Protection from MCU-Dependent Manganese Toxicity**. Cell Rep, 25, 1425-1435.

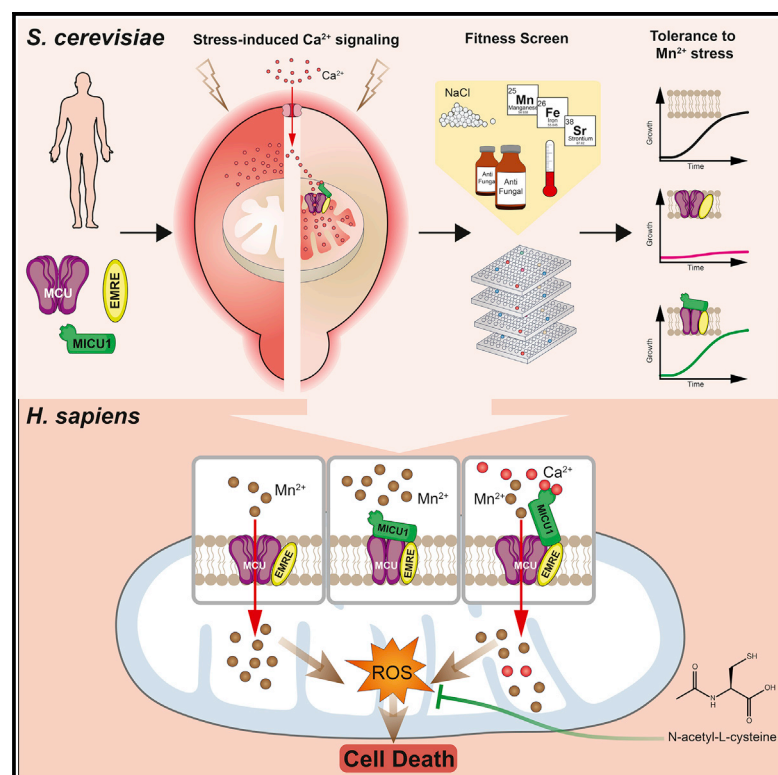
*equal author contributions

All experiments were designed together with Jennifer Wettmarshausen and Fabiana Perocchi. I had personally performed the experiments of Fig. 1C, 2E, 3D-F, 4A-B, 4F-H, S3, S4A-B, S4E-F, in collaboration with Jennifer Wettmarshausen for Fig. 1C and 2E. All the experiments and data in the figures as indicated were also analyzed and illustrated by myself. This manuscript was written together with Jennifer Wettmarshausen and Fabiana Perocchi.

Cell Reports

MICU1 Confers Protection from MCU-Dependent Manganese Toxicity

Graphical Abstract



Authors

Jennifer Wettmarshausen, Valerie Goh, Kai-Ting Huang, ..., Dejana Mokranjac, György Hajnóczky, Fabiana Perocchi

Correspondence

fabiana.perocchi@helmholtz-muenchen.de

In Brief

Wettmarshausen et al. develop a synthetic biology approach for *in vivo* dissection of functional interconnections between components of the mitochondrial calcium uniporter channel. They demonstrate an essential role of MICU1 in regulating MCU ion selectivity, finding that MICU1 prevents MCU-mediated Mn^{2+} overload and protects from Mn^{2+} -induced cell death.

Highlights

- MCU and MICU1 constitute the conserved unit of a eukaryotic uniporter
- Reconstitution of MCU-mediated Ca^{2+} uptake impairs yeast tolerance to Mn^{2+} stress
- MICU1 and MCU functional interaction confers a selective fitness advantage
- Loss of MICU1 hypersensitizes human cells to Mn^{2+} -dependent cell death



MICU1 Confers Protection from MCU-Dependent Manganese Toxicity

Jennifer Wettmarshausen,^{1,2,9} Valerie Goh,^{1,2,9} Kai-Ting Huang,³ Daniela M. Arduino,^{1,2} Utkarsh Tripathi,² Anja Leimpek,^{1,2} Yiming Cheng,^{1,2} Alexandros A. Pittis,^{4,5} Toni Gabaldón,^{4,5,6} Dejana Mokranjac,⁷ György Hajnóczky,³ and Fabiana Perocchi^{1,2,8,10,*}

¹Institute for Diabetes and Obesity, Helmholtz Diabetes Center (HDC), Helmholtz Zentrum München, 85764 Neuherberg, Germany

²Department of Biochemistry, Gene Center Munich, Ludwig-Maximilians Universität München, 81377 Munich, Germany

³Department of Pathology, Anatomy, and Cell Biology, MitoCare Center, Thomas Jefferson University, Philadelphia, PA 19107, USA

⁴Bioinformatics and Genomics Programme, Centre for Genomic Regulation (CRG), 08003 Barcelona, Spain

⁵Departament de Ciències Experimentals I de La Salut, Universitat Pompeu Fabra (UPF), 08003 Barcelona, Spain

⁶Institució Catalana de Recerca i Estudis Avançats (ICREA), 08010 Barcelona, Spain

⁷Biomedical Center Munich - Physiological Chemistry, Ludwig-Maximilians Universität München, 82152 Martinsried, Germany

⁸Munich Cluster for Systems Neurology, 81377 Munich, Germany

⁹These authors contributed equally

¹⁰Lead Contact

*Correspondence: fabiana.perocchi@helmholtz-muenchen.de

<https://doi.org/10.1016/j.celrep.2018.10.037>

SUMMARY

The mitochondrial calcium uniporter is a highly selective ion channel composed of species- and tissue-specific subunits. However, the functional role of each component still remains unclear. Here, we establish a synthetic biology approach to dissect the interdependence between the pore-forming subunit MCU and the calcium-sensing regulator MICU1. Correlated evolutionary patterns across 247 eukaryotes indicate that their co-occurrence may have conferred a positive fitness advantage. We find that, while the heterologous reconstitution of MCU and EMRE *in vivo* in yeast enhances manganese stress, this is prevented by co-expression of MICU1. Accordingly, MICU1 deletion sensitizes human cells to manganese-dependent cell death by disinhibiting MCU-mediated manganese uptake. As a result, manganese overload increases oxidative stress, which can be effectively prevented by NAC treatment. Our study identifies a critical contribution of MICU1 to the uniporter selectivity, with important implications for patients with MICU1 deficiency, as well as neurological disorders arising upon chronic manganese exposure.

INTRODUCTION

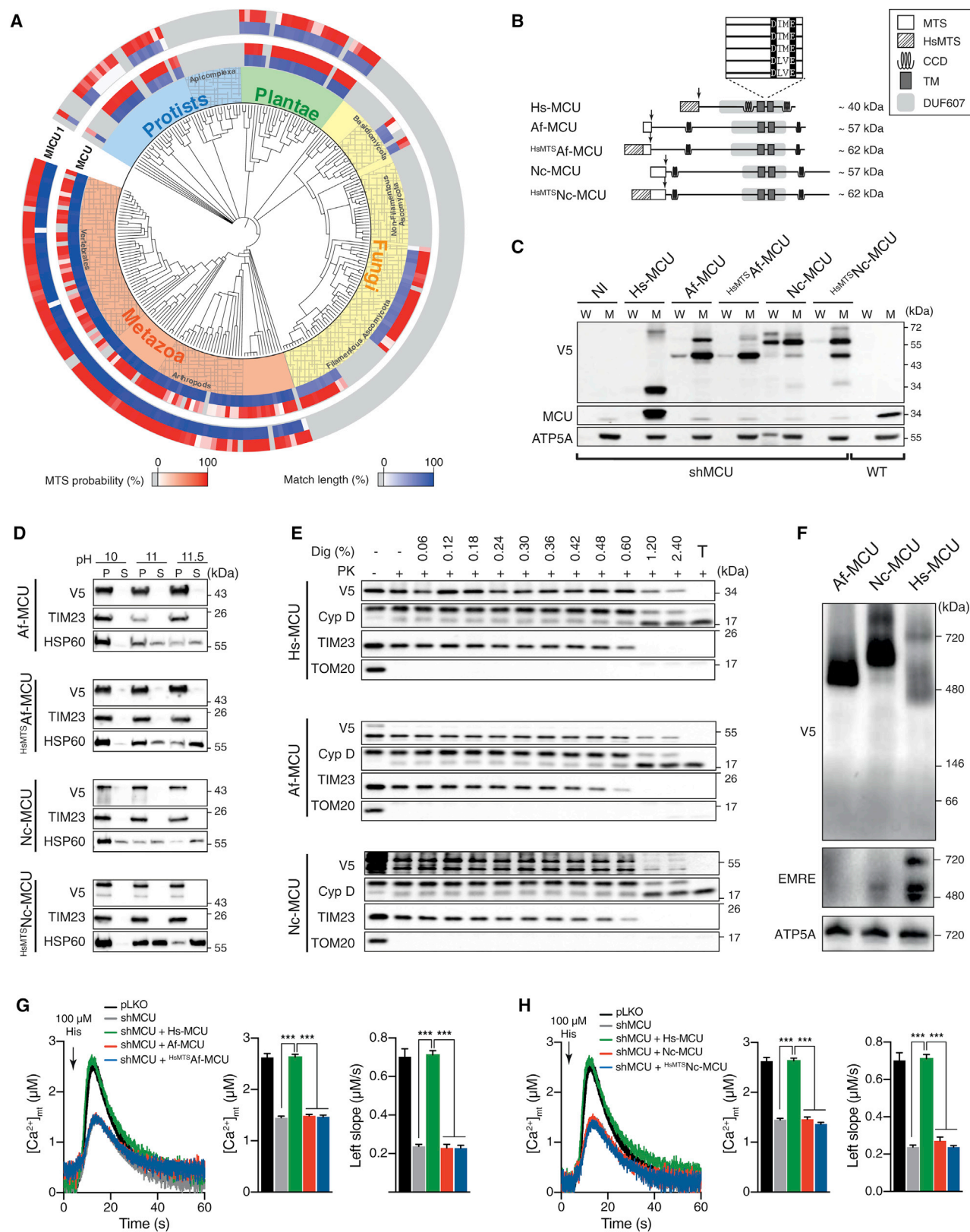
Mitochondria from several organisms are able to regulate intracellular calcium (Ca^{2+}) dynamics due to their ability to rapidly and transiently uptake Ca^{2+} . This occurs through an electrophoretic uniporter mechanism that makes use of the steep electrochemical gradient generated by the respiratory chain (Carafoli and Lehninger, 1971; Deluca and Engstrom, 1961; Vasington

and Murphy, 1962) and is mediated by a highly selective Ca^{2+} channel located at the inner mitochondrial membrane (Kirichok et al., 2004). However, the molecular identity of the mitochondrial Ca^{2+} uniporter has remained a mystery for decades. Recently, a functional genomics approach has allowed the discovery of the first peripheral Ca^{2+} -dependent regulator (MICU1) (Perocchi et al., 2010) and the transmembrane pore-forming subunit of the uniporter (MCU) (Baughman et al., 2011; De Stefani et al., 2011), paving the way for the identification of several other inhibitory and enhancing effectors of mitochondrial Ca^{2+} (mt- Ca^{2+}) uptake such as MCUB, MICU2, MICU3, and EMRE (De Stefani et al., 2016).

Overall, the complex molecular nature of the mammalian uniporter highlights the physiological relevance of achieving great plasticity and selectivity in mt- Ca^{2+} uptake. Due to the presence of a very large driving force for cation influx, the uniporter must at the same time limit mt- Ca^{2+} accumulation when the cell is at rest to prevent vicious Ca^{2+} cycling and rapidly transmit a cytosolic Ca^{2+} (cyt- Ca^{2+}) signal to the mitochondrial matrix during signaling. The highly selective permeability of the uniporter for Ca^{2+} is thought to derive from the high-affinity binding of the ion to the DXE motif at the MCU pore (Arduino et al., 2017; Baughman et al., 2011; Cao et al., 2017; Chaudhuri et al., 2013; Oxenoid et al., 2016), whereas both gating and cooperative activation of the uniporter have been attributed to its interaction with hetero-oligomers of MICU1 and MICU2 or MICU3 (Csordás et al., 2013; Kamer et al., 2017; Mallilankaraman et al., 2012; Patron et al., 2014, 2018). However, the respective functional and mechanistic roles of those subunits in regulating uniporter activity have been thus far investigated in mammalian systems, in which the interpretation of results is hampered by differences in the degree of gene silencing, tissue-specific protein composition (Murgia and Rizzuto, 2015; Vecellio Reane et al., 2016), stoichiometry, and compensatory remodeling (Liu et al., 2016; Paillard et al., 2017) of the channel.

The budding yeast *Saccharomyces cerevisiae* represents an ideal testbed for dissecting the functional contribution of each





(legend on next page)

component of the human uniporter, given that it completely lacks any detectable MCU homolog (Bick et al., 2012; Cheng and Perocchi, 2015) and endogenous mt- Ca^{2+} transport activity (Arduino et al., 2017; Carafoli and Lehninger, 1971; Kovács-Bogdán et al., 2014; Yamamoto et al., 2016), while enabling the facile expression and targeting of human mitochondrial proteins. Moreover, we and others have shown that mt- Ca^{2+} uptake can be readily reconstituted *in vitro* in isolated yeast mitochondria by co-expressing the human MCU and EMRE subunits (Arduino et al., 2017; Kovács-Bogdán et al., 2014; Yamamoto et al., 2016). Here, we establish a yeast-based heterologous system to investigate the functional interconnection between MCU and MICU1 *in vivo*. By screening for stress conditions whereby the expression of MICU1 in an MCU-reconstituted yeast strain would confer a fitness advantage, we identify a protective role of MICU1 against MCU-dependent manganese (Mn^{2+}) toxicity. Consistent with these findings, human HEK293 cells lacking MICU1 become permeable to Mn^{2+} , whose uptake is genetically and chemically prevented by the re-introduction of wild-type (WT) MICU1 and by ruthenium red (RuRed), respectively. As a consequence, MICU1 knockout (KO) cells are greatly sensitized to Mn^{2+} -induced cell death that is triggered by an increase in oxidative stress and prevented by *N*-acetyl-L-cysteine (NAC) treatment. Our findings highlight a previously unknown role of MICU1 in regulating the selectivity of the uniporter, with potential implications for both MICU1 and Mn^{2+} -related human disorders.

RESULTS

Phylogenetic Profiling of MCU and MICU1 across 247 Eukaryotes

We examined the co-evolution and predicted mitochondrial co-localization of MCU and MICU1 across 247 fully sequenced eukaryotic species (Figure 1A) from multiple taxonomic levels at different evolutionary distances to maximize the resolution of coupled evolutionary patterns (see also <https://itol.embl.de/tree/774755176425021526503446>) (Cheng and Perocchi, 2015). We found that MCU homologs were widely distributed in all of the major eukaryotic groups, present in nearly all Metazoa and Plantae, but only in some Protozoa (e.g., *Trypanosoma cruzi*, *Leishmania major*) and few Fungi. Instead, they apparently had been lost in all Apicomplexa (e.g., *Plasmodium falciparum*), mitochondrial-devoid, single-cell eukaryotes (e.g., *Entamoeba histolytica*, *Giardia lamblia*, *E. cuniculi*), and Saccharomycota (e.g., *S. cerevisiae*, *Schizosaccharomyces pombe*, *Candida*

glabrata). We observed a largely overlapping distribution of MICU1 and MCU homologs, pointing to a strong functional association between the two proteins, which we now know to be part of the same complex. Only a few species within Basidiomycota and Ascomycota fungal clades, such as *Neurospora crassa* and *Aspergillus fumigatus*, contained MCU-like proteins without any detectable MICU1 orthologs.

Given that Fungi also lack EMRE (Sancak et al., 2013), we reasoned that fungal MCU homologs should be self-sufficient to drive mt- Ca^{2+} uptake, similarly to the MCU ortholog from *Dicostillium discoideum* (Dd-MCU) (Arduino et al., 2017; Kovács-Bogdán et al., 2014). Therefore, we analyzed their ability to complement MCU loss of function in human cells. We expressed *A. fumigatus* (Af-MCU), *N. crassa* (Nc-MCU), or human MCU (Hs-MCU) with a C-terminal V5 tag in MCU knockdown (shMCU) HeLa cells (Figure 1B). To ensure the targeting of fungal MCUs to human mitochondria, we also tested chimera proteins consisting of the Hs-MCU mitochondrial targeting sequence (HsMTS) fused to the full-length form of Nc-MCU (^{HsMTS}Nc-MCU) and Af-MCU (^{HsMTS}Af-MCU). We showed that all constructs were properly localized (Figure 1C) and inserted (Figure 1D) into the inner mitochondrial membrane of shMCU HeLa cells, with the C termini facing the matrix side, similar to Hs-MCU (Figure 1E). Furthermore, on a native gel, both Af-MCU and Nc-MCU formed a large protein complex of a size comparable to that of cells expressing Hs-MCU (Figure 1F). Next, we quantified mt- Ca^{2+} uptake transients in intact (Figures 1G and 1H) and digitonin-permeabilized (Figure S1) shMCU HeLa cells expressing Hs-MCU, Af-MCU, or Nc-MCU, together with a mitochondrial matrix-targeted WT aequorin (mt-AEQ) as a Ca^{2+} sensor. Although the expression of Hs-MCU fully rescued mt- Ca^{2+} uptake, neither Af-MCU nor Nc-MCU, with and without HsMTS, were able to functionally complement Hs-MCU loss of function.

The strong co-evolution of MCU and MICU1, together with the apparent lack of functional MCU homologs in *A. fumigatus*, *N. crassa*, and several other fungal species (Baradaran et al., 2018) that do not express any MICU1-like component, suggest that MCU and MICU1 constitute the conserved unit of a eukaryotic uniporter, and their functional interaction could be required to provide a fitness advantage.

In Vivo Reconstitution of Mitochondrial Calcium Uptake in Yeast

Yeast uses cyt- Ca^{2+} signaling to activate pro-survival, adaptive responses to diverse environmental stresses (Cyert, 2003). We

Figure 1. Evolutionary Analysis of MCU and MICU1 across 247 Eukaryotes

(A) Phylogenetic distribution of MCU and MICU1 homologs (blue, percentage of amino acids match length). MTS, mitochondrial targeting sequence.
(B) Schematic of ectopically expressed fungal MCU constructs and protein domains. DXE motif and MTS cleavage site prediction (arrow) are also shown. CCD, coiled-coil domain; TM, transmembrane domain.
(C) Analysis of whole-cell (W) and mitochondrial (M) fractions from pLKO (WT) or shMCU HeLa cells stably expressing human (Hs-MCU), *N. crassa* (Nc-MCU), or *A. fumigatus* (Af-MCU) MCU fused to a C-terminal V5-tag. HsMTS, mitochondrial targeting sequence of human MCU; NI, not infected.
(D) Analysis of mitochondrial soluble (S) and membrane pellet (P) fractions.
(E) Analysis of fungal MCU protein topology by proteinase K (PK) treatment. Dig, digitonin; T, triton (1%).
(F) Macromolecular protein complex analysis of fungal MCU constructs by blue native (BN)-PAGE.
(G and H) Representative traces and quantification of mt- Ca^{2+} transients in pLKO (WT) or shMCU HeLa cells stably expressing MCU from human (Hs-MCU) and *A. fumigatus* (Af-MCU) (G) or *N. crassa* (Nc-MCU) (H) upon histamine (His) stimulation.
All data represent means \pm SEMs; n = 6–8; ***p < 0.001, one-way ANOVA with Tukey's multiple comparisons test.
See also Figure S1.

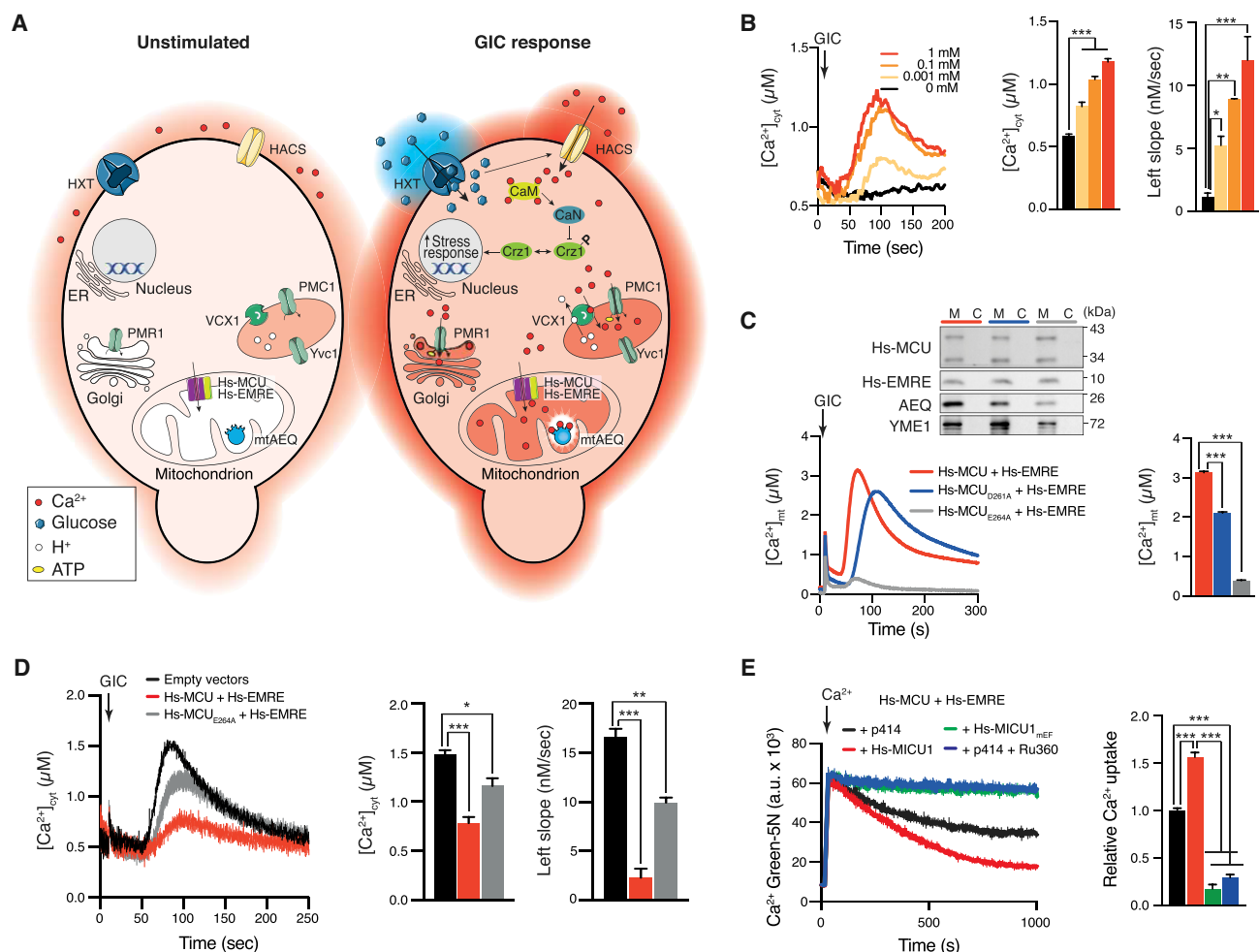


Figure 2. In vivo Reconstitution of mt- Ca^{2+} Uptake in Yeast

(A) Schematic of the Ca^{2+} homeostasis system and glucose-induced calcium (GIC) signaling in *S. cerevisiae*. CaM, calmodulin; CaN, calcineurin; Crz1, calcineurin-dependent transcription factor; Crz1^P, phosphorylated Crz1; ER, endoplasmic reticulum; HACs, high-affinity Ca^{2+} transport system; HXT, hexose transporter; mtAEQ, mitochondria-targeted aequorin; PMC1, vacuolar Ca^{2+} -ATPase; PMR1, ER/Golgi Ca^{2+} -ATPase; VCX1, vacuolar $\text{H}^{+}/\text{Ca}^{2+}$ exchanger; Yvc1, transient receptor potential cation (TRPC)-type Ca^{2+} channel.

(B) Cyt- Ca^{2+} transients in yeast cells upon GIC stimulation in the presence of different extracellular CaCl_2 concentrations (n = 3); *p < 0.05, **p < 0.01, ***p < 0.001; one-way ANOVA with Dunnett's multiple comparisons test.

(C) Mt- Ca^{2+} transients in yeast cells expressing WT mtAEQ, Hs-EMRE, and either WT or mutated Hs-MCU upon GIC stimulation in the presence of 1 mM CaCl_2 (n = 3); ***p < 0.0001; one-way ANOVA with Tukey's multiple comparisons test. Inset: immunoblot analysis of cytosolic (C) and mitochondrial (M) fractions.

(D) Cyt- Ca^{2+} transients in yeast cells expressing empty vectors (p425, p423) or Hs-EMRE with either WT or mutant Hs-MCU upon GIC stimulation in the presence of 1 mM CaCl_2 (n = 3); *p < 0.05, **p < 0.01, ***p < 0.001; one-way ANOVA with Dunnett's multiple comparisons test.

(E) Extracellular Ca^{2+} clearance by mitochondria isolated from the yeast strains expressing Hs-MCU, Hs-EMRE, and either an empty vector (p414), human WT MICU1 (Hs-MICU1), or EF-hands mutant MICU1 (Hs-MICU1^{mEF}), (n = 3); ***p < 0.001; one-way ANOVA with Tukey's multiple comparisons test.

All data represent means \pm SEMs.

See also Figure S2.

therefore asked whether the reconstitution of MCU-mediated mt- Ca^{2+} uptake in yeast would affect the activation of cyt- Ca^{2+} dynamics *in vivo*. As an extracellular stimulus, we chose glucose-induced calcium (GIC) activation, whereby the addition of glucose and extracellular Ca^{2+} to cells starved for >2 hr in hexose-free medium triggers cyt- Ca^{2+} transients (Figures 2A and 2B) (Groppi et al., 2011). Next, we generated yeast strains expressing WT mt-AEQ together with Hs-MCU, Hs-EMRE, or

both and confirmed that their co-expression was necessary and sufficient to drive mt- Ca^{2+} uptake *in vivo* (Figure S2A) and to respond to a wide dynamic range of external Ca^{2+} concentrations (Figure S2B). Accordingly, Hs-MCU mutants in highly conserved acidic residues within the DXE motif (Hs-MCU_{D261A}; Hs-MCU_{E264A}) were either partially functional (Hs-MCU_{D261A}) or almost completely unable (Hs-MCU_{E264A}) to fully transfer GIC-induced cyt- Ca^{2+} signals into the mitochondrial matrix

(Figure 2C). Likewise, yeast strains expressing Af-MCU or Nc-MCU (Figure S2C) were unable to drive Ca^{2+} uptake in the organelle, compared to cells reconstituted with Dd-MCU (Figure S2D). As hypothesized, the *in vivo* reconstitution of MCU-mediated mt- Ca^{2+} uptake resulted in a prompt buffering of GIC-induced cyt- Ca^{2+} elevations (Figure 2D). We then tested whether the expression of WT human MICU1 (Hs-MICU1) (Figure S2E) would be sufficient to reconstitute a Ca^{2+} -regulated uniporter in yeast. Similar to mammalian cells (Csordás et al., 2013; Kamer et al., 2017; Mallilankaraman et al., 2012), the presence of WT but not EF-hands mutant (Hs-MICU1_{mEF}) significantly increased the MCU-dependent mt- Ca^{2+} level upon GIC activation in intact cells (Figure S2F) and a bolus of high Ca^{2+} in isolated mitochondria (Figure 2E).

These results validate our *in vivo*, heterologous experimental system for the study of uniporter-mediated Ca^{2+} uptake. They also demonstrate that the expression of Hs-MCU, Hs-EMRE, and Hs-MICU1 in yeast is sufficient to reconstitute Ca^{2+} -regulated uniporter activity in response to physiological stimuli that activate intracellular Ca^{2+} signaling.

MCU Impairs Yeast Tolerance to Metal Stress

We then searched for biological conditions in which the reconstitution of MCU-mediated mt- Ca^{2+} uptake in the absence of the regulatory subunit MICU1 would lead to fitness impairment. We compared the fitness of yeast strains expressing a functional (Hs-MCU/EMRE) or an inactive (Hs-MCU_{E264A}/EMRE) uniporter to that of WT cells upon different environmental stresses (Figure 3), including heat shock, fungicide treatment, high salt, and heavy metals. To this end, we used growth rate as a proxy for cell survival and proliferation and ensured their reliance on functional mitochondria by using lactate as a non-fermentable carbon source. Overall, we observed comparable doubling times among the three different strains during normal growth at 30°C in lactate medium, which was >2-fold higher upon heat shock (37°C) (Figure 3A). Likewise, treatment with increasing doses of two antifungal drugs, miconazole and amiodarone, either decreased the growth rate of the yeast cultures by >2-fold (miconazole, 100 ng/mL) (Figure 3B) or resulted in a complete cessation of growth (amiodarone, 20 μM) (Figure 3C), regardless of the genetic background. The three strains also showed similar sensitivities to salt stress (NaCl and CaCl_2) within the range of the tested concentrations (Figures 3D, 3E, and S3A).

Instead, we observed notable differences among strains in their responses to heavy metals-induced stress (Sr^{2+} , Cu^{2+} , Zn^{2+} , Fe^{2+} , Mn^{2+}) (Figure 3F). Those cations are essential for normal growth and metabolism when present at minimal levels in the medium, but at high concentrations they can induce cytotoxicity (Wysocki and Tamás, 2010). Accordingly, with the exception of Sr^{2+} (Figure S3B), the doubling time of WT yeast cultures was >2-fold higher in the presence of high extracellular concentrations of CuCl_2 , FeCl_2 , and ZnCl_2 (Figure 3F). While all strains showed a similar tolerance to CuCl_2 and ZnCl_2 , we observed a greater hypersensitivity of the functional MCU-reconstituted strain to both Fe^{2+} and Mn^{2+} toxicity, which manifested as a drastic reduction in cell proliferation at concentrations >10 and 1 mM, respectively (Figure 3F). In addition, expression of Hs-MCU_{E264A} did not impair tolerance to Mn^{2+}

stress, whereas the same mutation was not sufficient to prevent Fe^{2+} -induced toxicity, suggesting a potentially different coordination of Fe^{2+} with the DXXE motif.

These observations indicate that in the absence of MICU1, MCU may mediate the cytotoxic accumulation of heavy metals in mitochondria.

MICU1 Protects Human Cells from MCU-Dependent Mn^{2+} Toxicity

We speculate that the co-occurrence of MCU and MICU1 could confer an evolutionary advantage by shielding mitochondria from an unwanted accumulation of heavy metals. Thus, we tested whether the reconstitution of an MICU1-regulated uniporter would be sufficient to protect yeast cells from MCU-dependent Mn^{2+} and Fe^{2+} stresses. We found that the expression of either Hs-MICU1 or Hs-MICU1_{mEF} significantly rescued the hypersensitivity of the MCU-reconstituted strain toward both Fe^{2+} (Figure S4A) and Mn^{2+} (Figure 4A) stresses. This finding indicated that MICU1 interaction with Hs-MCU and Hs-EMRE, rather than functional EF-hands, was required to prevent Fe^{2+} and Mn^{2+} entry into mitochondria, most probably by keeping the channel in a close conformation.

Next, we recapitulated the above findings in mammalian cells. To this end, we compared the viability of WT and MICU1-KO HEK293 cells upon treatment with increasing concentrations of either FeCl_2 or MnCl_2 for 48 hr. Unlike yeast, neither WT nor MICU1-KO HEK293 cells showed an increased sensitivity to Fe^{2+} treatment (Figure S4B), even at high non-physiological concentrations, indicating major differences in the mechanisms used by fungal and mammalian cells to regulate Fe^{2+} homeostasis and cope with its overload (Philpott, 2012). Instead, we observed a dramatic decrease in cell viability when MICU1-KO cells were treated with concentrations of Mn^{2+} >10 μM , which did not affect WT cells (Figure 4B). As observed in yeast, the protective role of MICU1 toward Mn^{2+} toxicity was not dependent on having functional Ca^{2+} -sensing domains, as a genetic rescue with either Hs-MICU1 or Hs-MICU1_{mEF} resulted in a significantly higher tolerance than MICU1-KO cells to 25 μM Mn^{2+} (Figures S4C and S4D).

These results pointed toward a critical role of MICU1 in inhibiting MCU-dependent Mn^{2+} toxicity, which could be exerted by directly regulating Mn^{2+} entry through the uniporter. We therefore measured mitochondrial Mn^{2+} uptake in WT and MICU1-KO HEK293 cells by monitoring the quenching of the fluorescence signal from mitochondrial compartmentalized Fura-FF upon Mn^{2+} entry in the mitochondrial matrix (Csordás and Hajnóczky, 2003). We confirmed previous findings showing that in the presence of submicromolar cyt- Ca^{2+} levels, mitochondria from WT cells are not permeable to Mn^{2+} (Figure 4C). Instead, in the same conditions, MICU1 KO cells displayed robust mitochondrial Mn^{2+} uptake, as indicated by the time-dependent quenching of the fluorescence signal upon addition of 20 μM Mn^{2+} (Figure 4C). This uptake was completely inhibited by RuRed and fully rescued by the expression of WT MICU1 in the HEK293 KO genetic background (Figure 4D), validating that the observed Mn^{2+} transport was mediated by MCU. Moreover, we showed that the pre-addition of 30 μM Ca^{2+} , a concentration at which the uniporter is disinhibited, resulted in Mn^{2+} entry also

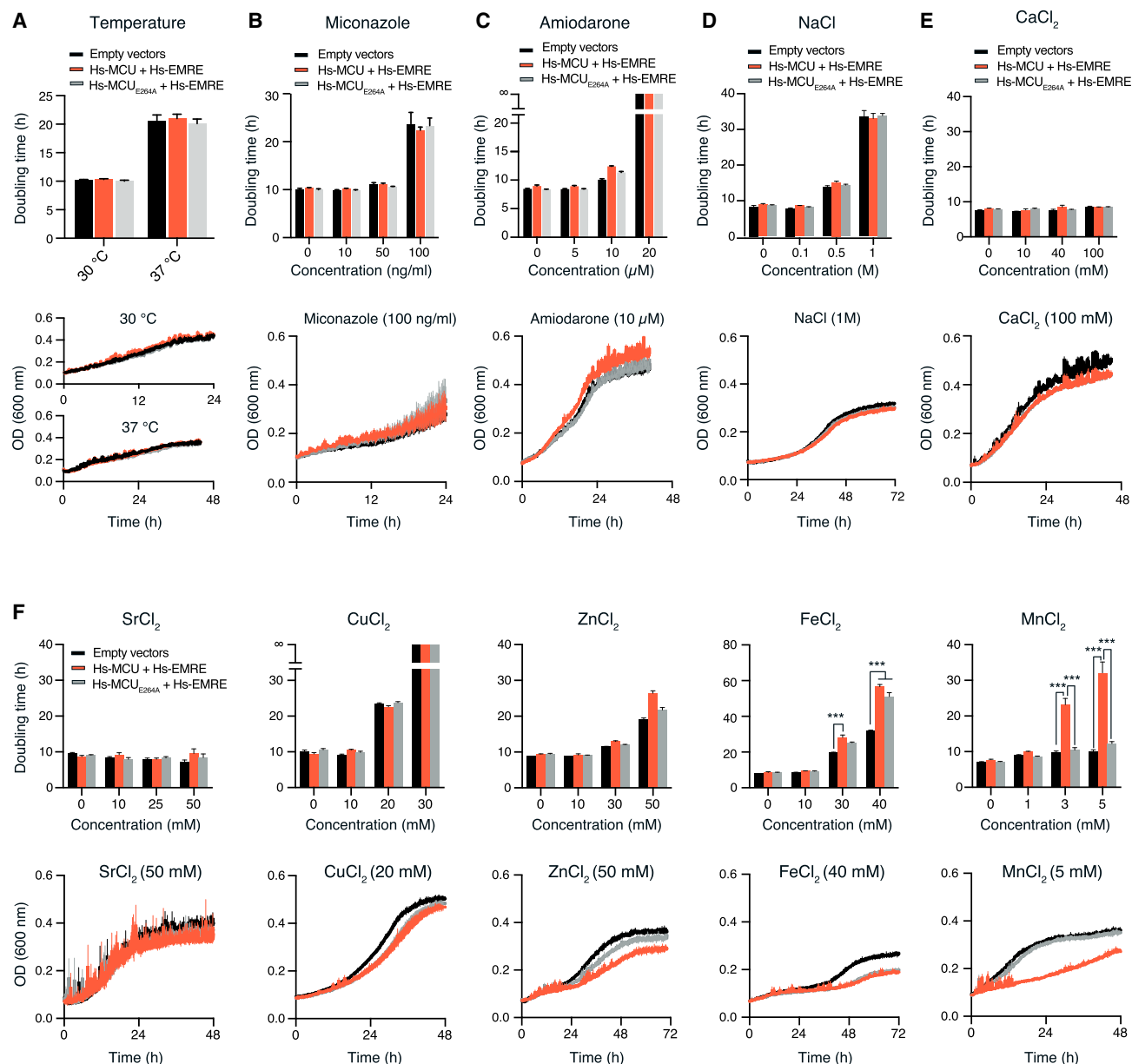


Figure 3. MCU Impairs Yeast Tolerance to Iron and Manganese Stresses

(A–F) Quantification of growth rate and average growth curve of yeast strains expressing empty vectors (p423 and p425) or Hs-EMRE with WT or mutated Hs-MCU at 30°C and 37°C (A), and at increasing concentrations of miconazole (B), amiodarone (C), NaCl (D), CaCl₂ (E), or heavy metals (F).

Data represent means ± SEMs; n = 4; ***p < 0.0001; one-way ANOVA with Tukey's multiple comparisons test.

See also Figure S3.

in HEK293 WT cells (Figure 4E), which is consistent with previous results in rat basophilic leukemia (RBL)-2H3 mast cells (Csordás and Hajnóczky, 2003).

Although the mechanism of mitochondrial Mn²⁺ toxicity is not entirely understood, it is believed that increased oxidative stress triggered by Mn²⁺ overload plays a role in the induction of cell death (Smith et al., 2017). Thus, we measured reactive oxygen species (ROS) production in MICU1-KO cells exposed to high extracellular Mn²⁺ concentrations. As shown in Figure 4F,

MICU1-KO cells exhibited a significant increase in intracellular ROS production upon 25 μM Mn²⁺ treatment, which is comparable to the level induced by treatment with H₂O₂. We then searched for strategies that could prevent Mn²⁺-induced toxicity. Fe²⁺ supplementation has already been proposed as a therapeutic strategy to treat or prevent neurological disorders due to a chronic increase of Mn²⁺ level in the blood (O'Neal and Zheng, 2015; Tai et al., 2016), as both cations compete for the same plasma membrane divalent metal transporter.

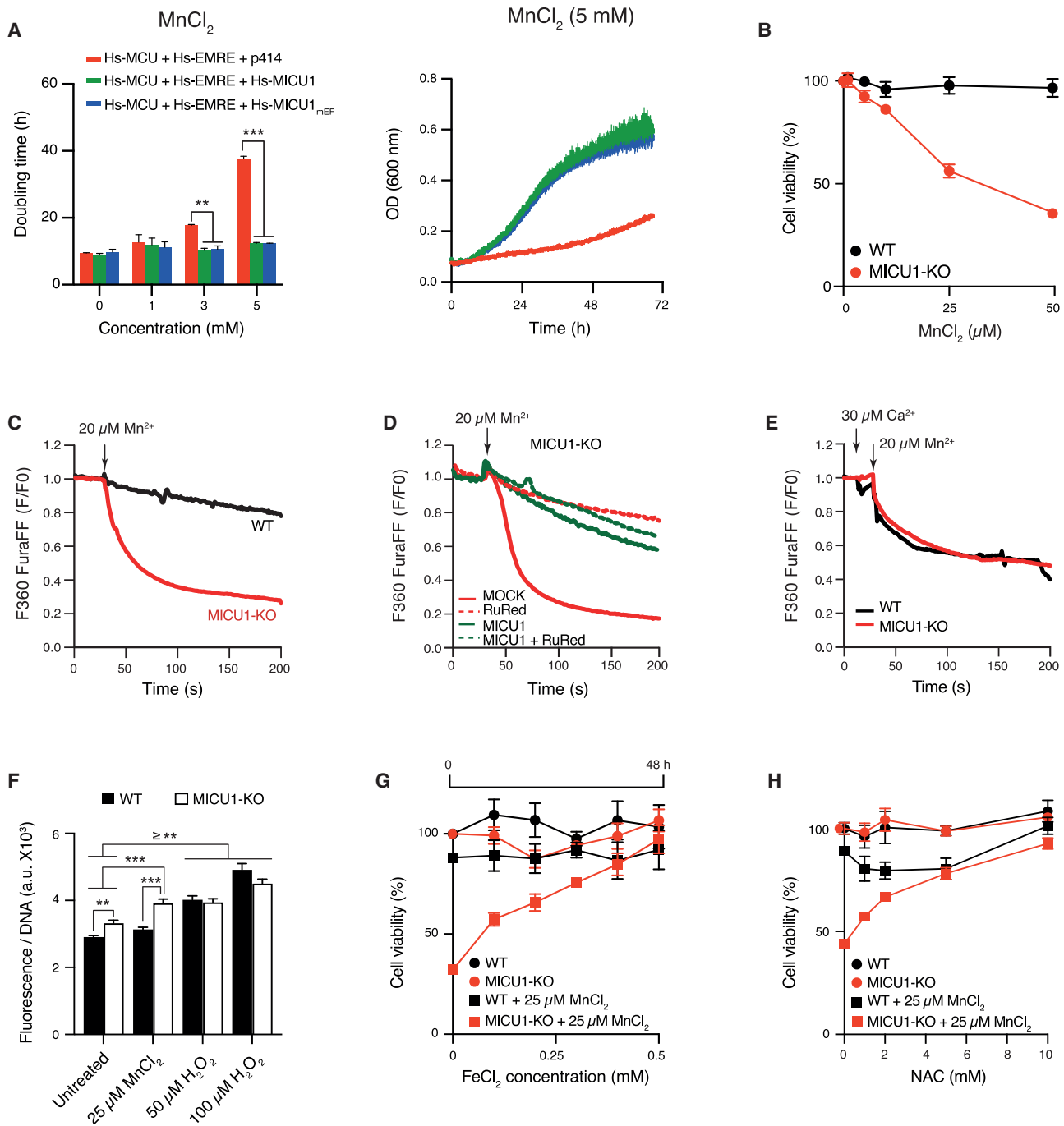


Figure 4. MICU1 Protects from Manganese-Induced Cell Death

(A) Quantification of growth rate and average growth curve of yeast strains treated with $MnCl_2$; $n = 4$; $**p < 0.01$; $***p < 0.001$; one-way ANOVA with Tukey's multiple comparisons test.

(B) Cell viability of wild-type (WT) and MICU1 knockout (MICU1-KO) HEK293 cells treated for 48 hr with $MnCl_2$; $n = 4$.

(C–E) Detection of mitochondrial Mn^{2+} uptake through the quench of compartmentalized Fura-FF in permeabilized single WT and MICU1-KO cells in the absence (C) or presence (D) of $CaCl_2$ and upon transfection with MICU1 or pcDNA in the absence and presence of 3 μM RuRed (E). Each trace represents the mean of 40–50 cells from one of three different cell cultures.

(F) Measurements of ROS by 5-(and-6)-chloromethyl-2', 7'-dichlorodihydrofluorescein diacetate (CM-H₂DCFDA) in WT and MICU1-KO cells treated for 48 hr with vehicle, $MnCl_2$, or H_2O_2 . Data represent means \pm SEMs; $n = 8$; $**p < 0.01$, $***p < 0.001$; one-way ANOVA with Tukey's multiple comparisons test.

(legend continued on next page)

Treatment of MICU1-KO cells with 25 μ M Mn^{2+} in the presence of 0.5 mM $FeCl_2$ (Figure 4G) consistently resulted in cell survival, whereas $FeCl_2$ pre-treatment for 24 hr was unable to confer protection to Mn^{2+} -induced stress (Figure S4E). We also tested the effect of several antioxidant compounds on Mn^{2+} -induced oxidative stress (Figure S4F) and found that NAC treatment was able to fully rescue Mn^{2+} -induced cell death in MICU1 KO cells (Figure 4H).

Our findings establish an essential role of MICU1 in regulating the permeability of the uniporter to Mn^{2+} , which is essential for preventing Mn^{2+} -induced cytotoxicity.

DISCUSSION

Our phylogenetic analysis (Figure 1) and a previous comparative genomics study (Bick et al., 2012) highlight a widespread co-occurrence of MCU and MICU1 across Metazoa, Plantae, and Protozoa, with the exception of Fungi. The presence of MCU homologs in several Ascomycota and Basidiomycota fungal clades devoid of any detectable MICU1 has led to the hypothesis that MCU could exist independently of a Ca^{2+} -sensing regulator. This is based on the assumption that fungal MCU homologs are able per se to mediate mt- Ca^{2+} uptake, with properties similar to the mammalian uniporter. Our results from functional complementation analyses in human shMCU cells (Figures 1 and S1) and from *in vivo* reconstitution in yeast (Figure S2) show that MCU orthologs from *N. crassa* and *A. fumigatus* are unable to drive mt- Ca^{2+} uptake, despite proper expression, mitochondrial localization, topology, and assembly. Those findings are consistent with previous observations from Carafoli and Lehninger (1971) and from Gonçalves et al. (2015) that mitochondria of *N. crassa* have a limited ability to accumulate Ca^{2+} , which occurs in the range of hours, are only partially inhibited by Ru360, and are not driven by membrane potential. Recently, it was reported that a putative MCU ortholog could mediate Ca^{2+} transport into *A. fumigatus* mitochondria (Song et al., 2016) and the structures of MCU orthologs from several Fungi (Baradaran et al., 2018; Fan et al., 2018; Nguyen et al., 2018), including *N. crassa* (Yoo et al., 2018), have been characterized. However, Af-MCU-KO elicited only a 50% decrease in Ca^{2+} uptake into *A. fumigatus* mitochondria. Moreover, there is currently no direct evidence that MCU orthologs from *Nassarius fischeri* (Nguyen et al., 2018), *Fusarium graminearum*, and *Metarhizium acridum* (Fan et al., 2018) mediate mt- Ca^{2+} uptake in those organisms, neither that other fungal MCUs can reconstitute mt- Ca^{2+} uptake when expressed in yeast or mammalian cells (Baradaran et al., 2018). These results would lead to conjecture that either the MCU-like sequences found in some Fungi encode for proteins that have lost Ca^{2+} uptake ability or they could be involved in Ca^{2+} transport through mechanisms that are different from the mammalian uniporter. Further experiments will be neces-

sary to uncover the function of those MCU-like proteins in Fungi and to resolve the paradox of species with MCU-like sequences without MICU1 orthologs.

To investigate the direct contribution of MICU1 to the uniporter activity, we used the yeast *S. cerevisiae* as a model system. Previous results, including ours, have shown that Hs-MCU and Hs-EMRE are sufficient to drive Ca^{2+} uptake *in vitro* into the matrix of isolated mitochondria (Arduino et al., 2017; Kovács-Bogdán et al., 2014; Yamamoto et al., 2016). Here, we show that they can reconstitute mt- Ca^{2+} entry *in vivo* in yeast in response to a physiological increase in cyt- Ca^{2+} (Figure 2). Furthermore, similar to mammalian cells, the expression of Hs-MICU1 in MCU-reconstituted yeast cells exerts a synergistic effect on mt- Ca^{2+} uptake, which is dependent on its Ca^{2+} -sensing domains. Therefore, we searched for biological conditions whereby a positive MCU-MICU1 genetic interaction would provide a selective fitness advantage over a yeast strain reconstituted with MCU without its regulator (Figure 3). We found that MCU-reconstituted yeast cells are more susceptible to the increase of Mn^{2+} levels in the extracellular medium, which is likely due to its permeation across the uniporter (Cao et al., 2017; Csordás and Hajnóczky, 2003; Mela and Chance, 1968; Romslo and Flatmark, 1973; Saris, 2012; Vinogradov and Scarpa, 1973). Co-expression with MICU1 conferred full protection against uniporter-dependent Mn^{2+} toxicity (Figure 4), regardless of functional EF-hand domains. All of these findings were recapitulated in HEK293 cells, where the KO of MICU1 hypersensitized cells to Mn^{2+} -dependent cell death. Thus, unlike Ca^{2+} , the binding of Mn^{2+} to EF-hands (Senguen and Grabarek, 2012; Shirran and Barran, 2009) would be insufficient to trigger in MICU1 the conformational change needed for the opening of the MCU channel, a hypothesis that was recently validated by Kamer et al. (2018).

Our findings are of great relevance for patients with MICU1 loss-of-function mutations (Lewis-Smith et al., 2016; Logan et al., 2014; Musa et al., 2018). So far, the disease phenotypes observed in human patients and recapitulated in MICU1-KO mice (Antony et al., 2016; Liu et al., 2016) were attributed to high basal mt- Ca^{2+} levels, possibly due to the loss of MICU1-dependent gatekeeping of the uniporter. In light of our results, those could also result from Mn^{2+} accumulation in mitochondria, which would have an additive effect: it would increase mt- Ca^{2+} levels by inhibiting both Na^{+} -dependent and Na^{+} -independent mt- Ca^{2+} efflux routes (Gavin et al., 1990), and it would increase oxidative stress and trigger cell death (Smith et al., 2017). Accordingly, antioxidant treatment with NAC fully prevented Mn^{2+} -induced cell death in MICU1-KO cells. This result is consistent with previous findings showing that treatment of cells, mice, rats, and nonhuman primates with NAC during exposure to high doses of $MnCl_2$ is protective against Mn^{2+} cytotoxicity (Smith et al., 2017). Finally, our findings also suggest MICU1 as a possible target for neurological diseases related to chronic

(G) Cell viability of WT and MICU1-KO cells treated for 48 hr with $MnCl_2$ in the presence of $FeCl_2$ ($n = 3$).

(H) Cell viability of WT and MICU1-KO cells treated for 48 hr with $MnCl_2$ in the presence of *N*-acetyl-L-cysteine (NAC) ($n = 3$).

All data represent means \pm SEMs and are reported as the percentage of viable cells in untreated samples.

See also Figure S4.

exposure to environmental sources of Mn^{2+} such as, for example, Mn^{2+} -rich foods, Mn^{2+} aerosols and dusts in mines and smelters, and air pollution from the combustion of gasoline containing methylcyclopentadienyl Mn^{2+} tricarbonyl (O'Neal and Zheng, 2015).

In summary, our study demonstrates the power of combining comparative genomics analyses with the use of yeast as a model system for dissecting the functional and mechanistic role of each component of the mammalian uniporter. The reconstitution of an MICU1-regulated uniporter in yeast offers an incomparable advantage over similar investigations of MICU1 and MCU interdependence in mammalian cells, in which MICU1 KO or knock-down also has confounding effects on the expression of other uniporter subunits, such as MICU2 and MICU3 (Patron et al., 2014, 2018; Plovanich et al., 2013). Importantly, we unraveled a key role of MICU1 in regulating the selectivity of the uniporter towards Ca^{2+} ions, with important implications for patients with MICU1 deficiency.

STAR★METHODS

Detailed methods are provided in the online version of this paper and include the following:

- KEY RESOURCES TABLE
- CONTACT FOR REAGENT AND RESOURCE SHARING
- EXPERIMENTAL MODEL AND SUBJECT DETAILS
 - Cell lines
 - Yeast Strains
- METHOD DETAILS
 - Phylogenetic Profiling of MICU1 and MCU
 - Protein Domains
 - Plasmids and Reagents
 - Isolation of Crude Mitochondria from HeLa Cells
 - Topology Analysis of Mitochondrial Proteins
 - Blue Native – PAGE Analysis
 - Measurements of Mitochondrial Calcium Uptake in Intact HeLa Cells
 - Measurements of Mitochondrial Calcium Uptake in Digitonin-Permeabilized HeLa Cells
 - Subcellular Fractionation of Yeast Cells
 - Measurements of Calcium Transients in Intact Yeast Cells
 - Measurements of Mitochondrial Calcium Uptake in Isolated Yeast Mitochondria
 - Yeast Growth Measurement
 - Cell Viability Analysis
 - Mitochondrial Mn^{2+} Transport Measurement in Human Cells
 - ROS Measurement
- QUANTIFICATION AND STATISTICAL ANALYSIS
 - Quantification of Calcium Transients
 - Data Analysis

SUPPLEMENTAL INFORMATION

Supplemental Information includes four figures and can be found with this article online at <https://doi.org/10.1016/j.celrep.2018.10.037>.

ACKNOWLEDGMENTS

We acknowledge support from the German Research Foundation (DFG) under the Emmy Noether Programme (PE 2053/1-1 to F.P. and J.W.), the Munich Center for Systems Neurology (SyNergy EXC 1010 to F.P.), the Juniorverbund in der Systemmedizin “mitOmics” (FKZ 01ZX1405B to V.G. and A.L.), The Bert L & N Kuggie Vallee Foundation (to F.P. and D.M.A.), the DFG (MO1944/1-2 to D.M.), the Spanish Ministry of Economy, Industry, and Competitiveness (MEIC; BFU2015-67107), the European Union's Horizon 2020 research and innovation program under grant agreement ERC-2016-724173 (to T.G. and A.A.P.), and the NIH (RO1 GM102724 to G.H.).

AUTHOR CONTRIBUTIONS

Conceptualization, F.P.; Methodology, F.P., V.G., J.W., K.-T.H., D.M., T.G., and G.H.; Validation, V.G., J.W., K.-T.H., U.T., and A.L.; Formal Analysis, V.G., J.W., K.-T.H., A.A.P., D.M.A., and Y.C.; Investigation, V.G., J.W., and K.-T.H.; Resources, F.P., D.M., G.H., and T.G.; Writing - Original Draft, F.P., V.G., and J.W.; Writing - Review & Editing, F.P., T.G., D.M., G.H., and D.M.A.; Visualization, F.P., V.G., J.W., K.-T.H., and G.H.; Supervision, F.P., G.H. and T.G.; Funding Acquisition, F.P., D.M., T.G. and G.H.

DECLARATION OF INTERESTS

The authors declare no competing interests.

Received: June 30, 2018

Revised: August 9, 2018

Accepted: October 8, 2018

Published: November 6, 2018

REFERENCES

- Antony, A.N., Paillard, M., Moffat, C., Juskeviciute, E., Correnti, J., Bolon, B., Rubin, E., Csordás, G., Seifert, E.L., Hoek, J.B., and Hajnóczky, G. (2016). MICU1 regulation of mitochondrial Ca^{2+} uptake dictates survival and tissue regeneration. *Nat. Commun.* 7, 10955.
- Arduino, D.M., Wettmarshausen, J., Vais, H., Navas-Navarro, P., Cheng, Y., Leimpek, A., Ma, Z., Delrio-Lorenzo, A., Giordano, A., Garcia-Perez, C., et al. (2017). Systematic identification of MCU modulators by orthogonal inter-species chemical screening. *Mol. Cell* 67, 711–723.e7.
- Baradaran, R., Wang, C., Siliciano, A.F., and Long, S.B. (2018). Cryo-EM structures of fungal and metazoan mitochondrial calcium uniporters. *Nature* 559, 580–584.
- Baughman, J.M., Perocchi, F., Girgis, H.S., Plovanich, M., Belcher-Timme, C.A., Sancak, Y., Bao, X.R., Strittmatter, L., Goldberger, O., Bogorad, R.L., et al. (2011). Integrative genomics identifies MCU as an essential component of the mitochondrial calcium uniporter. *Nature* 476, 341–345.
- Bick, A.G., Calvo, S.E., and Mootha, V.K. (2012). Evolutionary diversity of the mitochondrial calcium uniporter. *Science* 336, 886.
- Bonora, M., Giorgi, C., Bononi, A., Marchi, S., Patergnani, S., Rimessi, A., Rizzuto, R., and Pinton, P. (2013). Subcellular calcium measurements in mammalian cells using jellyfish photoprotein aequorin-based probes. *Nat. Protoc.* 8, 2105–2118.
- Cao, C., Wang, S., Cui, T., Su, X.-C., and Chou, J.J. (2017). Ion and inhibitor binding of the double-ring ion selectivity filter of the mitochondrial calcium uniporter. *Proc. Natl. Acad. Sci. USA* 114, E2846–E2851.
- Carafoli, E., and Lehninger, A.L. (1971). A survey of the interaction of calcium ions with mitochondria from different tissues and species. *Biochem. J.* 122, 681–690.
- Chaudhuri, D., Sancak, Y., Mootha, V.K., and Clapham, D.E. (2013). MCU encodes the pore conducting mitochondrial calcium currents. *eLife* 2, e00704.
- Cheng, Y., and Perocchi, F. (2015). ProtPhylo: identification of protein-phenotype and protein-protein functional associations via phylogenetic profiling. *Nucleic Acids Res.* 43, W160–W168.

- Csordás, G., and Hajnóczky, G. (2003). Plasticity of mitochondrial calcium signaling. *J. Biol. Chem.* 278, 42273–42282.
- Csordás, G., Golenár, T., Seifert, E.L., Kamer, K.J., Sancak, Y., Perocchi, F., Moffat, C., Weaver, D., de la Fuente Perez, S., Bogorad, R., et al. (2013). MICU1 controls both the threshold and cooperative activation of the mitochondrial Ca^{2+} uniporter. *Cell Metab.* 17, 976–987.
- Cyert, M.S. (2003). Calcineurin signaling in *Saccharomyces cerevisiae*: how yeast go crazy in response to stress. *Biochem. Biophys. Res. Commun.* 311, 1143–1150.
- De Stefani, D., Raffaello, A., Teardo, E., Szabò, I., and Rizzuto, R. (2011). A forty-kilodalton protein of the inner membrane is the mitochondrial calcium uniporter. *Nature* 476, 336–340.
- De Stefani, D., Rizzuto, R., and Pozzan, T. (2016). Enjoy the trip: calcium in mitochondria back and forth. *Annu. Rev. Biochem.* 85, 161–192.
- Deluca, H.F., and Engstrom, G.W. (1961). Calcium uptake by rat kidney mitochondria. *Proc. Natl. Acad. Sci. USA* 47, 1744–1750.
- Fan, C., Fan, M., Orlando, B.J., Fastman, N.M., Zhang, J., Xu, Y., Chambers, M.G., Xu, X., Perry, K., Liao, M., and Feng, L. (2018). X-ray and cryo-EM structures of the mitochondrial calcium uniporter. *Nature* 559, 575–579.
- Gavin, C.E., Gunter, K.K., and Gunter, T.E. (1990). Manganese and calcium efflux kinetics in brain mitochondria. Relevance to manganese toxicity. *Biochem. J.* 266, 329–334.
- Gonçalves, A.P., Cordeiro, J.M., Monteiro, J., Lucchi, C., Correia-de-Sá, P., and Videira, A. (2015). Involvement of mitochondrial proteins in calcium signaling and cell death induced by staurosporine in *Neurospora crassa*. *Biochim. Biophys. Acta* 1847, 1064–1074.
- Groppi, S., Belotti, F., Brandão, R.L., Martegani, E., and Tisi, R. (2011). Glucose-induced calcium influx in budding yeast involves a novel calcium transport system and can activate calcineurin. *Cell Calcium* 49, 376–386.
- Kamer, K.J., and Mootha, V.K. (2014). MICU1 and MICU2 play non redundant roles in the regulation of the mitochondrial calcium uniporter. *EMBO Rep* 15, 299–307.
- Kamer, K.J., Grabarek, Z., and Mootha, V.K. (2017). High-affinity cooperative Ca^{2+} binding by MICU1-MICU2 serves as an on-off switch for the uniporter. *EMBO Rep.* 18, 1397–1411.
- Kamer, K.J., Sancak, Y., Fomina, Y., Meisel, J.D., Chaudhuri, D., Grabarek, Z., and Mootha, V.K. (2018). MICU1 imparts the mitochondrial uniporter with the ability to discriminate between Ca^{2+} and Mn^{2+} . *Proc. Natl. Acad. Sci. USA* 115, E7960–E7969.
- Kirichok, Y., Krapivinsky, G., and Clapham, D.E. (2004). The mitochondrial calcium uniporter is a highly selective ion channel. *Nature* 427, 360–364.
- Kovács-Bogdán, E., Sancak, Y., Kamer, K.J., Plovanich, M., Jambhekar, A., Huber, R.J., Myre, M.A., Blower, M.D., and Mootha, V.K. (2014). Reconstitution of the mitochondrial calcium uniporter in yeast. *Proc. Natl. Acad. Sci. USA* 111, 8985–8990.
- Lewis-Smith, D., Kamer, K.J., Griffin, H., Childs, A.M., Pysden, K., Titov, D., Duff, J., Pyle, A., Taylor, R.W., Yu-Wai-Man, P., et al. (2016). Homozygous deletion in MICU1 presenting with fatigue and lethargy in childhood. *Neurol. Genet.* 2, e59.
- Liu, J.C., Liu, J., Holmström, K.M., Menazza, S., Parks, R.J., Fergusson, M.M., Yu, Z.X., Springer, D.A., Halsey, C., Liu, C., et al. (2016). MICU1 serves as a molecular gatekeeper to prevent in vivo mitochondrial calcium overload. *Cell Rep.* 16, 1561–1573.
- Logan, C.V., Szabadkai, G., Sharpe, J.A., Parry, D.A., Torelli, S., Childs, A.M., Kriek, M., Phadke, R., Johnson, C.A., Roberts, N.Y., et al.; UK10K Consortium (2014). Loss-of-function mutations in MICU1 cause a brain and muscle disorder linked to primary alterations in mitochondrial calcium signaling. *Nat. Genet.* 46, 188–193.
- Mallilankaraman, K., Doonan, P., Cárdenas, C., Chandramoorthy, H.C., Müller, M., Miller, R., Hoffman, N.E., Gandhirajan, R.K., Molgó, J., Birnbaum, M.J., et al. (2012). MICU1 is an essential gatekeeper for MCU-mediated mitochondrial Ca^{2+} uptake that regulates cell survival. *Cell* 151, 630–644.
- Mela, L., and Chance, B. (1968). Spectrophotometric measurements of the kinetics of Ca^{2+} and Mn^{2+} accumulation in mitochondria. *Biochemistry* 7, 4059–4063.
- Mumberg, D., Müller, R., and Funk, M. (1995). Yeast vectors for the controlled expression of heterologous proteins in different genetic backgrounds. *Gene* 156, 119–122.
- Murgia, M., and Rizzuto, R. (2015). Molecular diversity and pleiotropic role of the mitochondrial calcium uniporter. *Cell Calcium* 58, 11–17.
- Musa, S., Eyaïd, W., Kamer, K., Ali, R., Al-Mureikhi, M., Shahbeck, N., Al-Mesaifri, F., Makhseed, N., Mohamed, Z., AlShehhi, W.A., et al. (2018). A Middle Eastern founder mutation expands the genotypic and phenotypic spectrum of mitochondrial MICU1 deficiency: a report of 13 patients. *JIMD Rep.* Published online May 3, 2018. https://doi.org/10.1007/8904_2018_107.
- Nguyen, N.X., Armache, J.P., Lee, C., Yang, Y., Zeng, W., Mootha, V.K., Cheng, Y., Bai, X.C., and Jiang, Y. (2018). Cryo-EM structure of a fungal mitochondrial calcium uniporter. *Nature* 559, 570–574.
- O’Neal, S.L., and Zheng, W. (2015). Manganese toxicity upon overexposure: a decade in review. *Curr. Environ. Health Rep.* 2, 315–328.
- Oxenoid, K., Dong, Y., Cao, C., Cui, T., Sancak, Y., Markhard, A.L., Grabarek, Z., Kong, L., Liu, Z., Ouyang, B., et al. (2016). Architecture of the mitochondrial calcium uniporter. *Nature* 533, 269–273.
- Paillard, M., Csordás, G., Szanda, G., Golenár, T., Debattisti, V., Bartok, A., Wang, N., Moffat, C., Seifert, E.L., Spät, A., and Hajnóczky, G. (2017). Tissue-specific mitochondrial decoding of cytoplasmic Ca^{2+} signals is controlled by the stoichiometry of MICU1/2 and MCU. *Cell Rep.* 18, 2291–2300.
- Patron, M., Checchetto, V., Raffaello, A., Teardo, E., Vecellio Reane, D., Mantoan, M., Granatiero, V., Szabò, I., De Stefani, D., and Rizzuto, R. (2014). MICU1 and MICU2 finely tune the mitochondrial Ca^{2+} uniporter by exerting opposite effects on MCU activity. *Mol. Cell* 53, 726–737.
- Patron, M., Granatiero, V., Espino, J., Rizzuto, R., and De Stefani, D. (2018). MICU3 is a tissue-specific enhancer of mitochondrial calcium uptake. *Cell Death Differ.* Published online May 3, 2018. <https://doi.org/10.1038/s41418-018-0113-8>.
- Perocchi, F., Gohil, V.M., Girgis, H.S., Bao, X.R., McCombs, J.E., Palmer, A.E., and Mootha, V.K. (2010). MICU1 encodes a mitochondrial EF hand protein required for Ca^{2+} uptake. *Nature* 467, 291–296.
- Philpott, C.C. (2012). Coming into view: eukaryotic iron chaperones and intracellular iron delivery. *J. Biol. Chem.* 287, 13518–13523.
- Plovanich, M., Bogorad, R.L., Sancak, Y., Kamer, K.J., Strittmatter, L., Li, A.A., Girgis, H.S., Kuchimanchi, S., De Groot, J., Speciner, L., et al. (2013). MICU2, a paralog of MICU1, resides within the mitochondrial uniporter complex to regulate calcium handling. *PLoS One* 8, e55785.
- Romslo, I., and Flatmark, T. (1973). Energy-dependent accumulation of iron by isolated rat liver mitochondria. II. Relationship to the active transport of Ca^{2+} . *Biochim. Biophys. Acta* 325, 38–46.
- Sancak, Y., Markhard, A.L., Kitami, T., Kovács-Bogdán, E., Kamer, K.J., Udeshi, N.D., Carr, S.A., Chaudhuri, D., Clapham, D.E., Li, A.A., et al. (2013). EMRE is an essential component of the mitochondrial calcium uniporter complex. *Science* 342, 1379–1382.
- Saris, N.-E. (2012). Mitochondrial uptake of Ca^{2+} and other bivalent cations. *Biochem. Anal. Biochem.* 1, 112.
- Schreiner, B., Westerburg, H., Forne, I., Imhof, A., Neupert, W., and Mokranjac, D. (2012). Role of the AAA protease Yme1 in folding of proteins in the intermembrane space of mitochondria. *Mol. Biol. Cell* 23, 4335–4346.
- Senguen, F.T., and Grabarek, Z. (2012). X-ray structures of magnesium and manganese complexes with the N-terminal domain of calmodulin: insights into the mechanism and specificity of metal ion binding to an EF-hand. *Biochemistry* 51, 6182–6194.
- Shirran, S.L., and Barran, P.E. (2009). The use of ESI-MS to probe the binding of divalent cations to calmodulin. *J. Am. Soc. Mass Spectrom.* 20, 1159–1171.
- Sikorski, R.S., and Hieter, P. (1989). A system of shuttle vectors and yeast host strains designed for efficient manipulation of DNA in *Saccharomyces cerevisiae*. *Genetics* 122, 19–27.

- Smith, M.R., Fernandes, J., Go, Y.M., and Jones, D.P. (2017). Redox dynamics of manganese as a mitochondrial life-death switch. *Biochem. Biophys. Res. Commun.* **482**, 388–398.
- Song, J., Liu, X., Zhai, P., Huang, J., and Lu, L. (2016). A putative mitochondrial calcium uniporter in *A. fumigatus* contributes to mitochondrial Ca^{2+} homeostasis and stress responses. *Fungal Genet. Biol.* **94**, 15–22.
- Tai, Y.K., Chew, K.C., Tan, B.W., Lim, K.L., and Soong, T.W. (2016). Iron mitigates DMT1-mediated manganese cytotoxicity via the ASK1-JNK signaling axis: implications of iron supplementation for manganese toxicity. *Sci. Rep.* **6**, 21113.
- Vasington, F.D., and Murphy, J.V. (1962). Ca ion uptake by rat kidney mitochondria and its dependence on respiration and phosphorylation. *J. Biol. Chem.* **237**, 2670–2677.
- Vecellio Reane, D., Vallese, F., Checchetto, V., Acquasaliente, L., Butera, G., De Filippis, V., Szabó, I., Zanotti, G., Rizzuto, R., and Raffaello, A. (2016). A MICU1 splice variant confers high sensitivity to the mitochondrial Ca^{2+} uptake machinery of skeletal muscle. *Mol. Cell* **64**, 760–773.
- Vinogradov, A., and Scarpa, A. (1973). The initial velocities of calcium uptake by rat liver mitochondria. *J. Biol. Chem.* **248**, 5527–5531.
- Wettmarshausen, J., and Perocchi, F. (2017). Isolation of functional mitochondria from cultured cells and mouse tissues. *Methods Mol. Biol.* **1567**, 15–32.
- Wysocki, R., and Tamás, M.J. (2010). How *Saccharomyces cerevisiae* copes with toxic metals and metalloids. *FEMS Microbiol. Rev.* **34**, 925–951.
- Yamamoto, T., Yamagoshi, R., Harada, K., Kawano, M., Minami, N., Ido, Y., Kuwahara, K., Fujita, A., Ozono, M., Watanabe, A., et al. (2016). Analysis of the structure and function of EMRE in a yeast expression system. *Biochim. Biophys. Acta* **1857**, 831–839.
- Yoo, J., Wu, M., Yin, Y., Herzik, M.A., Jr., Lander, G.C., and Lee, S.Y. (2018). Cryo-EM structure of a mitochondrial calcium uniporter. *Science* **361**, 506–511.

STAR★METHODS

KEY RESOURCES TABLE

REAGENT or RESOURCE	SOURCE	IDENTIFIER
Antibodies		
Rabbit polyclonal anti-MCU	Sigma-Aldrich	Cat#HPA016480; Lot#C0114358; RRID: AB_2071893
Rabbit polyclonal anti-EMRE - C22orf32 (clone C-12)	Santa Cruz Biotechnology	Cat#sc-86337; Lot#K0215; RRID: AB_2250685
Mouse monoclonal anti-Aequorin (clone 6E3.2)	Merck/Millipore	Cat#MAB4405; RRID: AB_94900; RRID: AB_94900
Rabbit polyclonal anti-MICU1	Sigma-Aldrich	Cat#HPA037480; Lot#N107141; RRID: AB_10696934
Anti-Sc-Yme1 produced in rabbit	Schreiner et al., 2012	N/A
Mouse monoclonal anti-TIM23	BD Bioscience	Cat#611222; Lot#3067849; RRID: AB_398754
Rabbit polyclonal anti-MICU1	Atlas Antibody	Cat#HPA037479; Lot#R34024; RRID: AB_2675495
Mouse monoclonal anti-Cyclophilin D [E11AE12BD4]	Abcam	Cat#ab110324; Lot#GR134866-15; RRID: AB_10864110
Mouse monoclonal anti-ATP5A	Invitrogen	Cat#43-9800; Lot#TA2516391; RRID: AB_2533548
Mouse monoclonal anti-V5	Life Technologies	Cat#R96025; Lot#1792242; RRID: AB_2556564
Mouse monoclonal anti-HSP60	R&D System	Cat#MAB1800; Lot#UNG02; RRID: AB_11212084
Mouse monoclonal anti-TOMM20	Abcam	Cat#Ab56783; Lot#GR3188177-1; RRID: AB_945896
Mouse monoclonal anti-β-Actin	Sigma-Aldrich	Cat#A2228; Lot#085M4754V; RRID: AB_476697
Chemicals, Peptides, and Recombinant Proteins		
Amiodarone hydrochloride	Sigma-Aldrich	Cat#A8423; CAS: 19774-82-4
Antioxidant Supplement (1000 ×)	Sigma-Aldrich	Cat#A1345
Calcium chloride dihydrate	Merck/Millipore	Cat#208290; CAS: 10035-04-8
Calcium Green-5N, Hexapotassium Salt, cell impermeant	Thermo Fisher Scientific	Cat#C3737; CAS: 153130-66-6
CM-H2DCFDA (General Oxidative Stress Indicator)	Thermo Fisher Scientific	Cat#C6827
Coelenterazine, native	Abcam	Cat#ab145165; CAS: 55779-48-1
Copper(II) chloride	Sigma-Aldrich	Cat#751944; CAS: 7447-39-4
Digitonin	Sigma-Aldrich	Cat#D141; CAS: 11024-24-1
Hydrogen peroxide 30% (w/w) solution	Sigma-Aldrich	Cat#H1009; CAS: 7722-84-1
Idebenone	Santhera Pharmaceuticals	CAS: 58186-27-9; Lot#99826G001B
Iron(II) chloride tetrahydrate	Merck/Millipore	Cat#1038610250; CAS: 13478-10-9
L-Glutathione reduced	Sigma-Aldrich	Cat#G6013; CAS: 70-18-8
Mn ²⁺ (II) chloride tetrahydrate	Merck/Millipore	Cat#1059271000; CAS: 13446-34-9
Miconazole nitrate salt	Sigma-Aldrich	Cat#M3512; CAS: 22832-87-7
N-Acetyl-L-cysteine	Sigma-Aldrich	Cat#A9165; CAS: 616-91-1
Native Mark Unstained Protein Standard-5	Life Technologies	Cat#LC0725
Native PAGE 20x Cathode Buffer	Life Technologies	Cat#BN2002
Native PAGE Novex 3-12%, Bis-Tris Protein, 10well	Life Technologies	Cat#BN1001
Native PAGE Running Buffer (20x)	Life Technologies	Cat#BN2001
NativePAGE 5% G-250 Sample Additive	Life Technologies	Cat#BN2004
NativePAGE Sample Buffer (4x)	Life Technologies	Cat#BN2003
Ru360	Calbiochem	Cat#557440
Strontium chloride hexahydrate	Merck/Millipore	Cat#1078650250; CAS: 10025-70-4
Thiazolyl Blue Tetrazolium Bromide (MTT)	Sigma-Aldrich	Cat#M5655; CAS: 298-93-1
Zinc chloride	Sigma-Aldrich	Cat#Z0152; CAS: 7646-85-7
Zymolyase 20T from <i>Arthrobacter luteus</i>	Amsbio	Cat#120491-1
6-Hydroxy-2,5,7,8-tetramethylchromane-2-carboxylic acid (Trolox)	Sigma-Aldrich	Cat#238813; CAS: 53188-07-1

(Continued on next page)

Continued

REAGENT or RESOURCE	SOURCE	IDENTIFIER
Ruthenium Red	Sigma	R2751
Fura-2 low affinity (AM)	Teflabs	0-136
Thapsigargin	Enzo Life Sciences	BML-PE180-0005
CGP-37157	Enzo Life Sciences	BML-CM119-0005
Lipofectamine 3000	Life Technologies	L3000008
Critical Commercial Assays		
Pierce BCA Protein Assay Kit	Thermo Fisher Scientific	Cat#23227
CyQUANT Cell Proliferation Assay Kit	Thermo Fisher Scientific	Cat#C7026
Experimental Models: Cell Lines		
HEK293T cells	ATCC	CRL-11268
MICU1-knockout HEK293T cells (MICU1-KO)	Vamsi K. Mootha Laboratory	Kamer and Mootha (2014); Kamer et al. (2017)
MICU1-KO HEK293T cells rescued with WT MICU1	This paper	N/A
MICU1-knockout HEK293T cells rescued with EF-hands mutant MICU1	This paper	N/A
pLKO HeLa cells stably expressing WT mt-AEQ	This paper	N/A
shMCU HeLa cells stably expressing WT mt-AEQ	This paper	N/A
shMCU HeLa cells stably expressing WT mt-AEQ + HsMCU	This paper	N/A
shMCU HeLa cells stably expressing WT mt-AEQ + HsMTS ^A MCU	This paper	N/A
shMCU HeLa cells stably expressing WT mt-AEQ + AfMCU	This paper	N/A
shMCU HeLa cells stably expressing WT mt-AEQ + NcMCU	This paper	N/A
shMCU HeLa cells stably expressing WT mt-AEQ + HsMTS ^N NcMCU	This paper	N/A
Experimental Models: Organisms/Strains		
<i>S. cerevisiae</i> : Strain background: YPH499 expressing HsMCU + HsEMRE + WT mt-AEQ	Arduino et al., 2017	N/A
<i>S. cerevisiae</i> : Strain background: YPH499 expressing HsMCU _{E264A} + HsEMRE + WT mt-AEQ	This paper	N/A
<i>S. cerevisiae</i> : Strain background: YPH499 expressing HsMCU _{D261A} + HsEMRE + WT mt-AEQ	This paper	N/A
<i>S. cerevisiae</i> : Strain background: YPH499 expressing HsMCU + WT mt-AEQ	This paper	N/A
<i>S. cerevisiae</i> : Strain background: YPH499 expressing DdMCU + WT mt-AEQ	This paper	N/A
<i>S. cerevisiae</i> : Strain background: YPH499 expressing AfMCU + WT mt-AEQ	This paper	N/A
<i>S. cerevisiae</i> : Strain background: YPH499 expressing NcMCU + WT mt-AEQ	This paper	N/A
<i>S. cerevisiae</i> : Strain background: YPH499 expressing HsEMRE + WT mt-AEQ	This paper	N/A
<i>S. cerevisiae</i> : Strain background: YPH499 expressing HsMCU + HsEMRE + HsMICU1 + WT mt-AEQ	This paper	N/A
<i>S. cerevisiae</i> : Strain background: YPH499 expressing HsMCU + HsEMRE + HsMICU1 _{mEF} + WT mt-AEQ	This paper	N/A
<i>S. cerevisiae</i> : Strain background: YPH499 + p414GPD expressing HsMCU + HsEMRE + WT mt-AEQ	This paper	N/A

(Continued on next page)

Continued

REAGENT or RESOURCE	SOURCE	IDENTIFIER
<i>S. cerevisiae</i> : Strain background: YPH499 +p423GPD + p425GPD expressing WT mt-AEQ	This paper	N/A
<i>S. cerevisiae</i> : Strain background: YPH499 expressing WT mt-AEQ	This paper	N/A
Oligonucleotides		
MCU shRNA targeting sequence: 5'-GCAAGGAGTTTCTTTCTTT-3'	RNAi Consortium, Broad Institute	TRCN0000133861
Recombinant DNA		
p316GPD (plasmid)	Arduino et al., 2017	N/A
p423GPD (plasmid)	Mumberg et al., 1995	N/A
p425GPD (plasmid)	Mumberg et al., 1995	N/A
p414GPD (plasmid)	Mumberg et al., 1995	N/A
MCU full-length with V5-tag (pLX304)	Arduino et al., 2017	N/A
AfMCU full-length with V5-tag (pLX304)	This paper	N/A
^{HsMTS} AfMCU full-length with V5-tag (pLX304)	This paper	N/A
^{HsMTS} NcMCU full-length with V5-tag (pLX304)	This paper	N/A
NcMCU full-length with V5-tag (pLX304)	This paper	N/A
DdMCU full-length with V5-tag (pLX304)	This paper	N/A
MCU full-length with V5-tag (p423GPD)	Arduino et al., 2017	N/A
AfMCU full-length with V5-tag (p423GPD)	This paper	N/A
NcMCU full-length with V5-tag (p423GPD)	This paper	N/A
DdMCU full-length with V5-tag (p423GPD)	This paper	N/A
pcDNA-dest40-MICU1-HA	(Kamer et al., 2017)	N/A
Software and Algorithms		
GraphPad Prism 5.0 or newer	GraphPad Software	N/A
MATLAB R2014b	MathWorks	N/A
ProtPhylo	Cheng and Perocchi, 2015	www.protphylo.org
Phylogenetic tree generator	N/A	https://phylo.t.biobyte.de/
iTOL	N/A	https://itol.embl.de/
Canvas X	N/A	N/A
SigmaPlot 12.5	N/A	N/A

CONTACT FOR REAGENT AND RESOURCE SHARING

Further information and requests for resources and reagents should be directed to and will be fulfilled by the Lead Contact, Fabiana Perocchi (fabiana.perocchi@helmholtz-muenchen.de).

EXPERIMENTAL MODEL AND SUBJECT DETAILS

Cell lines

All mammalian cells were grown in high-glucose Dulbecco's modified Eagle's medium (DMEM) (Sigma-Aldrich; D6429) supplemented with 10% FBS (Sigma-Aldrich, F7524) at 37°C and 5% CO₂. HeLa cells stably expressing a WT mitochondrial matrix-targeted GFP-aequorin (mt-AEQ HeLa) were generated as previously described ([Arduino et al., 2017](#)) and selected with 100 µg/ml geneticin (Thermo Fisher Scientific, 10131027). Mt-AEQ HeLa cells stably expressing either an empty vector (pLKO; Addgene, 8453) or a pLKO vector expressing a shRNA targeting Hs-MCU (shMCU; Sigma Aldrich, TRCN0000133861) were generated as previously described ([Baughman et al., 2011](#)) and selected with 2 µg/mL puromycin (Life Technologies, A11138) and 100 µg/ml geneticin. MCU-knockdown mtAEQ HeLa cells stably expressing Hs-MCU, Nc-MCU, Af-MCU, ^{HsMTS}Af-MCU and ^{HsMTS}Nc-MCU from the pLX304 lentiviral vector were generated by transduction. Lentivirus production and infection were performed according to guidelines from the Broad RNAi Consortium and infected cell lines were selected 48 hr post-transduction with the respective selection markers. MICU1-knockout HEK293 cells were kindly provided by Prof. Vamsi Mootha (Howard Hughes Medical Institute). MICU1-knockout

HEK293 cells stably expressing either wild-type (Hs-MICU1) or mutant Hs-MICU1 (Hs-MICU1_{mEF}) from the pLX304 vector were generated by transduction and selected with 10 μ g/mL blasticidin.

Yeast Strains

Yeast strains expressing mt-AEQ or cyt-AEQ were generated by transforming the wild-type yeast strain YPH499 and selecting transformants in glucose medium lacking uracil (Sikorski and Hieter, 1989). Yeast strains expressing Dd-MCU, Af-MCU, Nc-MCU, Hs-EMRE, Hs-MCU, Hs-MICU1 and their mutants were generated by transforming the YPH499 strain with the respective plasmids and by selecting transformants on glucose medium lacking uracil (empty vector p316GPD or mt-AEQ and cyt-AEQ), histidine (empty vector p423GPD or Hs-MCU, Hs-MCU_{D261A}, Hs-MCU_{E264A}, Dd-MCU, Af-MCU, and Nc-MCU), leucine (empty vector p425GPD or Hs-EMRE), and tryptophan (empty vector p414GPD or Hs-MICU1, Hs-MICU1_{mEF}) as selection markers.

METHOD DETAILS

Phylogenetic Profiling of MICU1 and MCU

Homologs of human MCU and MICU1 across 247 eukaryotes were retrieved from ProtPhylo (www.protphylo.org) (Cheng and Perocchi, 2015) using OrthoMCL with more than 0% match length and inflation index of 1.1 for orthology assignment. The percentage of amino acids match length was determined based on BLASTp-NIH. The phylogenetic tree of 247 eukaryotes was reconstructed using the phylogenetic tree generator (<https://phylot.biobyte.de/>) and visualized using iTOL (<https://itol.embl.de/>). The mitochondrial-targeting sequence (MTS) probability was determined with MitoProt (<https://ihg.gsf.de/ihg/mitoprot.html>).

Protein Domains

Protein sequences of *Homo sapiens* MCU (Hs-MCU, NP_612366.1) *Neurospora crassa* MCU (Nc-MCU, XP_959658.1), and *Aspergillus fumigatus* MCU (Af-MCU, XP_751795.1) were analyzed to predict MTS, DUF607 motif, coiled coil domains (CCD) (https://embnet.vital-it.ch/software/COILS_form.html), and transmembrane domains (TM) (TMHMM 2.0). Clustal Omega was used for proteins alignment and sequence similarities above 80% were color-coded with the Sequence Manipulation Suite tool.

Plasmids and Reagents

The lentiviral vector pLX304 was obtained from the Broad Institute's RNAi Consortium and used for expressing V5- tagged cDNAs. Full-length, human wild-type EMRE (Hs-EMRE), MCU (Hs-MCU), MICU1 (Hs-MICU1) and their mutants (Hs-MCU_{D261A}, Hs-MCU_{E264A}, and Hs-MICU1_{mEF}) cDNAs without a stop codon were obtained from Addgene. Hs-MICU1_{mEF} contains two point mutations in both first (D231A, E242K) and second (D421A, E432K) EF-hand domains as described in (Perocchi et al., 2010).

Dd-MCU, Af-MCU and Nc-MCU with (^{HsMTS}Af-MCU and ^{HsMTS}Nc-MCU) and without the N-terminal MTS of Hs-MCU (aminoacids 1-56) and without a stop codon were codon optimized for human expression, synthesized *de novo* in the PuC57 vector (GenScript) and amplified with flanked attB1 and attB2 sites by PCR using the following primers: fw-DdMCU (5'-GGG GAC AAG TTT GTA CAA AAA AGC AGG CTT AGC CAC CAT GAA CTC CTT TGT CAT CAG-3'); rv-DdMCU (5'-GGG GAC AAG TTT GTA CAA AAA AGC AGG CTT AGC CAC CAT GAA TTG CGT GAG AAT GAG ACT C-3'); fw-NcMCU (5'-GGG GAC AGG TTT GTA CAA AAA AGC AGG CTT AGC CAC CAT GAA TTG CGT GAG AAT GAG ACT C-3'); rv-NcMCU (5'-GGG GAC CAC TTT GTA CAA GAA AGC TGG GTT ACT GTC TCC GCT GGT CTC TTT-3'); fw-AfMCU (5'-GGG GAC AAG TTT GTA CAA AAA AGC AGG CTT AGC CAC CAT GGT CCT GTC TTG TGA TAC TAG A-3'); rv-AfMCU (5'-GGG GAC CAC TTT GTA CAA GAA AGC TGG GTT GTC GTC ATC TCG GTC ATC GTT-3'); fw-HsMTS (5'-GGG GAC AAG TTT GTA CAA AAA AGC AGG CTT AGC CAC CAT GGC GGC CGC CGC AGG TAG A-3'). PCR products were integrated into the pDONR221 vector using a site-specific recombination system (GATEWAY cloning technology) according to manufacturer's instructions (Life Technologies). For the expression in mammalian cells, cDNAs were integrated from the pDONR221 Gateway vector (Thermo Fisher Scientific, 1253607), by site-specific recombination, into the pLX304 vector according to manufacturer's instructions (Life Technologies).

Cytosolic aequorin (cyt-AEQ) plasmid was kindly provided by Prof. Teresa Alonso (University Valladolid) and a mitochondria-targeted GFP-aequorin (mt-AEQ) plasmid was generated as previously described in (Arduino et al., 2017). cDNAs of Dd-MCU, Af-MCU, Nc-MCU, Hs-EMRE, Hs-MCU, Hs-MICU1 and their mutants were amplified by PCR using the following primers: fw-DdMCU (5'-CCC TCT AGA ATG AAC TCC TTT GTC ATC AG-3'); fw-AfMCU (5'-CCC TCT AGA ATG GTC CTG TCT TGT GAT AC-3'); fw-NcMCU (5'-CCC TCT AGA ATG AAT TGC GTG AGA ATG AG-3'); rv-V5 (5'-GGG CTC GAG CTA CGT AGA ATC GAG ACC GAG-3'); fw-HsEMRE (5'-CCC GGA TCC ATG GCG TCC GGA GCG GCT CGC-3'); rv-HsEMRE (5'-GGG CTC GAG TTA GTC ATC ATC ATC ATC CTC-3'); fw-HsMCU (5'-CCC TCT AGA ATG GCG GCC GCC GCA GGT AG-3'); rv-HsMCU (5'-GGG CTC GAG TTA ATC TTT TTC ACC AAT TTG TCG-3'); fw-HsMICU1 (5'-CCC GGA TCC ATG TTT CGT CTG AAC TCA CTT TC-3'); rv-HsMICU1 (5'-GGG CTC GAG TTA CTG TTT GGG TAA AGC GAA G-3'), and cloned into the yeast expression plasmids p423GPD (Dd-MCU, Af-MCU, Nc-MCU, Hs-MCU, Hs-MCU_{D261A}, Hs-MCU_{E264A}), p414GPD (Hs-MICU1, Hs-MICU1_{mEF}) and p425GPD (Hs-EMRE) as in (Mumberg et al., 1995).

Isolation of Crude Mitochondria from HeLa Cells

Crude mitochondria were prepared from cultured HeLa cells as previously described (Wettmarshausen and Perocchi, 2017). Briefly, HeLa cells were grown to confluency in 245 × 245 × 20 mm cell culture plates. Culture medium was removed and cells were rinsed

with 30 mL PBS, scraped down and resuspended in 5 mL PBS. After 5 minutes of centrifugation at 600 x g, 4°C, the cell pellet was resuspended in ~15 mL of ice cold isolation buffer (IB; 220 mM mannitol, 70 mM sucrose, 5 mM HEPES-KOH pH 7.4, 1 mM EGTA-KOH pH 7.4), with one protease inhibitor tablet added per 50 mL of buffer. Cell suspension was immediately subjected to nitrogen cavitation at 600 psi for 10 minutes at 4°C. Nuclei and intact cells were pelleted by centrifugation at 600 x g for 10 minutes at 4°C. Supernatants were transferred into new tubes and centrifuged at 8000 x g for 10 minutes at 4°C. The resulting pellet containing crude mitochondria was resuspended in 50–200 μ L IB for further analyses.

Topology Analysis of Mitochondrial Proteins

Alkaline carbonate extraction from crude mitochondria was performed as described previously (Baughman et al., 2011). Briefly, 100 μ g of mitochondria were pelleted by centrifugation at 8000 x g for 10 minutes at 4°C. Pellets were resuspended in 0.1 M Na_2CO_3 at pH 10, pH 11 or pH 12 and incubated for 30 minutes on ice. Samples were then centrifuged at 45,000 x g for 10 minutes at 4°C. Pellets were resuspended in 100 μ L of 2 x Laemmli buffer, boiled at 98°C for 5 minutes and stored at –80°C until further use (pellet sample). Supernatants were mixed with 40 μ L of 100% TCA and incubated overnight at –20°C. On the following day, supernatants were centrifuged at 16,000 x g for 25 min at 4°C. Pellets were then washed twice with cold acetone, air-dried for 20–30 minutes at room temperature, resuspended in 100 μ L of 2 x Laemmli buffer and heated up to 98°C for 5 minutes (supernatant sample). 25 μ L of supernatant and pellet samples were analyzed by SDS-PAGE. TIM23 and HSP60, integral inner membrane and soluble matrix targeted proteins, respectively, are used as controls.

Proteinase K protection assay was performed by incubating 30 μ g of mitochondria in 30 μ L of isolation buffer with increasing concentrations of digitonin or 1% Triton X-100 in the presence of 100 μ g/mL proteinase K to sequentially permeabilize outer and inner membranes. The reaction was carried out at room temperature for 15 minutes and was stopped by the addition of 5 mM PMSF, followed by incubation on ice for 10 minutes. Samples were mixed with 10 μ L of 4 X Laemmli buffer containing 10% 2-mercaptoethanol and boiled for 5 minutes at 98°C. Samples were then loaded at 10 μ L per lane and were analyzed by SDS-PAGE. TOM20 and cyclophilin D (Cyp D), an integral outer membrane and a soluble matrix protein, respectively, were used as controls.

Blue Native – PAGE Analysis

Samples for BN-PAGE analysis were prepared by incubating 10 μ g of crude mitochondria on ice for 10 minutes in 9.5 μ L of Invitrogen 1X NativePAGE™ sample buffer containing 1% digitonin. Samples were centrifuged at 20,000 x g for 30 minutes at 4°C. Supernatants were transferred into new tubes and 0.5 μ L of NativePAGE™ 5% G-250 Sample Additive was added to a final concentration of 0.25%. Anode and cathode buffers for gel electrophoresis were prepared according to the manufacturer's protocol for the Invitrogen NativePAGE™ Novex® Bis-Tris Gel System and were cooled to 4°C before use. Electrophoresis was performed at 4°C and gels were performed at 40 V for 1 hour. The voltage was then increased to 60 V for 30 minutes and subsequently to 100 V until the dye front had traveled through 1/3 of the gel, at which point the Dark Blue Cathode Buffer was replaced with Light Blue Cathode Buffer. Electrophoresis was continued at 100 V for 30 minutes and then increased to 150 V until completed. Proteins were transferred onto PVDF membranes by electrophoretic wet transfer overnight at 40 V, 4°C. After transfer, proteins were fixed on the membrane by incubating in 8% acetic acid for 15 minutes at room temperature on a shaker. Immunoblot analyses were performed with the following antibodies: anti-MCU (Sigma Aldrich, HPA01648), anti-V5 (Life Technologies, R96025), and anti-ATP5A (Abcam, MS507), anti-TIM23 (BD Bioscience, 611222), and anti-HSP60 (R&D System, MAB1800), anti-TOM20 (Abcam, ab56783), and anti-Cyclophilin D (Abcam, ab110324).

Measurements of Mitochondrial Calcium Uptake in Intact HeLa Cells

Mitochondrial Ca^{2+} uptake was measured in mt-AEQ HeLa cells as previously described (Arduino et al., 2017). Briefly, HeLa cells stably expressing mt-AEQ were seeded in white 96-well plates at 25,000 cells/well in growth medium. After 24 hours, mt-AEQ was reconstituted with 2 μ M native coelenterazine (Abcam, ab145165) for 2 hours at 37°C. Mt-AEQ-based measurements of Ca^{2+} -dependent light kinetics were performed upon 100 μ M histamine stimulation. Light emission was measured in a luminescence counter (MicroBeta2 LumiJET Microplate Counter, PerkinElmer) at 469 nm every 0.1 s. At the end of each experiment, cells were lysed with a solution containing 0.5% Triton X-100 and 10 mM CaCl_2 to release all the residual aequorin counts.

Measurements of Mitochondrial Calcium Uptake in Digitonin-Permeabilized HeLa Cells

HeLa cells stably expressing mt-AEQ were harvested at a density of 500,000 cells/mL in growth medium supplemented with 20 mM HEPES (pH 7.4/NaOH) and the photoprotein aequorin was reconstituted by incubation with 3 μ M native coelenterazine for 2.5 hours at room temperature. Cells were then centrifuged at 300 g for 3 minutes and the pellet was re-suspended in an extracellular-like buffer containing 145 mM NaCl, 5 mM KCl, 1 mM MgCl_2 , 10 mM glucose, 10 mM HEPES and 500 μ M EGTA (pH 7.4/NaOH), supplemented with 200 nM thapsigargin. After 20 minutes at room temperature, cells were collected by centrifugation at 300 g for 3 minutes and the pellet was resuspended in an intracellular-like buffer containing 140 mM KCl, 1 mM $\text{KH}_2\text{PO}_4/\text{K}_2\text{HPO}_4$, 1 mM MgCl_2 , 20 mM HEPES, 100 μ M EGTA (pH 7.2/KOH), supplemented with 1 mM Na^+ -pyruvate, 1 mM ATP/ MgCl_2 and 2 mM Na^+ -succinate. Cells were permeabilized with 60 μ M digitonin for 5 minutes, collected by centrifugation at 300 g for 3 minutes and resuspended in intracellular-like buffer at a density of ~900 cells/ μ L. Then, 90 μ L of cell suspension was dispensed into a white 96-well plate (PerkinElmer). Cells were incubated for 5 minutes at room temperature and Ca^{2+} -stimulated light signal was recorded at 469 nm every 0.1 s using a luminescence counter (MicroBeta2 LumiJET Microplate Counter, PerkinElmer). Ru360 (10 μ M) was used as a positive control.

Subcellular Fractionation of Yeast Cells

To test the expression and subcellular localization of heterologous proteins, yeast cells were grown at 30°C in a selective lactate medium (S-LAC) containing 8.5 g/L yeast nitrogen base, 25 g/L ammonium sulfate, 2% (v/v) lactic acid (90%), 0.1% glucose (pH 5.5/KOH), supplemented with the respective selection markers. At an OD ~0.8, cells were harvested at 1000 g for 5 minutes at room temperature. The cell pellet was re-suspended in SHK buffer (0.6 M sorbitol, 20 mM HEPES/KOH pH 7.2, 80 mM KCl, and 1 mM PMSF) and vortexed five times for 30 s with glass beads (425–600 µm diameter), with a 30 s cooling interval in between. This sample was then centrifuged at 1000 g for 5 minutes at 4°C and the supernatant was further centrifuged at 20,000 g for 10 minutes at 4°C to obtain the mitochondrial fraction (pellet). The resulting supernatant (cytosolic fraction) was precipitated with trichloroacetic acid at –20°C for 1 hour, washed once with cold acetone and centrifuged at 20,000 g for 10 minutes at 4°C to obtain the cytosolic fraction (pellet). Both cytosolic and mitochondrial fractions were directly resuspended in Laemmli buffer and separated under reducing conditions in 12 or 14% SDS-PAGE gels. Immunoblotting was performed according to the standard procedures using the following antibodies: anti-MCU (Sigma-Aldrich, HPA016480); anti-EMRE (Santa Cruz Biotechnology, sc- 86337); anti-MICU1 (Sigma Aldrich, HPA037480); anti-YME1 (ThermoFisher/Novex, 459250); anti-AEQ (Merck/Millipore, MAB4405).

Measurements of Calcium Transients in Intact Yeast Cells

In vivo analyses of cytosolic and mitochondrial Ca²⁺ dynamics in yeast cells were performed as described by (Groppi et al., 2011) with some modifications. Yeast were grown in S-LAC at 30°C overnight to an OD ~0.8, (~24x10⁶ cells/mL), and cells were harvested by centrifugation at 3,500 g for 5 minutes at room temperature. Yeast cell pellet was washed three times with milliQ water and resuspended in a nutrient-free buffer (NFB; 100 mM Tris, pH 6.5) at a density of 1x10⁸ cells/mL. Cells were incubated for 1.5 hours at room temperature (starvation), collected by centrifugation at 3,500 rpm for 5 minutes and concentrated in the same buffer to a density of 25x10⁸ cells/mL. The photoprotein aequorin was then reconstituted with 50 µM native coelenterazine in the dark for 30 minutes at room temperature. Excess of coelenterazine was washed thrice with NFB and the cell pellet was resuspended to a final density of 5x10⁸ cells/mL. Then, a suspension of 0.5x10⁸ cells/well were plated into a white 96-well plate and Ca²⁺-dependent aequorin light signal was recorded upon stimulation with containing 1 mM CaCl₂ and 100 mM glucose, at 0.5 s interval in a MicroBeta2 LumiJET Microplate Counter. At the end of each experiment, a lysis solution containing 5 mM digitonin, 450 mM EGTA, 100 mM Tris (pH 6.5/KOH) was added at a ratio of 1:5 for 5 minutes at 37°C and light response was measured upon the addition of CaCl₂ to a final concentration of 140 mM to release all the residual aequorin counts.

Measurements of Mitochondrial Calcium Uptake in Isolated Yeast Mitochondria

Crude mitochondria were isolated from yeast strains as described previously (Arduino et al., 2017). Mitochondria were then resuspended in a buffer containing 0.6 M sorbitol, 20 mM HEPES, 2 mM MgCl₂, 10 mM KH₂PO₄, 3 mM glutamate, 3 mM malate, 3 mM succinate, 50 µM EDTA, and 0.1 µM Calcium Green-5N (Life technologies, C3737) and seeded into a black 96-well plate at 150 µg/100 µL. Calcium Green-5N fluorescence (excitation 506 nm, emission 531 nm) was monitored every 2 s at room temperature using a CLARIOstar microplate reader (BMG Labtech Perkin-Elmer Envision) after injection of CaCl₂ (100 µM final concentration). The MCU inhibitor Ru360 (10 µM) was used as a positive control.

Yeast Growth Measurement

For growth assays in liquid media, overnight yeast cultures grown at 30°C in S-LAC were diluted to an OD of 0.1 (3x10⁶ cells/mL) and then 0.3x10⁶ cells/well were seeded in a black, gas-permeable Lumox 96-well plate. Absorbance measurements of yeast suspension light scattering were performed at λ_{max} = 600 nm and intervals of 340 s using a CLARIOstar microplate reader (BMG Labtech) for 48–72 hours with shaking at 30°C, 37°C, or in the presence of sterile solutions of sodium chloride (NaCl, 0.1–1 M), calcium chloride (CaCl₂, 10–100 mM), copper (II) chloride (CuCl₂, 10–30 mM), iron (II) chloride (FeCl₂, 10–40 mM), Mn²⁺ (II) chloride (MnCl₂, 1–5 mM), strontium (II) chloride (SrCl₂, 10–50 mM), zinc (II) chloride (ZnCl₂, 10–50 mM), or antifungal drugs (miconazole, 10–100 ng/ml; amiodarone, 5–20 µM). The average time taken by the yeast culture to double in the log-growth phase (doubling time) was calculated using the following equation:

$$\text{Doubling time} = \frac{(T_f - T_i) * \log(2)}{\log(N_f) - \log(N_i)}$$

where T is the time between the log-growth phase from T_i to T_f and N the number of cells measured as an optical density at λ_{max} = 600 nm at the time point T_i (N_i) and T_f (N_f).

For spot assays, yeast cultures grown at 30°C in S-LAC were harvested at an OD of 1.0 (30x10⁶ cells/mL) at 3200 g for 5 minutes at room temperature. The cell pellet was re-suspended in sterile water to 30x10⁶ cells/mL and diluted in a 10-fold series. Aliquots of 5 µL from each dilution were spotted onto a S-LAC plate with or without the respective treatment (CaCl₂, 100–600 mM; SrCl₂, 50–500 mM). Plates were then incubated at 30°C for 72 h.

Cell Viability Analysis

A colorimetric 3-(4,5-dimethylthiazol-2-yl)-2,5-diphenyltetrazolium bromide (MTT) metabolic activity assay was used to determine cell viability. HEK293 cells were seeded at 50,000 cells/well in 1 mL of DMEM with high glucose and 10% FBS in a transparent

24-well plate at 37°C and 5% CO₂. After 24 hours, cells were incubated in the presence or absence of metal ions (FeCl₂, 0.1–1 mM; MnCl₂, 5–50 μM) or antioxidants (N-acetyl-L-cysteine, NAC, 1–10 mM; L-glutathione, GSH, 1–20 μM; antioxidant supplement, 1–20X concentration according to manufacturer's protocol; Trolox, 0.5–5 mM; Idebenone, 0.1 μM), together with 10–50 μM of MnCl₂, for further 48 hours. Afterward, 500 μL of medium was replaced, 50 μL of MTT solution (Sigma Aldrich, M5655; 5 mg/ml in PBS) was added, and cells were incubated for 3 hours at 37°C. Finally, cells were lysed with 500 μL of solubilization solution (1% SDS and 0.1 M HCl in isopropanol) for 15 minutes at 37°C and absorbance at λ_{max} 570 nm was monitored in a CLARIOstar microplate reader (BMG Labtech).

Mitochondrial Mn²⁺ Transport Measurement in Human Cells

Measurements of Mn²⁺ uptake in mitochondria were performed as previously described (Csordás and Hajnóczky, 2003). Briefly, cells were first loaded with Fura2FF/AM (4 μM for 60 min) and then rinsed with a Ca²⁺-free extracellular buffer containing 100 μM EGTA. Permeabilization was carried out in 1 mL ICM (120 mM KCl, 10 mM NaCl, 1 mM KH₂PO₄, 20 mM Tris-HEPES, 2 mM MgATP, and 1 μg/ml each of antipain, leupeptin and pepstatin at pH 7.2) supplemented with saponin (20 μg/ml) and 20 μM EGTA/Tris (pH 7.4) in the incubation chamber for 5 min (35°C). Subsequently, fresh ICM supplemented with succinate (2 mM) and CGP (20 μM) to energize mitochondria and to inhibit mitochondrial Ca²⁺ efflux, respectively. Fluorescence imaging of Fura2FF-quenching by Mn²⁺ was carried out using a multiwavelength beamsplitter/emission filter combination and a high quantum-efficiency cooled CCD camera. Fura2FF was excited at 360 nm (Mn²⁺ quench). Image analysis was performed using custom-made software (Spectralyzer). Genetic rescue of MICU1-KO HEK293 cells was performed with either WT MICU1 or pcDNA 48 hr before imaging.

ROS Measurement

HEK293 cells were loaded with 10 μM of 5-(and-6)-chloromethyl-2', 7'-dichlorodihydrofluorescein diacetate (CM-H₂DCFDA) in Krebs buffer (140 mM NaCl, 5 mM KCl, 1 mM MgCl₂, 5.6 mM D-glucose, 20 mM HEPES, 1.5 mM CaCl₂, 1 mM NaH₂PO₄, pH 7.4) for 30 minutes at 37°C. Cells were washed once with PBS, re-suspended in DMEM (without phenol red, REF, source ID), supplemented with 5 mM glucose, 1 mM pyruvate, 2 mM L-glutamine and 10% FBS, seeded at 20,000 cells/well in a black 96-well plate, and treated with 25 μM of MnCl₂ for 48 hours. H₂O₂ (50–100 μM) was used as a positive control. Fluorescence was measured at an excitation and emission wavelength of 485 nm and 520 nm respectively. Data was normalized to cell number quantified using a CyQUANT Cell Proliferation Assay Kit (Thermo Fisher Scientific).

QUANTIFICATION AND STATISTICAL ANALYSIS

Quantification of Calcium Transients

Quantification of mt-Ca₂₊ concentration was performed using a MATLAB software as previously described in (Arduino et al., 2017). The dynamics of mt-Ca²⁺-dependent luminescence signal was smoothed by the cubic spline function:

$$p \sum_{i=1}^n (y_i - f(x_i))^2 + (1 - p) \int \left(\frac{d^2 f}{dx^2} \right)^2 dx$$

Where, p is a smoothing parameter, controlling the tradeoff between fidelity to the data and roughness of the function estimate, f is the estimated cubic spline function to minimize the above function, and x_i and y_i are the dynamical data points. Here, p is set at 0.5. Parametrization of the Ca²⁺-dependent luminescence kinetics was performed in order to determine the maximal amplitude of the luminescence signal (peak) and the left slope of the bell-shaped kinetic trace. Aequorin-based luminescence signal calibration into mt-Ca²⁺ concentration was performed using the algorithm reported in (Bonora et al., 2013) for wild-type aequorin and native coelenterazine, with the following formula:

$$[Ca^{2+}](M) = \frac{\left(\frac{L}{L_{max}} \times \lambda \right)^{\frac{1}{n}} + \left(\left(\frac{L}{L_{max}} \times \lambda \right)^{\frac{1}{n}} \times K_{TR} \right) - 1}{K_R - \left(\left(\frac{L}{L_{max}} \times \lambda \right)^{\frac{1}{n}} \times K_R \right)}$$

Where $\lambda = 1$, $K_R = 7.23 \times 10^6$, $K_{TR} = 120$ and $n = 2.99$ are the calibration values used for WT aequorin and native coelenterazine.

Data Analysis

Data are represented as mean ± SEM and the statistical analysis of each experiment is described in the figure legends including the statistical tests used and the exact value of n . Here n represents the number of biological replicates. For each biological replicate experiment at least 3 technical replicates were used for quantification and data analysis. Normal distribution was tested by Shapiro-Wilk normality test. Differences between two datasets were evaluated by two-tailed unpaired Student's t test. Statistical tests between multiple datasets and conditions were carried out using one-way analysis of variance (ANOVA) followed by Tukey's or Dunnett's Multiple Comparison tests. Statistical analyses were performed using GraphPad Prism (GraphPad Software, version 7).

Supplemental Information

**MICU1 Confers Protection
from MCU-Dependent Manganese Toxicity**

Jennifer Wettmarshausen, Valerie Goh, Kai-Ting Huang, Daniela M. Arduino, Utkarsh Tripathi, Anja Leimpek, Yiming Cheng, Alexandros A. Pittis, Toni Gabaldón, Dejana Mokranjac, György Hajnóczky, and Fabiana Perocchi

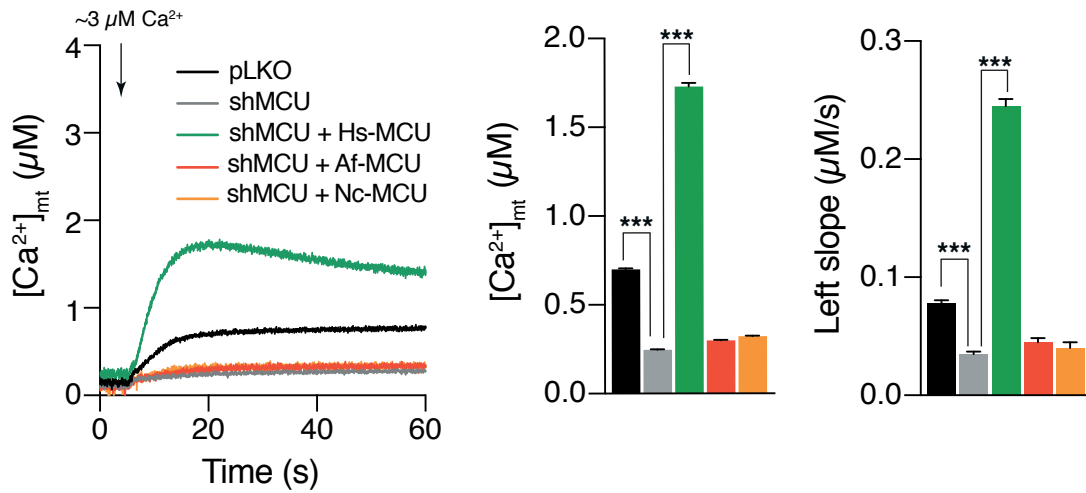


Figure S1. Mt- Ca^{2+} uptake in permeabilized shMCU HeLa cells expressing MCU orthologs from *N. crassa* and *A. fumigatus*. Related to Figure 1. Representative traces and quantification of mt- Ca^{2+} transients in digitonin-permeabilized control (pLKO) and shMCU HeLa cells expressing human and fungal MCU constructs. All data represent mean \pm SEM; n=6-12; ***p < 0.001, one-way ANOVA with Tukey's Multiple Comparison Test.

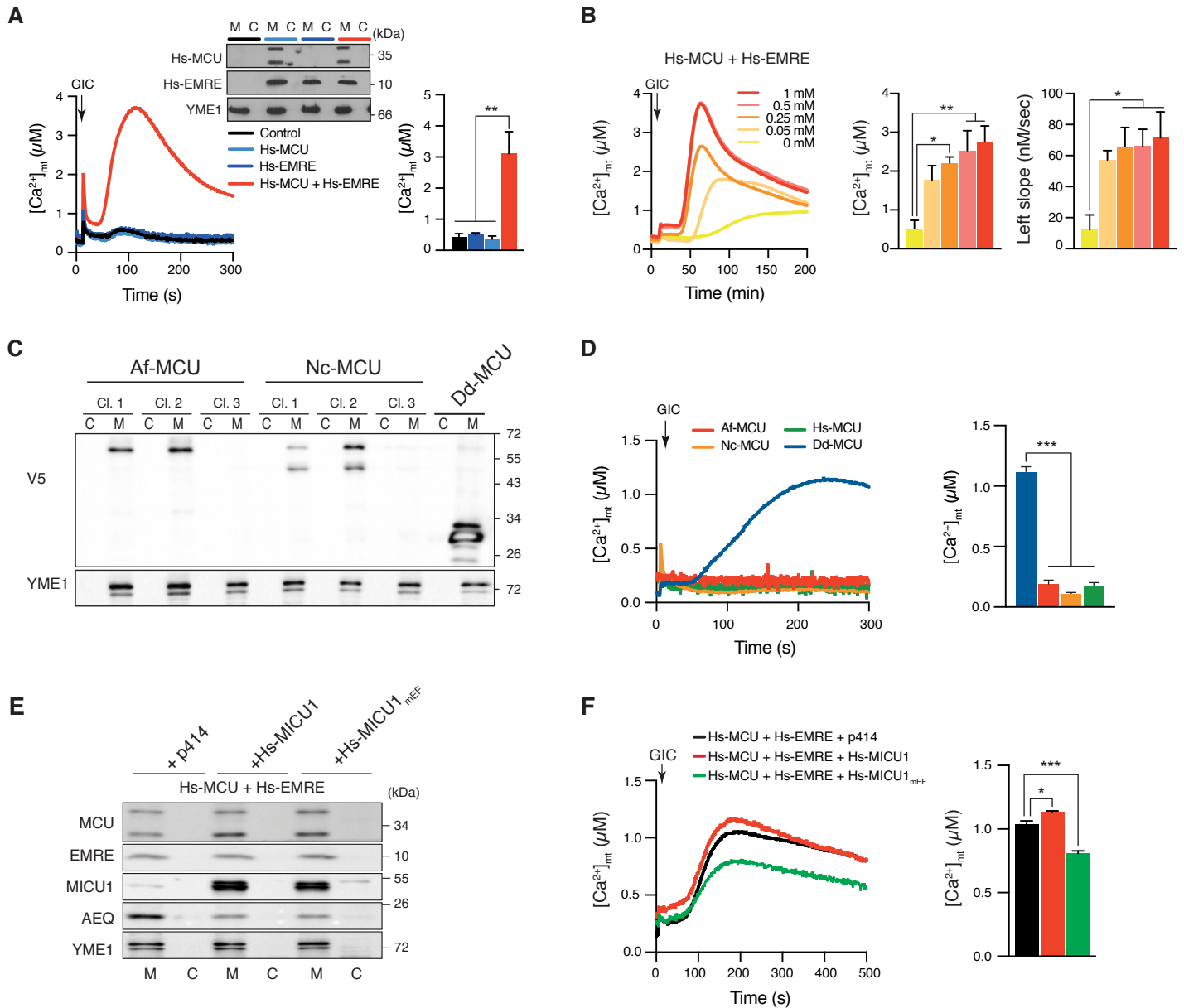


Figure S2. Reconstitution of mt- Ca^{2+} uptake in yeast cells. Related to Figure 2. **(A)** Representative traces and quantification of mt- Ca^{2+} transients in yeast cells expressing WT mtAEQ with either empty vector (control), Hs-EMRE, Hs-MCU, or both upon GIC stimulation in presence of 1 mM CaCl_2 (n=3); ***p < 0.001, one-way ANOVA with Tukey's Multiple Comparisons test. Inset, immunoblot analysis of cytosolic (C) and mitochondrial (M) fractions. **(B)** Mt- Ca^{2+} transients in Hs-MCU and Hs-EMRE reconstituted yeast cells upon GIC stimulation in presence of different extracellular CaCl_2 concentrations (n=3); *p < 0.05, **p < 0.01, one-way ANOVA with Dunnett's Multiple Comparisons Test. **(C)** Analysis of cytosolic (C) and mitochondrial (M) fractions from yeast clones (Cl. 1-3) expressing MCU orthologs from *N. crassa* (Nc-MCU), *A. fumigatus* (Af-MCU) or *D. discoideum* (Dd-MCU) fused to a C-terminal V5-tag. **(D)** Representative traces and quantification of mt- Ca^{2+} transients in yeast cells expressing WT mtAEQ with MCU orthologs from *N. crassa* (Cl. 2), *A. fumigatus* (Cl. 2), or *D. discoideum* upon GIC stimulation in presence of 1 mM CaCl_2 (n=4); ***p < 0.001, one-way ANOVA with Tukey's Multiple Comparisons Test. **(E)** Immunoblot analysis of cytosolic (C) and mitochondrial (M) fractions isolated from yeast strains expressing Hs-MCU, Hs-EMRE and either an empty vector (p414), human WT MICU1 (Hs-MICU1), or EF-hands mutant MICU1 (Hs-MICU1_{MEF}). **(F)** Mt- Ca^{2+} transients in the yeast strains described in (E) upon GIC stimulation in presence of 1 mM CaCl_2 (n=3); *p < 0.05, ***p < 0.001, one-way ANOVA with Dunnett's Multiple Comparisons Test.

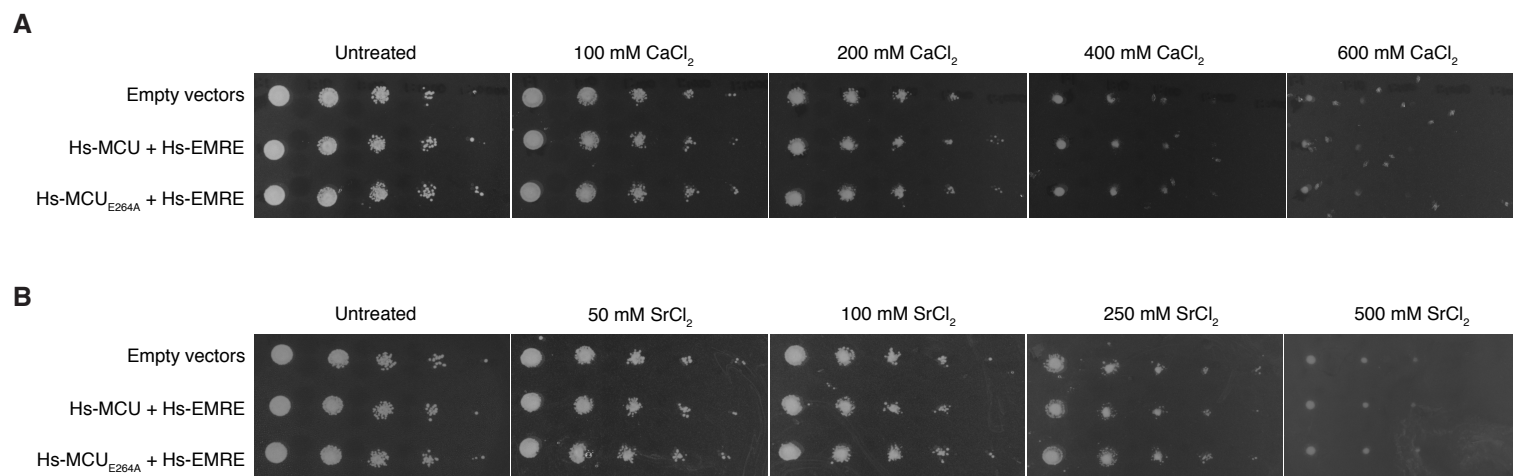


Figure S3. Yeast tolerance to calcium and strontium stress. Related to Figure 3. Growth assay of ten-fold serial dilutions of yeast strains expressing empty vectors (p423 and p425) or Hs-EMRE with WT or mutated Hs-MCU at 30°C on S-LAC plates containing increasing concentrations of CaCl_2 (**A**) and SrCl_2 (**B**).

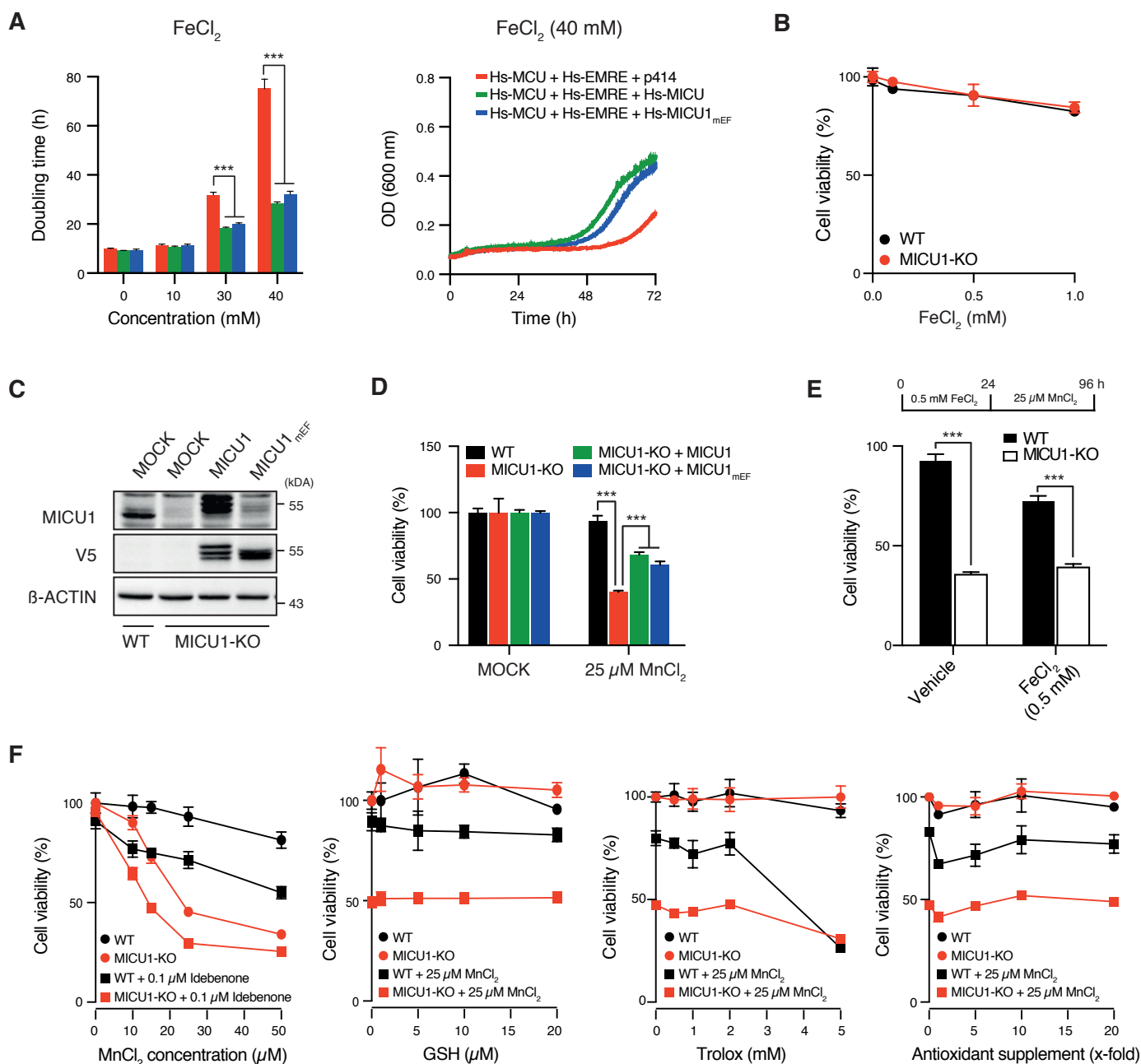


Figure S4. Role of MICU1 in manganese-induced cytotoxicity. Related to Figure 4. **(A)** Quantification of growth rate and average growth curve of yeast strains expressing Hs-MCU, Hs-EMRE and either empty vector (p414), Hs-MICU1 or Hs-MICU1_{mEF} and treated with FeCl_2 ; $n=4$; *** $p < 0.001$, one-way ANOVA with Tukey's Multiple Comparisons Test. **(B)** Cell viability assays of wild-type (WT) and MICU1 knockout (MICU1-KO) HEK-293 cells treated for 48 hours with FeCl_2 ; $n=4$. **(C)** Immunoblot analysis of whole cell lysates from WT and MICU1-KO cells that were either MOCK-treated or rescued by lentiviral expression of Hs-MICU1 or Hs-MICU1_{mEF}. **(D)** Cell viability assays of uninfected WT and MICU1-KO cells that were either MOCK-treated or rescued by lentiviral expression of Hs-MICU1 or Hs-MICU1_{mEF} upon MnCl_2 treatment for 48 hours; $n=4$; *** $p < 0.001$, one-way ANOVA with Tukey's Multiple Comparisons Test. **(E)** Cell viability assays of WT and MICU1-KO HEK-293 cells pre-treated with either FeCl_2 or vehicle (water) for 24 hours followed by 48 hours of incubation with MnCl_2 ($n=3$). **(F)** Cell viability assays of WT and MICU1-KO HEK-293 cells treated for 48 hours with MnCl_2 in the presence of idebenone, L-glutathione (GSH), trolox, or an antioxidant supplement from Sigma, ($n=3$). Data are reported as the percentage of viable cells in untreated samples. All data represent mean \pm SEM.

Publication II

Alexandros A. Pittis*, **Valerie Goh***, Alberto Cebrian-Serrano, Jennifer Wettmarshausen, Fabiana Perocchi & Toni Gabaldón, 2020. **Discovery of EMRE in fungi resolves the true evolutionary history of the mitochondrial calcium uniporter**. Nature communications, 11, 4031.

*equal author contributions

All experiments were designed together with Alexandros A. Pittis, Fabiana Perocchi and Toni Gabaldón. I had personally performed the experiments of Fig. 3B-C, 4C-F, Supplementary Fig. 3-4, 7-12. All the experiments and data in the figures as indicated were also analyzed and illustrated by myself. This manuscript was revised together with Alexandros A. Pittis, Fabiana Perocchi and Toni Gabaldón.



ARTICLE



<https://doi.org/10.1038/s41467-020-17705-4>

OPEN

Discovery of EMRE in fungi resolves the true evolutionary history of the mitochondrial calcium uniporter

Alexandros A. Pittis^{1,2,3,8,10} , Valerie Goh^{4,10}, Alberto Cebrian-Serrano^{4,5}, Jennifer Wettmarshausen⁴, Fabiana Perocchi^{4,6,11}  & Toni Gabaldón^{1,2,7,9,11} 

Calcium (Ca^{2+}) influx into mitochondria occurs through a Ca^{2+} -selective uniporter channel, which regulates essential cellular processes in eukaryotic organisms. Previous evolutionary analyses of its pore-forming subunits MCU and EMRE, and gatekeeper MICU1, pinpointed an evolutionary paradox: the presence of MCU homologs in fungal species devoid of any other uniporter components and of mt- Ca^{2+} uptake. Here, we trace the mt- Ca^{2+} uniporter evolution across 1,156 fully-sequenced eukaryotes and show that animal and fungal MCUs represent two distinct paralogous subfamilies originating from an ancestral duplication. Accordingly, we find EMRE orthologs outside Holoza and uncover the existence of an animal-like uniporter within chytrid fungi, which enables mt- Ca^{2+} uptake when reconstituted in vivo in the yeast *Saccharomyces cerevisiae*. Our study represents the most comprehensive phylogenomic analysis of the mt- Ca^{2+} uptake system and demonstrates that MCU, EMRE, and MICU formed the core of the ancestral opisthokont uniporter, with major implications for comparative structural and functional studies.

¹ Centre for Genomic Regulation (CRG), The Barcelona Institute of Science and Technology, 08003 Barcelona, Spain. ² Universitat Pompeu Fabra (UPF), 08003 Barcelona, Spain. ³ Biodiversity Research Centre & Department of Botany, University of British Columbia (UBC), Vancouver, BC V6T 1Z4, Canada. ⁴ Institute for Diabetes and Obesity, Helmholtz Diabetes Center (HDC), Helmholtz Zentrum München, 85764 Neuherberg, Germany. ⁵ German Center for Diabetes Research (DZD), 85764 Neuherberg, Germany. ⁶ Munich Cluster for Systems Neurology, 81377 Munich, Germany. ⁷ ICREA, Pg. Lluís Companys 23, 08010 Barcelona, Spain. ⁸ Present address: Berlin Institute for Advanced Study, 14193 Berlin, Germany. ⁹ Present address: Barcelona Supercomputing Centre (BSC-CNC) and Institute for Research in Biomedicine (IRB), 08034 Barcelona, Spain. ¹⁰ These authors contributed equally: Alexandros A. Pittis, Valerie Goh. ¹¹ These authors jointly supervised this work: Fabiana Perocchi, Toni Gabaldón. ✉email: fabiana.perocchi@helmholtz-muenchen.de; toni.gabaldon.bcn@gmail.com

Mitochondria from several organisms play a key role in regulating intracellular Ca^{2+} signaling¹ due to their ability to rapidly uptake and buffer cytosolic Ca^{2+} . Mitochondrial Ca^{2+} (mt- Ca^{2+}) uptake is mediated by a highly selective channel, the mt- Ca^{2+} uniporter, that resides in the inner mitochondrial membrane and is powered by the negative transmembrane potential^{2–4}. However, the functional role of mt- Ca^{2+} uptake and its pathophysiology has remained largely unknown, as the molecular identity of the mt- Ca^{2+} uniporter channel was only recently discovered^{5–7}. To this end, comparative genomics analyses based on a few eukaryotic species, in combination with RNAi assays, were instrumental in identifying the first components of the mammalian uniporter, MCU and MICU1 (refs. 5–7). While MCU constitutes the pore-forming and Ca^{2+} -conducting subunit of the uniporter⁸, the EF-hand-containing and Ca^{2+} -sensitive protein MICU1 has been shown to function as a channel gatekeeper and cooperative activator⁹. Importantly, their discovery paved the way to the identification of additional structural and regulatory components of the mammalian uniporter, including a MCU-dominant-negative beta subunit (MCUB)¹⁰, three tissue-specific MICU1 paralogs or splice variants (MICU2 (refs. 11,12), MICU3 (ref. 13), and MICU1.1 (ref. 14)), and an essential MCU regulator (EMRE)¹⁵. When co-expressed with MCU, EMRE was shown to be necessary and sufficient to form a functional Ca^{2+} channel and to reconstitute mammalian-like uniporter activity even in yeast mitochondria^{15,16}, which are otherwise incapable of Ca^{2+} uptake^{16–18}.

Altogether, these findings have highlighted a complex multi-meric nature for the mammalian uniporter, whose composition, stoichiometry, and regulation need to be fine-tuned to the physiological demands of each cell and tissue. However, the functional and mechanistic role of each uniporter component and the molecular basis of their interdependence are still unclear. Furthermore, although several observations have pointed to an ancient eukaryotic origin of mt- Ca^{2+} uptake, the identification of several organisms with a different uniporter's composition in different clades have raised interest in understanding the structural basis of uniporter activity^{19–24}. For example, while MCU and MICU1 showed highly correlated evolutionary histories across 138 sequenced eukaryotic organisms, EMRE apparently lacked any homolog outside the metazoan lineage and was therefore suggested to be an animal-specific innovation^{25,26}. Consistently, *Dictyostelium discoideum*, an amoebozoan that diverged earlier than the origin of opisthokonts, expresses both MCU and MICU1 orthologs, which form a functional uniporter in the absence of EMRE¹⁶. Despite the ancient origin of their interaction and the overall observed high co-evolution between MCU and MICU1, most fungi represented an exception to this rule, with most fungal species encoding homologs of MCU but not of MICU1 (refs. 25,26). The identification of MCU as the only uniporter component in Basidiomycota and filamentous Ascomycota (e.g., *Neurospora crassa* and *Aspergillus fumigatus*) has been described as an evolutionary paradox (see ref. 27), but has also been interpreted as indicating that fungal MCUs could be sufficient for mt- Ca^{2+} uptake and regulated independently of MICU1 (refs. 25,26). Based on the assumption of an orthologous relationship between human and fungal MCUs^{25,26,28}, several independent structural studies of Ascomycota MCUs have been performed to understand the basic principles of uniporter channel assembly and function^{21–24}. However, those organisms had been shown to lack uniporter activity^{29,30} and their MCU homologs were unable to mediate mt- Ca^{2+} uptake when heterologously expressed in HeLa or yeast cells^{17,24}. Not surprisingly, significant structural and sequence differences were found between fungal MCUs and their animal counterparts^{20–24}, raising

the question of whether fungal MCUs function as classical Ca^{2+} uniporters at all.

Here, we perform a comprehensive evolutionary analysis of the mt- Ca^{2+} uniporter and show that a gene duplication at the opisthokont common ancestor of animals and fungi resulted in two distinct MCU paralogous clades, differentially retained in the two groups. When only the animal-like clade is considered, we observe fully consistent co-evolutionary patterns between MCU and MICU (MICU1's family), across eukaryotes, and of these with EMRE, across opisthokonts. We find that only three early diverging fungi contain both the fungal paralog and the complete animal-like MCU complex (MCU, MICU, and EMRE). Consistently, we find that the heterologous expression of MCU and EMRE from fungal species with an animal-like MCU complex results in the functional reconstitution of Ca^{2+} uptake in mitochondria of HeLa and yeast cells. Conversely, representatives of the fungal paralogs do not show uniporter activity, suggestive of an alternative function or of the requirement for a yet unidentified regulator. Altogether, our phylogenomic and functional analyses of the mt- Ca^{2+} uptake system demonstrate that MCU, EMRE, and MICU represent the minimal core components of the ancestral opisthokont uniporter and pinpoint key targets for comparative structural and functional studies. Finally, this study also confirms the importance and power of thorough evolutionary analyses to understand the molecular basis of functional interactions within a protein complex.

Results

The mitochondrial calcium uniporter evolution. We assessed the evolution of each uniporter component across 1156 fully-sequenced eukaryotic genomes (see Supplementary Data 1), using a combination of profile-based sequence searches, protein domain composition assessment, and phylogenetics. As shown in Fig. 1 (Supplementary Fig. 1), the overall taxonomic distributions of MCU and MICU1 homologs were largely congruent with that of previous genomics surveys^{25,26}. We confirmed the presence of MCU in at least some species of the major eukaryotic groups (Unikonts, the SAR clade, Plants, and Euglenozoa), and its absence in all sequenced Apicomplexans, Microsporidia, *Trichomonas*, and *Giardia*, and all yeasts in Saccharomycotina and most in Schizosaccharomycetes. Hence, mt- Ca^{2+} uptake appeared to have been lost many times independently during the evolution of eukaryotes. A significant number of these losses correlated with extreme streamlining of mitochondrial metabolism, as most MCU/MICU-lacking lineages encompassed relict forms of anaerobic mitochondria, such as mitosomes (microsporidians, *Entamoeba*, *Giardia*, *Cryptosporidium*) or hydrogenosomes (*Trichomonas*)³¹. Our homology-based results confirmed the above-mentioned anomaly that most fungal genomes, for which our dataset is particularly rich—776 species as compared to 50 in previous studies^{25,26}—encode for MCU but not MICU or EMRE. Unexpectedly, our analysis uncovered the presence of EMRE outside Holozoa, identifying reliable orthologs in three chytrid fungi—an early diverging zoosporic fungal lineage: *Allomyces macrogynus*, *Catenaria anguillulae*, and *Spizellomyces punctatus*. Additional searches in public databases confirmed that EMRE was not present in other sequenced fungi.

To clarify the underlying evolutionary history of the uniporter, we reconstructed and inspected the molecular phylogenies of MCU (Fig. 2a, Supplementary Fig. 2a) and MICU1 (Fig. 2b, Supplementary Fig. 2b) homologs across eukaryotes. We found that the evolution of both MCU and MICU gene families was driven by numerous gene duplications and losses, some of them having occurred in parallel in different lineages, implying an ancient and tight functional relationship. Furthermore, we

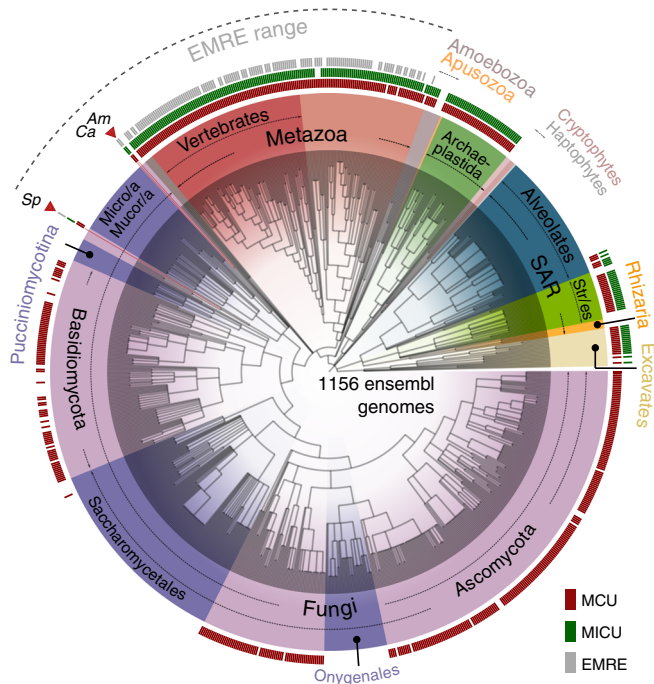


Fig. 1 Phylogenetic distribution of mt-Ca²⁺ uniporter protein families.

The phylogenetic distribution of MCU (red), MICU (green), and EMRE (gray) homologs across 1156 eukaryotic genomes is shown on the NCBI taxonomy tree. Viridiplantae and Rhodophyta (red algae) have been grouped together as Archaeplastida, and alveolates, stramenopiles (Str/es), and rhizarians as the SAR clade. In all cases where data from various strains of a species are present with the same pattern, these have all been collapsed to the species level, resulting in 969 terminal nodes shown. The mt-Ca²⁺ uniporter complex has been completely lost in Apicomplexa within Alveolates, Rhizaria (5 genomes), red algae (3 genomes), Cryptophytes (3 genomes), Haptophytes (1 genome), and the Entamoeba clade within Amoebozoa. Within fungi (in purple), all major clades that have completely lost MCU homologs are indicated with a darker purple color, namely Onygenales, Saccharomycetales, Pucciniomycotina, Mucoromycotina (Mucor/a), and Microsporidia (Micro/a). The only three early diverging fungal species (*A. macrogynus*-Am, *C. anguillulae*-Ca, *S. punctatus*-Sp) that encode also MICU and EMRE are highlighted with a red arrowhead. The NCBI taxonomy and the presence/absence profile were visualized using the ETE toolkit⁴¹. For a version of the profile, which includes the species names, see Supplementary Fig. 1.

showed that evolutionary-independent duplications at the base of several main eukaryotic lineages—vertebrates, streptophytes, oomycetes, kinetoplastids, and ciliates—resulted in the existence of multiple MCU paralogous copies in each of these clades. As a result, orthology relationships within the MCU gene family are complex and of the type many-to-many³². This means, for instance, that human MCU and MCUB are equally distant evolutionarily (co-orthologous) to each non-vertebrate animal MCUs, and also to all MCUs from protists and plants, explaining why *Trypanosoma*'s MCUB does not functionally complement human MCUB^{33,34}. It also implies that shared physical interactions between paralogous MCU proteins in hetero-oligomers in different organisms, as shown for human and *Trypanosoma brucei* MCUB proteins^{10,33,34}, are the result of parallel evolution. Importantly, one duplication event in the MCU gene family occurred in the common ancestor of opisthokonts and was followed by differential losses that distinguished Holomycota (fungi and their relatives, including *Fonticula alba*) from the other opisthokonts, i.e. the Holozoa (animals and their unicellular

close relatives). Most fungal species kept only one of the two MCU paralogs that is referred here as the fungal-specific MCU paralog (MCUP). Holozoa, instead, retained the other MCU paralog, the bona-fide animal MCU. Only three chytrid fungi in our dataset, *A. macrogynus*, *C. anguillulae*, and *S. punctatus* retained both the MCUP and the animal MCU, and these are also the only fungi encoding MICU1 and EMRE homologs. This striking, previously undetected, co-evolution pattern between MCU, MICU, and EMRE in chytrids suggests a strong interdependence, and even stronger considering that Blastocladales (*Allomyces* and *Catenaria*) and *Spizellomyces* do not form a monophyletic clade³⁵. Based on these findings, we hypothesized that these animal-like MCUs present in chytrids should require EMRE to drive mt-Ca²⁺ uptake, similarly to their human ortholog.

Reconstitution of mt-Ca²⁺ uptake by chytrid MCU and EMRE.

The above-mentioned finding of bona-fide EMRE orthologs in these three chytrids (Fig. 1) placed back the origin of an animal-like mt-Ca²⁺ uptake in the opisthokont ancestor, preceding the diversification of animals and fungi. Consistently, the heterologous expression of MCU from *Dictyostelium discoideum*, representing an amoebozoan lineage that diverged earlier than the origin of opisthokonts, is alone sufficient to reconstitute mt-Ca²⁺ uptake in yeast mitochondria, while human (Hs-) MCU only does so in the presence of EMRE¹⁶. Similarly, we hypothesized that co-expression of animal MCU and EMRE proteins from chytrids would be necessary and sufficient to reconstitute uniporter activity. The phylogenetic distribution profile (presence/absence) across the MCU complex components revealed a strong co-evolution pattern, when only the true orthologous sequences were considered (Fig. 3a). Strikingly, we detected mt-Ca²⁺ uptake in yeast strains expressing animal MCUs from either *A. macrogynus* (Am-MCUa) or *S. punctatus* (Sp-MCU) with their respective EMREs (Am-EMRE1-2, Sp-EMRE) (Fig. 3b, c, Supplementary Fig. 3). Particularly, in *A. macrogynus* that encodes two MCU proteins, Am-MCUa and Am-MCUB, mt-Ca²⁺ uptake activity was detected only for the former, and showed different efficiency with its two encoded EMRE variants (Am-EMRE1 higher than Am-EMRE2). In contrast, we did not detect any mt-Ca²⁺ uptake in yeast strains expressing MCUP proteins from *A. macrogynus* (Am-MCUP1) and *S. punctatus* (Sp-MCUP), despite proper expression and localization (Supplementary Fig. 3, Supplementary Fig. 4). Similar results would be expected in other Holozoa despite the inability to detect EMRE by similarity searches. Indeed, the co-expression of MCU from the sea anemone *Nematostella vectensis* (Nv-MCU) with Hs-EMRE in yeast was able to reconstitute mt-Ca²⁺ uptake to a similar extent of a strain expressing Hs-MCU and Hs-EMRE (Supplementary Fig. 5). These results, together with the absence of MICU proteins in most fungal lineages, indicate that mt-Ca²⁺ uptake in fungal mitochondria, if it exists, is not mediated by MCUPs, or that a different—yet unknown—regulator is necessary. Instead, animal-like MCUs from chytrid fungi and Holozoa function similarly to the mammalian uniporter, in an EMRE-dependent fashion. Altogether, our evolutionary analyses and experimental results confirmed that MCU-EMRE interaction is conserved, and was already present in the last common ancestor of fungi and animals.

Consistent with our hypothesis that MCUPs do not represent true functional orthologs of Hs-MCU, when comparing MCU sequences across eukaryotes we found that MCUPs lacked key residues conserved in the animal-like MCUs, despite retaining a DXXE motif (Fig. 4a, Supplementary Fig. 6a). Those residues have been previously shown to be important for MCU function and its interaction with EMRE³⁶. Notably, animal and chytrid

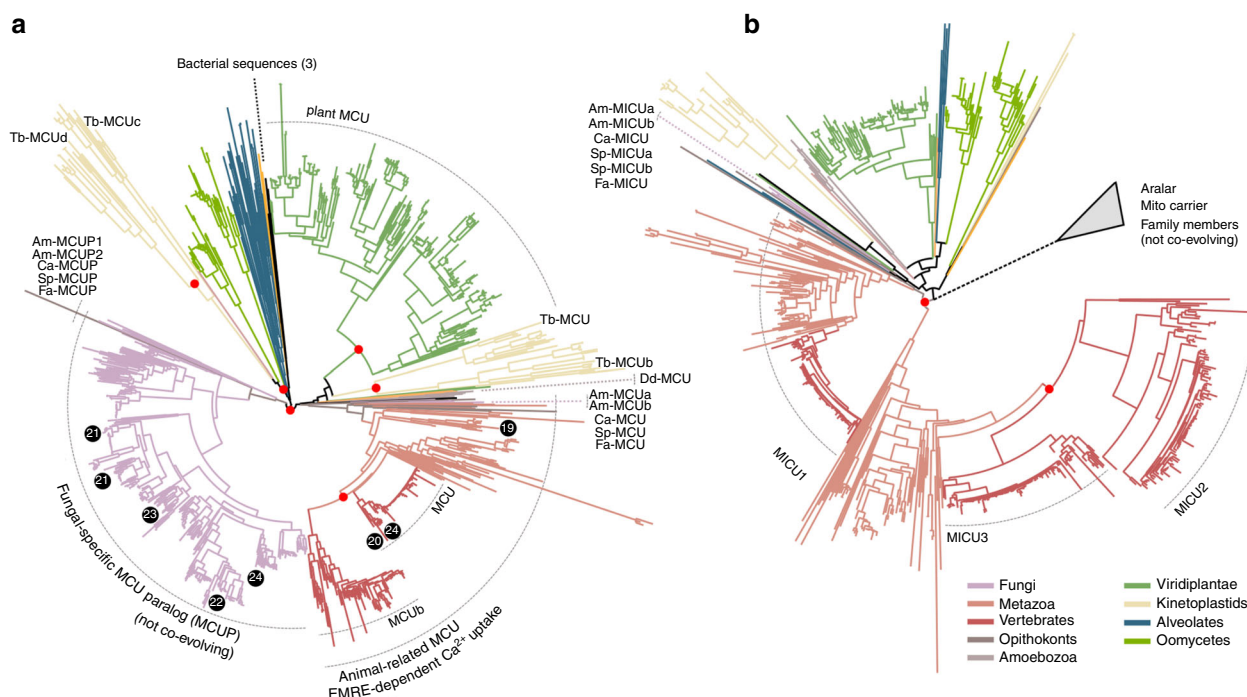


Fig. 2 The fungal-specific MCU is a paralogous distinct phylogenetic clade. Maximum Likelihood phylogenetic trees of MCU (a) and MICU (b) families. The two families have been expanded through duplication rounds in various independent lineages. Major duplication events are indicated with a red sphere on the relevant tree node. The co-occurrence between the two families is almost perfect, if only the true orthologous sequences are considered. MCUP (fungal-specific MCU paralog) and Aralar (MICU distant homolog) sequences are not co-evolving with MCU and MICU, respectively (see also Methods). In both a and b names and relative positions in the trees of members from Holomycota and few other representative species are shown. The main sub-families (MCU/MCUB and MICU1/2/3) are named after the human/mouse sequences within the phylogenetic clades. The phylogenetic positions of MCUs or MCUPs from published structural data are shown in black circles, and the numbers refer to the publication reference. The number of bacterial sequences included in the tree is indicated in brackets. The raw phylogenetic trees in newick format are provided in Supplementary Data 2.

EMREs appeared highly divergent (Fig. 4b, Supplementary Fig. 6b), although the MCU interacting domain GXXXA/S/G and the polyaspartate tail necessary for the binding to MICU1 (ref. 36) were fully conserved. Interestingly, the fungal EMRE sequences contained an extra C-terminal domain that was not found in Holozoa, suggesting some degree of specialization. Thus, we hypothesized that Am-MCUa and Sp-MCU would have evolved to interact with EMRE proteins from the same or related species. To this goal, we measured mt- Ca^{2+} uptake in HeLa cells infected with lentiviral particles expressing either Hs-MCU or Am-MCUa and Sp-MCU (Supplementary Fig. 7a). Those proteins were expressed in addition to the endogenous Hs-MCU and Hs-EMRE. We found that mt- Ca^{2+} uptake in HeLa cells expressing either Am-MCUa or Sp-MCU was similar to uninfected control cells in response to histamine, differently from the overexpression of Hs-MCU, which resulted in a gain-of-function phenotype. We then measured mt- Ca^{2+} uptake in HeLa cells where MCU was stably knocked-down (sh-MCU) (Supplementary Fig. 7b). Here, we either re-introduced Hs-MCU or fungal MCU homologs (MCU and MCUP). As expected, the re-introduction of Hs-MCU resulted in a complete rescue of mt- Ca^{2+} uptake, which was similar to uninfected control cells (pLKO). Instead, unlike Hs-MCU, all the fungal MCUs and MCUPs were unable to rescue mt- Ca^{2+} uptake despite showing proper expression and insertion into the inner mitochondrial membrane (Supplementary Fig. 8), with a peak concentration of mt- Ca^{2+} similar to that of cells with MCU knock-down, due to the absence of a fungal EMRE. Furthermore, the expression of Am-MCUa and Sp-MCU in yeast mitochondria was unable to

reconstitute mt- Ca^{2+} uptake in the presence of Hs-EMRE (Fig. 4c, Supplementary Fig. 9). Instead, Hs-MCU was functional when co-expressed with either Am-EMRE or Sp-EMRE (Fig. 4d, Supplementary Fig. 9). Altogether, these results suggested that the C-terminal domain of chytrid EMREs was dispensable for a functional interaction with Hs-MCU but necessary to activate animal-like fungal MCUs. Accordingly, we observed that the co-expression of Am-MCUa and Sp-MCU with Am-EMRE and Sp-EMRE lacking the extra C-terminal domain (EMRE-t) was unable to efficiently reconstitute mt- Ca^{2+} uptake (Fig. 4e, Supplementary Fig. 10a). However, while the fusion of Hs-EMRE with this extra chytrid C-terminal domain did not affect the function of Hs-MCU and thus of mt- Ca^{2+} uptake, it was not sufficient to reconstitute mt- Ca^{2+} uptake when co-expressed with Am-MCUa and Sp-MCU (Fig. 4f, Supplementary Fig. 10b). On the one hand, these findings hint at a possible activating role of the extra C-terminal domain of the fungal EMRE for the efficient regulation of animal-like MCUs function. On the other hand, they suggest that functional domains that are conserved between fungal and human EMREs are sufficient to regulate Hs-MCU activity.

Discussion

Altogether, our identification of a strong co-evolution pattern between MCU, MICU, and EMRE provides an explanation to an elusive evolutionary paradox: the presence of uniporter homologs in species with MCU but no MICU1 homologs and no detectable mt- Ca^{2+} uptake^{25,26}. We demonstrate that an animal-related MCU complex has been lost early within the evolution of most fungal clades, which retained only fungal-specific paralogous

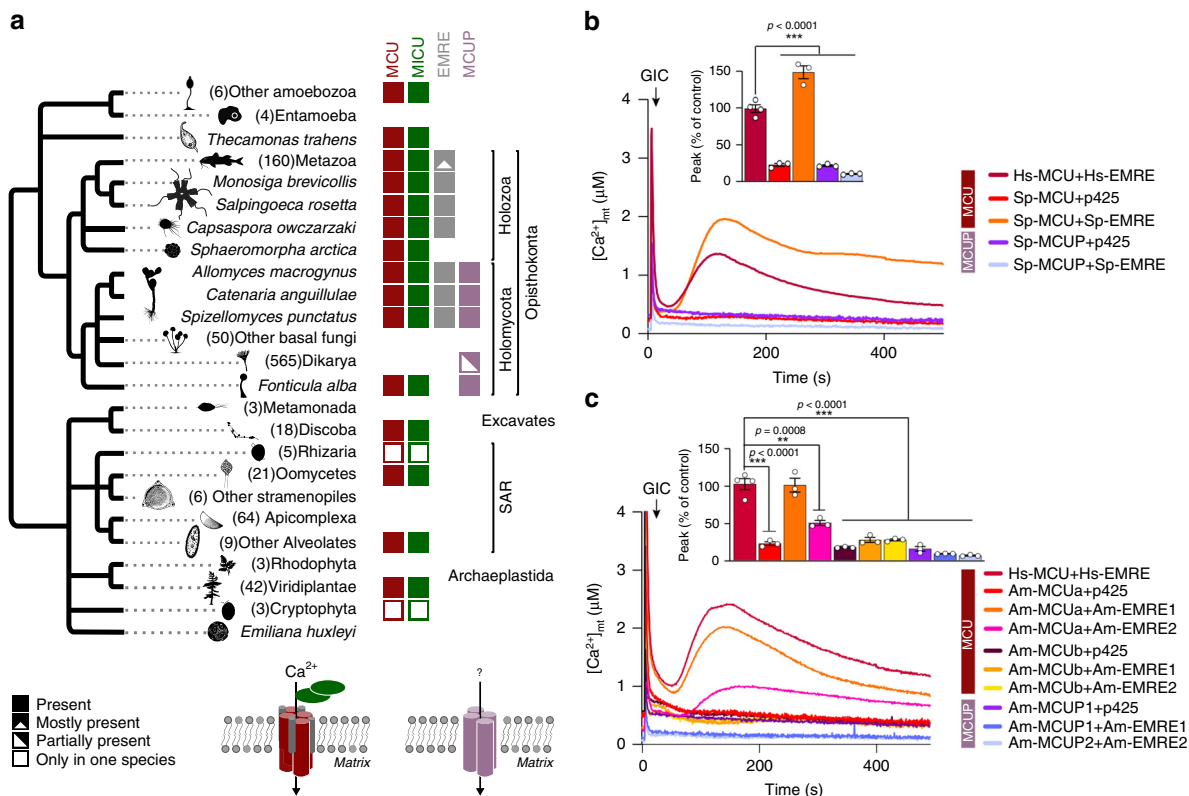


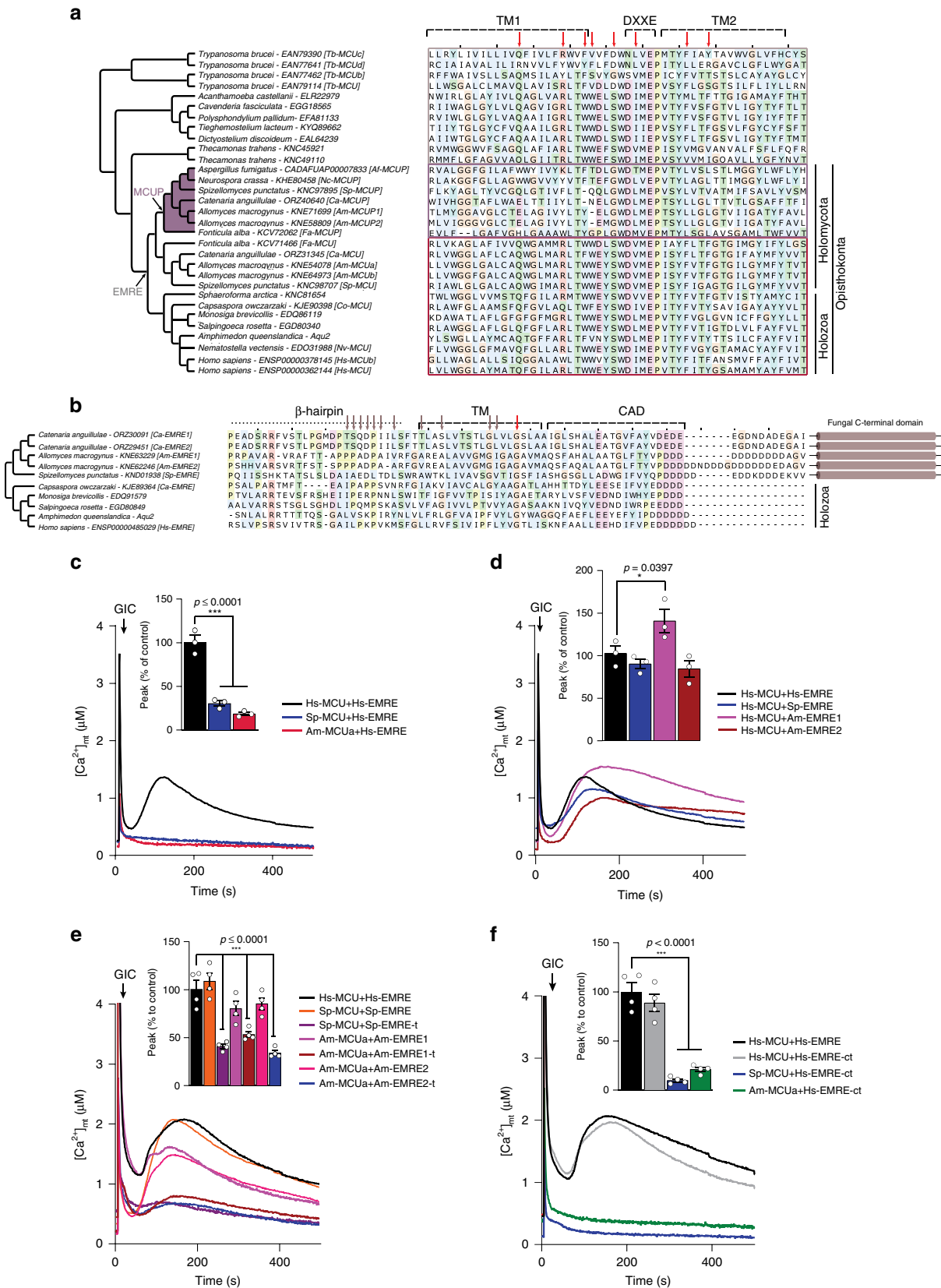
Fig. 3 Functional reconstitution of mt-Ca²⁺ uptake by fungal MCU and EMRE homologs. **a** Phylogenetic distribution profile (presence/absence) across MCU complex components. The distribution pattern of MICU (across eukaryotes) and EMRE (in opisthokonts) largely overlaps with that of the animal-like MCU, but not the MCUP. **b, c** Representative traces and quantification of mt-Ca²⁺ transients in yeast cells expressing human MCU and EMRE (n = 4) or animal-like or fungal-specific MCU orthologs from *S. punctatus* (n = 3) (b) and *A. macrogynus* (n = 3) (c) with either their respective EMRE proteins or empty vector (p425) upon glucose-induced calcium (GIC) stimulation in presence of 1 mM CaCl₂. All data represent mean ± SEM. P values are indicated in the different panels (b, c) ***p < 0.0001, one-way ANOVA with Dunnett's multiple comparisons test. The silhouette images in a representing the different lineages were downloaded from PhyloPic (<http://phylopic.org/>) or wikipedia (<https://www.wikipedia.org/>), or designed by A.A.P. in Inkscape (<https://inkscape.org/>). All downloaded images were available for reuse under a Public Domain license and do not require attribution. Source data of b and c are provided as a Source Data file.

MCU proteins (MCUPs). These MCUPs, which are paralogous to Hs-MCU, have been so far wrongly considered functionally equivalent to Hs-MCU and deeply studied for this reason. This is the case, for instance, of the Ascomycota MCUP proteins (e.g., *N. crassa*) that have been recently used as models for understanding structure and regulation of the human uniporter channel^{20–24}. Consistently, we and others find that fungal MCUPs are unable to reconstitute or rescue mt-Ca²⁺ uptake in yeast or HeLa cells lacking MCU, respectively^{17,24,29}. Similarly, the same fungal MCUP sequences used for investigating structure and function of the mammalian uniporter^{21,22,24} failed to mediate mt-Ca²⁺ uptake when expressed in yeast mitochondria or in MCU knockout HeLa cells (Supplementary Fig. 11). Instead, we show that only fungal species having both MCU and EMRE sequences (animal-like MCUs), such as *A. macrogynus* and *S. punctatus*, are able to mediate mt-Ca²⁺ uptake. Those observations together with the significant structural and sequence differences found between MCUs and MCUPs²⁰ question whether fungal MCUPs function as classical Ca²⁺ uniporters.

The remarkable presence/absence pattern across eukaryotes of MCU and MICU—when only the orthologs of the two protein families are considered—indicates strong co-evolution and functional interdependence. Indeed, MICU1 plays a key role in regulating the gating and activation properties of MCU⁹. Thus, the evolutionary coupling of uniporter's gating mechanism with its regulator suggests a dependency on MICU for Ca²⁺

homeostasis and cell physiology. Consistently, across the 1156 species in our analysis, MCU and MICU co-occur in 1144 (~99%), whereas only 12 species have one of the two components. Most such incongruencies are likely to result from assembly, annotation, or identification errors. In fact, we expect MICU to be encoded in all species with a functional MCU complex, with the only likely exception being Onchocercidae, a family of parasitic nematodes. In our dataset all three species in the clade (*Brugia malayi*, *Onchocerca volvulus*, and *Loa loa*) appear to lack MICU1 homologs in the presence of MCU (Supplementary Fig. 1), raising the possibility that MICU is indeed lost in the clade rather than being undetected. If this preliminary observation is confirmed, this would make these parasites interesting targets to explore further the physiological significance of MICU1.

Our phylogenomic analysis identifies non-metazoan EMRE sequences and demonstrates the ancestrally essential role of EMRE in mt-Ca²⁺ homeostasis. Our results imply that EMRE, previously thought to be an animal-specific innovation^{15,16,27}, formed part of an animal-like machinery in the common ancestor of opisthokonts, and was lost secondarily in the evolution of fungi, together with the other components of the animal-like mt-Ca²⁺ uptake machinery (Fig. 5). These results have major implications for structural and functional studies of the uniporter. Indeed, members of the orthologous MCU complex in basal fungi constitute relevant targets for future research and comparative structural analyses, particularly for identifying key MCU–EMRE



interactions. Our results show that human MCU can function in the presence of both human and chytrid EMREs, whereas chytrid MCUs such as Am-MCUa and Sp-MCU can only reconstitute mt- Ca^{2+} uptake when co-expressed with their corresponding

chytrid EMREs. These findings indicate a tight co-evolution between MCU and EMRE proteins, which we know to functionally and physically interact, and provide the framework to understand the sequence determinants of this interaction. Finally,

Fig. 4 Evolution of MCU-EMRE interaction. **a, b** Phylogenetic trees of members of MCU (**a**) and EMRE (**b**) protein families, and sequence diversity of major domains. The sequence alignment of TM1 and TM2 of MCU sequences from 20 species is shown in **a**. The program Multi-Harmony⁴³ was used to detect residues that are overall conserved but differ in the MCUP members (highest scoring positions are indicated with red arrows). The MCUP clade is shown in purple. The evolutionary point where the MCU proteins become EMRE dependent is shown in gray. The degree of conservation across the animal-related MCU members is very high in these loci, while few positions are Holomycota or Holozoa specific. Similarly, in **b** EMRE's sequence diversity across opisthokonts is shown for the β -hairpin, the TM, and CAD domain. Residues found important for the interaction between MCU and EMRE in ref. ²⁰ and fully conserved positions are indicated with gray and red arrows, respectively. **c–f** Representative traces and quantification of mt- Ca^{2+} transients in yeast cells expressing either human and animal-like *S. punctatus* and *A. macrogynus* MCU with human EMRE ($n = 3$) (**c**), species-specific EMRE with human MCU ($n = 3$) (**d**), animal-like *S. punctatus* and *A. macrogynus* MCU with their respective wild type or truncated (-t) EMREs ($n = 4$) (**e**) or with human EMRE fused to the chytrid extra C-terminal domain ($n = 4$) (**f**) upon glucose-induced calcium (GIC) stimulation in the presence of 1 mM CaCl_2 . All data represent mean \pm SEM. *P* values are indicated in the different panels (**c, e, f** *** $p < 0.001$, one-way ANOVA with Dunnett's multiple comparisons test; **d** * $p = 0.012$, one-way ANOVA with Dunnett's multiple comparisons test). Source data for **c–f** are provided as a Source Data file.

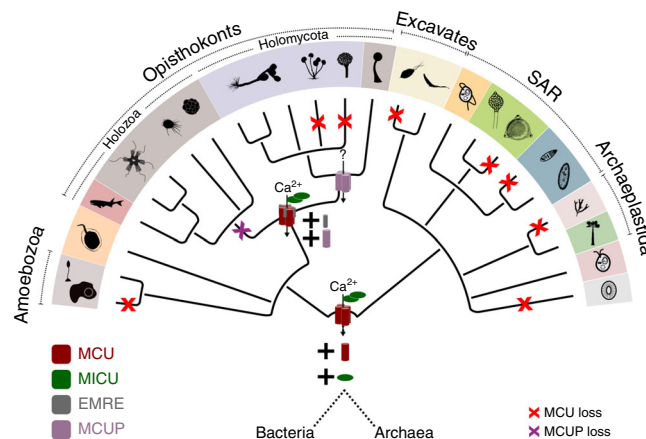


Fig. 5 Schematic representation of the evolution of the MCU complex in eukaryotes. Changes in the composition of the uniporter complex are shown in the respective taxonomic levels. The MCU-MICU complex emerges at the origin of eukaryotes, followed by the addition of EMRE in opisthokonts. MCUP is only found in Holomycota. Losses of MCU in the various eukaryotic lineages are indicated in red and the loss of MCUP in Holozoa in purple. The color code is the same as in Fig. 1, and the taxonomic tree structure and silhouette images of the different taxonomic groups are as in Fig. 3a.

our work underscores that accurate phylogenomic analyses can resolve apparent evolutionary riddles while making explicit functional predictions that can drive future experiments.

Methods

Sequence data and homology searches. The protein sequences encoded in 1156 completely sequenced eukaryotic genomes were retrieved from Ensembl DB v91, and v37 of Ensembl Metazoa, Plants, Fungi, and Protists (see Supplementary Data 1). Only the genome of *Catenaria anguillulae* PL171 was added from Ensembl Fungi v41. For each of the protein families studied, homologs were selected on the basis of sequence similarity and phylogenetic analysis. HMMER searches were performed using HMMER 3.1b2 (ref. ³⁷) and using the Gathering Cut-Off threshold (-cut_ga) when the raw HMM profile from Pfam was used, an *e*-value threshold of 10^{-2} otherwise. For all BLAST searches low-complexity regions in the query sequence (default parameter) were filtered out to minimize the number of false positives and an *E*-value threshold of 10^{-5} was used. Conserved domains in all retrieved sequences were annotated using the HMM profiles of Pfam release 30.0. For MCU, proteins in our database containing at least one MCU (Pfam: PF04678 [<https://pfam.xfam.org/family/PF04678>]) domain were detected using an HMMsearch. In total, 1076 protein sequences were selected for subsequent analysis. For MICU, 2105 protein sequences were retrieved from a BLAST search using Hs-MICU1 (Uniprot: Q9BPX6 [<https://www.uniprot.org/uniprot/Q9BPX6>]) as a query. HMMscan was used to search for additional domains in the retrieved sequences using all the Pfam domain profiles, and all the sequences with detected at least one Mito_carr domain (Pfam: PF00153 [<https://pfam.xfam.org/family/PF00153>]) were classified as the members of the mitochondrial carrier family (slc25a12-Aralar homologs). The Aralar-related sequences (Mito_carr domain containing) were clustered together clearly as a monophyletic clade in a phylogenetic tree, in the exclusion of known MICU sequences, and were excluded. The remaining 651 MICU sequences were re-aligned and a new phylogenetic tree with the same methods was reconstructed. EMRE sequences are characterized by a DDDD (Pfam: PF10161 [<https://pfam.xfam.org/family/PF10161>]) domain. Their short length and low sequence conservation makes detection strikingly difficult, which explains why in some cases EMRE appears to be missing even from some

animal genomes. HMMER searches with the “gathering” (-cut_ga) threshold were performed, and all detected homologs were retrieved and re-aligned, for a new HMM profile to be built and used to search back the genome database in a second iteration. One EMRE sequence was detected in *A. macrogynus* in the first search, while one more sequence in the same species, as well as in *S. punctatus* and *C. anguillulae*, were detected in the second iteration. The detected EMRE sequences in this second iteration are those that were further considered for all analyses. For NCLX (NCKX6), the Na_Ca_ex Pfam domain was initially used to retrieve protein sequences. However, this domain characterizes a ubiquitous superfamily of sodium/calcium exchangers that regulate intracellular Ca^{2+} concentrations in many cell types. Therefore, selection of NCKX6 (NCLX) homologs based on the Na_Ca_ex Pfam domain using HMMER returned 4024 hits. To narrow down the number of hits for more accurate alignment and phylogenetic reconstruction, we used the human NCLX sequence as a query (uniprot: Q6J4K2 [<https://www.uniprot.org/uniprot/Q6J4K2>]) for a blast search, retrieving 2105 sequences for phylogenetic analysis. Using the human members as reference, 1391 sequences across eukaryotes were selected as related to the NCLX clade (NCLX orthologs).

Phylogenetic analysis. Sequences of all the protein families described were aligned, and the alignment was trimmed and used to compute a phylogenetic tree. The selected homologous proteins were aligned with MAFFT v7.394 (ref. ³⁸) (E-INS-I for MICU, EMRE, and NCLX families and L-INS-i for the MCU family, based on their multi/single-domain architecture) and a soft trimming was applied, filtering out positions in the alignment with gaps in more than 99% of the sequences using trimAl³⁹ (-gt 0.01). IQ-TREE v1.6.8 (ref. ⁴⁰) was used to derive Maximum Likelihood (ML) trees. LG was selected as the base model to test all rate-heterogeneous models using the “-mset LG” parameter (26 protein models, combinations of invariable sites +I, discrete Gamma model with 4 rate categories +G, the FreeRate model +R with 2–10 categories, and empirical AA frequencies estimated by the data). The best-fit models, chosen according to the Bayesian information criterion (BIC), were LG + R10 for the MCU and MICU alignments and LG + F + R10 for NCLX alignment. Branch supports were obtained using the ultrafast bootstrap implemented in the IQ-TREE program with 1000 replicates. The ETE Toolkit⁴¹ was used for all taxonomic and phylogenetic tree operations and visualization. Sequence alignments were visualized using Jalview2 (ref. ⁴²), and

the Multi-Harmony⁴³ method was used identify patterns of variation across the different protein clades, positions conserved across the animal MCUs and the animal-like fungal MCUs but not in the MCUPs. Raw phylogenetic trees in newick format can be found in Supplementary Data 2.

Cell lines. HeLa cells stably expressing a wild-type mitochondrial matrix-targeted GFP-aequorin (mt-AEQ) were generated as in ref. ¹⁸. Mt-AEQ HeLa cells stably overexpressing Hs-MCU, Sp-MCUP, Sp-MCU, Am-MCUP1, Am-MCUa, Am-MCUB, Af-MCUP, and Nc-MCUP from the pLX304 lentiviral vector were then generated by viral transduction according to the manufacturer's instructions. MCU knock-down mt-AEQ HeLa cells were generated by viral transduction using a pLKO vector expressing an shRNA targeting Hs-MCU (sh-MCU; Sigma-Aldrich, TRCN0000133861). Control cells were generated using the empty vector pLKO (Addgene #8453). Mt-AEQ MCU knockout (MCU-KO) HeLa cells transiently expressing Hs-MCU, Ce-MCUP, Fg-MCUP, Ma-MCUP, and Nf-MCUP from the pLX304 lentiviral vector were generated by transfection using the X-tremeGene HP DNA transfection reagent (Roche), according to the manufacturer's instructions. cDNAs for Sp-MCUP, Sp-MCU, Am-MCUP1, Am-MCUa, Am-MCUB, Ce-MCUP, Fg-MCUP, Ma-MCUP, and Nf-MCUP expression without a stop codon were codon optimized for human expression, synthesized de novo in the PuC57 vector, and amplified with flanked attB1 and attB2 sites by PCR (see Supplementary Table 1). PCR products were first integrated into the pDONR221 vector and then into the pLX304 destination vector by site-specific recombination according to the manufacturer's instructions (Life Technologies). All cell lines were grown in high-glucose Dulbecco's modified Eagle's medium supplemented with 10% FBS at 37 °C and 5% CO₂.

Yeast strains. A yeast strain expressing mt-AEQ with Hs-MCU and Hs-EMRE was generated as in refs. ^{17,18}. To generate yeast strains co-expressing mt-AEQ together with different combinations of fungal and human MCU and EMRE orthologs, cDNAs were amplified from the pLX304 vector (see Supplementary Table 2) and cloned into the yeast expression plasmids p423GPD (Hs-MCU, Sp-MCUP, Sp-MCU, Am-MCUP1, Am-MCUa, Am-MCUB, Ce-MCUP, Fg-MCUP, Ma-MCUP, and Nf-MCUP) and p425GPD (Hs-EMRE, wild-type and C-terminal domain truncated Sp-EMRE, Am-EMRE1, and Am-EMRE2, and Hs-EMRE with an addition of chytid C-terminal domain from Sp-EMRE). The YPH499 strain was then transformed with the respective plasmids and transformants were selected on synthetic dextrose plates, with adenine, lysine, and tryptophan as selection markers.

MCU knockout in HeLa cells. Mt-AEQ HeLa cells with knockout of MCU were generated by CRISPR targeting⁴⁴. In brief, a cDNA encoding NLS-Cas9 was isolated from pX330 (Addgene #42230) by *EcoRI* digestion and cloned upstream of the ubiquitous CAG promoter. Two sets of single-guide RNA (sgRNA) were designed using an online tool CRISPOR (MCU-KO1 gRNA: 5'-CACCGC AGGAGCGATCTACCTGCGG-3'; MCU-KO2 gRNA: 5'-CACCGTGAAGTGAC AGCGTTACAGC-3'). For each sgRNA, complementary oligonucleotides containing the target sgRNA sequences were annealed and cloned into the *BbsI* site of the pX330-Puro-ccdB vector⁴⁵. After which, pX330-Puro-ccdB vector containing sgRNAs were transfected into mt-AEQ HeLa cells using the Lipofectamine 3000 Reagent (Life Technologies), according to the manufacturer's instructions and selected with 2 µg/ml puromycin for 2 days. Cells were then seeded at a density of 1 cell per well and expanded. Gene knockout was screened by PCR (MCU-KO Forward1: 5'-GCGTGTAGTTGAGAGTTACAGC-3'; MCU-KO Forward2: 5'-TT TTATAGCCAGTTCACAGAATAAAGCT-3'; MCU-KO Reverse: 5'-GTTTCATCC TTGCTCATGGCATT-3') and confirmed by sequencing and western blot using the following antibodies: anti-MCU (Sigma-Aldrich, HPA01648, 1:1000), anti-EMRE (Santa Cruz Biotechnology, sc-86337, 1:1000), anti-ACTIN (Sigma-Aldrich, A2228, 1:5000).

Isolation of crude mitochondria from HeLa cells. Crude mitochondria were isolated from HeLa cells as described¹⁷. Briefly, HeLa cells were grown to confluency, rinsed with PBS, and resuspended in ice-cold isolation buffer (IB: 220 mM mannitol, 70 mM sucrose, 5 mM HEPES-KOH pH 7.4, 1 mM EGTA-KOH pH 7.4, protease inhibitors). Cells were permeabilized by nitrogen cavitation at 600 psi for 10 min at 4 °C and then centrifuged at 600 × g for 10 min. The supernatant was transferred into new tubes and centrifuged at 8000 × g for 10 min at 4 °C. The resulting pellet containing crude mitochondria was resuspended in IB for protein topology analysis.

Analysis of mitochondrial protein topology. Proteinase K (PK) protection assay was performed on mitochondria isolated from HeLa cells¹⁷. Roughly, 30 µg of freshly isolated mitochondria were gently resuspended in 30 µl of IB buffer with either increasing concentrations of digitonin or 1% Triton X-100 in the presence of 100 µg/ml PK and incubated at room temperature for 15 min. The reaction was stopped by the addition of 5 mM PMSF, followed by incubation on ice for 10 min. Samples were mixed with 10 µl of 4× Laemmli buffer containing 10% 2-mercaptoethanol and boiled for 5 min at 98 °C for immunoblot analysis. Immunoblotting was performed according to the standard procedures using the following

antibodies: anti-V5 (Life Technologies, R96025, 1:5000); anti-TIM23 (BD Bioscience, 611222, 1:5000); anti-TOM20 (Abcam, ab56783, 1:1000); anti-Cyclophilin D (Cyp D) (Abcam, ab110324, 1:1000). TOM20, TIM23, and Cyp D were used as controls for integral mitochondrial outer membrane, inner membrane, and soluble matrix-targeted proteins, respectively.

Subcellular fractionation of yeast cells. Expression and subcellular localization of heterologous expressed proteins in yeast was tested by immunoblot analysis of cytosolic and mitochondrial fractions isolated from recombinant yeast strains¹⁷. Briefly, yeast cells were grown at 30 °C in a selective lactate medium supplemented with the respective selection markers till an OD ~0.8. The cell pellet was resuspended in a buffer containing 0.6 M sorbitol, 20 mM HEPES/KOH pH 7.2, 80 mM KCl, and 1 mM PMSF, and vortexed five times for 30 s with glass beads (425–600 µm diameter), with a 30 s cooling interval in between to break cell wall and plasma membrane. After the first centrifugation step at 1000 × g for 5 min at 4 °C, the supernatant was further centrifuged at 20,000 × g for 10 min at 4 °C to obtain the mitochondrial fraction (pellet). The supernatant (cytosolic fraction) was precipitated with trichloroacetic acid at –20 °C for 1 h, washed once with cold acetone, and centrifuged at 20,000 × g for 10 min at 4 °C. Both cytosolic and mitochondrial fractions were analyzed with immunoblotting according to the standard procedures using the following antibodies: anti-MCU (Sigma-Aldrich, HPA016480, 1:1000); anti-EMRE (Santa Cruz Biotechnology, sc-86337, 1:1000); anti-V5 (Life Technologies, R96025, 1:5000); anti-AEQ (Merck/Millipore, MAB4405, 1:1000); anti-YME1; anti-PGK1 (Life Technologies, 459250, 1:10,000).

Measurements of mitochondrial calcium uptake in yeast and HeLa cells. In vivo analyses of mitochondrial Ca²⁺ uptake in intact yeast and HeLa cells were performed using an aequorin-based measurement⁴⁶. Aequorin is widely used as a genetically encoded Ca²⁺ indicator (GECI) for measurements of mt-Ca²⁺ kinetics because it offers several advantages. Besides being targeted with precision to the organelle, it functions over a wide range of Ca²⁺ concentrations, and shows low buffering capacity, despite achieving a limited spatial resolution compared to fluorescent GECIs⁴⁶. Briefly, yeast cells were collected at an OD ~0.8, washed three times with milliQ water, and starved for 1.5 h at room temperature in a nutrient-free buffer (NFB, 100 mM Tris, pH 6.5 (1 × 10⁸ cells per ml). Afterwards, cells were collected at 3500 r.p.m. for 5 min and resuspended in NFB to a higher density (25 × 10⁸ cells per ml) in the presence of 50 µM native coelenterazine (Abcam, ab145165) to reconstitute the photoprotein aequorin. After 30 min in the dark at room temperature, 0.5 × 10⁸ cells per well were plated into a white 96-well plate and Ca²⁺-dependent light kinetics was recorded upon stimulation with 1 mM CaCl₂ and 100 mM glucose, at 469 nm every 0.5 s interval in a MicroBeta2 LumijET Microplate Counter. At the end of each experiment, cells were lysed with 1 mM digitonin for 5 min at 37 °C and any residual aequorin counts were collected upon the addition of CaCl₂ to a final concentration of 140 mM. For mt-Ca²⁺ uptake measurement in mt-AEQ HeLa cells, those were seeded at 25,000 cells/well of white 96-well plates in growth medium overnight. Afterwards, mt-AEQ was reconstituted with 2 µM native coelenterazine for 2 h at 37 °C and Ca²⁺-dependent light kinetics were recorded upon 100 µM histamine stimulation at 469 nm every 0.1 s interval. At the end of each experiment, cells were lysed with a solution containing 0.5% Triton X-100 and 10 mM CaCl₂ to record the released residual aequorin counts.

Quantification of calcium transients. Quantification of mt-Ca²⁺ concentration was performed using a MATLAB software as in ref. ¹⁸. The dynamics of mt-Ca²⁺-dependent luminescence signal was smoothed by the cubic spline function:

$$p \sum_i^n (y_i - f(x_i))^2 + (1 - p) f\left(\frac{d^2 f}{dx^2}\right)^2 dx, \quad (1)$$

where p is a smoothing parameter, controlling the tradeoff between fidelity to the data and roughness of the function estimate, f is the estimated cubic spline function to minimize the above function, and x_i and y_i are the dynamical data points. Here, p is set at 0.5. Parametrization of the Ca²⁺-dependent luminescence kinetics was performed in order to determine the maximal amplitude of the luminescence signal (peak) and the left slope of the bell-shaped kinetic trace. Aequorin-based luminescence signal calibration into mt-Ca²⁺ concentration was performed using the algorithm reported in ref. ⁴⁶ for wild-type aequorin and native coelenterazine, with the following formula:

$$[Ca^{2+}](M) = \frac{\left(\frac{L}{L_{max}} \times \lambda\right)^{\frac{1}{n}} + \left(\frac{L}{L_{max}} \times \lambda\right)^{\frac{1}{n}} \times K_{TR}}{K_R - \left(\frac{L}{L_{max}} \times \lambda\right)^{\frac{1}{n}} \times K_R}, \quad (2)$$

where $\lambda = 1$, $K_R = 7.23 \times 10^6$, $K_{TR} = 120$, and $n = 2.99$ are the calibration values used for WT aequorin and native coelenterazine.

Experimental data analysis. Data are represented as mean ± SEM and the statistical analysis of each experiment is described in the figure legends including the statistical tests used and the exact value of biological replicates. For each biological replicate experiment at least three technical replicates were used for quantification

and data analysis. Normal distribution was tested by Shapiro–Wilk normality test. Statistical tests between multiple datasets and conditions were carried out using one-way analysis of variance followed by Dunnett’s multiple comparison tests. Statistical analyses were performed using GraphPad Prism (GraphPad Software, version 8).

Reporting summary. Further information on research design is available in the Nature Research Reporting Summary linked to this article.

Data availability

The data that support the findings of this study are available from the corresponding authors upon reasonable request. All genome data and predicted peptide sets are publicly available and were downloaded from Ensembl-v91 (<https://www.ensembl.org/>), and Ensembl fungi (<https://fungi.ensembl.org/>), metazoa (<https://metazoa.ensembl.org/>), plants (<https://plants.ensembl.org/>) and protists (<https://protists.ensembl.org/index.html>) v37. The raw HMM profiles of the different protein families were downloaded from Pfam release 30.0 (<https://pfam.xfam.org/>). Hs-MICU1 (MICU1_HUMAN) and NCLX (NCLX_HUMAN) sequences were downloaded from the Uniprot database (<https://www.uniprot.org/uniprot/Q9BPX6> and <https://www.uniprot.org/uniprot/Q6J4K2>). The source data underlying Figs. 3b, c, 4c–f, and Supplementary Figs 3, 4, 5, 7, 8, 9, 10, and 11 are provided as a Source Data file. Full scans of the blots are available in Supplementary Fig. 12. All genomic data sources and versions analyzed in the study and the raw phylogenetic trees in newick format are provided in Supplementary Data 2. The silhouette images used in Figs. 3 and 5 were downloaded from PhyloPic (<http://phylopic.org/>) or wikipedia (<https://www.wikipedia.org/>), or designed by the A.P. in Inkscape (<https://inkscape.org/>).

Code availability

There is no specific new code developed for this project; custom python scripts and different programs were used as described in the Methods. These are available with no restriction under request.

Received: 12 March 2020; Accepted: 6 July 2020;

Published online: 12 August 2020

References

- Berridge, M. J., Bootman, M. D. & Roderick, H. L. Calcium signalling: dynamics, homeostasis and remodelling. *Nat. Rev. Mol. Cell Biol.* **4**, 517–529 (2003).
- Kirichok, Y., Krapivinsky, G. & Clapham, D. E. The mitochondrial calcium uniporter is a highly selective ion channel. *Nature* **427**, 360–364 (2004).
- Deluca, H. F. & Engstrom, G. W. Calcium uptake by rat kidney mitochondria. *Proc. Natl Acad. Sci. USA* **47**, 1744–1750 (1961).
- Vasington, F. D. & Murphy, J. V. Ca ion uptake by rat kidney mitochondria and its dependence on respiration and phosphorylation. *J. Biol. Chem.* **237**, 2670–2677 (1962).
- Baughman, J. M. et al. Integrative genomics identifies MCU as an essential component of the mitochondrial calcium uniporter. *Nature* **476**, 341–345 (2011).
- De Stefani, D., Raffaello, A., Teardo, E., Szabó, I. & Rizzuto, R. A forty-kilodalton protein of the inner membrane is the mitochondrial calcium uniporter. *Nature* **476**, 336–340 (2011).
- Perocchi, F. et al. MICU1 encodes a mitochondrial EF hand protein required for Ca(2+) uptake. *Nature* **467**, 291–296 (2010).
- Chaudhuri, D., Sancak, Y., Mootha, V. K. & Clapham, D. E. MCU encodes the pore conducting mitochondrial calcium currents. *Elife* **2013**, e00704 (2013).
- Csordás, G. et al. MICU1 controls both the threshold and cooperative activation of the mitochondrial Ca2+ uniporter. *Cell Metab.* **17**, 976–987 (2013).
- Raffaello, A. et al. The mitochondrial calcium uniporter is a multimer that can include a dominant-negative pore-forming subunit. *EMBO J.* **32**, 2362–2376 (2013).
- Plovanich, M. et al. MICU2, a paralog of MICU1, resides within the mitochondrial uniporter complex to regulate calcium handling. *PLoS ONE* **8**, e55785 (2013).
- Patron, M. et al. MICU1 and MICU2 finely tune the mitochondrial Ca2+ uniporter by exerting opposite effects on MCU activity. *Mol. Cell* **53**, 726–737 (2014).
- Patron, M., Granatiero, V., Espino, J., Rizzuto, R. & De Stefani, D. MICU3 is a tissue-specific enhancer of mitochondrial calcium uptake. *Cell Death Differ.* **26**, 179–195 (2019).
- Vecellio Reane, D. et al. A MICU1 splice variant confers high sensitivity to the mitochondrial Ca2+ uptake machinery of skeletal muscle. *Mol. Cell* **64**, 760–773 (2016).
- Sancak, Y. et al. EMRE is an essential component of the mitochondrial calcium uniporter complex. *Science* **342**, 1379–1382 (2013).
- Kovács-Bogdán, E. et al. Reconstitution of the mitochondrial calcium uniporter in yeast. *Proc. Natl Acad. Sci. USA* **111**, 8985–8990 (2014).
- Wettmarshausen, J. et al. MICU1 confers protection from MCU-dependent manganese toxicity. *Cell Rep.* **25**, 1425–1435.e7 (2018).
- Arduini, D. M. et al. Systematic identification of MCU modulators by orthogonal interspecies chemical screening. *Mol. Cell* **67**, 711–723.e7 (2017).
- Oxenoid, K. et al. Architecture of the mitochondrial calcium uniporter. *Nature* **533**, 269–273 (2016).
- Wang, Y. et al. Structural mechanism of EMRE-dependent gating of the human mitochondrial calcium uniporter. *Cell* **177**, 1252–1261.e13 (2019).
- Fan, C. et al. X-ray and cryo-EM structures of the mitochondrial calcium uniporter. *Nature* **559**, 575–579 (2018).
- Nguyen, N. X. et al. Cryo-EM structure of a fungal mitochondrial calcium uniporter. *Nature* **559**, 570–574 (2018).
- Yoo, J. et al. Cryo-EM structure of a mitochondrial calcium uniporter. *Science* **361**, 506–511 (2018).
- Baradaran, R., Wang, C., Siliciano, A. F. & Long, S. B. Cryo-EM structures of fungal and metazoan mitochondrial calcium uniporters. *Nature* **559**, 580–584 (2018).
- Bick, A. G., Calvo, S. E. & Mootha, V. K. Evolutionary diversity of the mitochondrial calcium uniporter. *Science* **336**, 886 (2012).
- Li, Y., Calvo, S. E., Gutman, R., Liu, J. S. & Mootha, V. K. Expansion of biological pathways based on evolutionary inference. *Cell* **158**, 213–225 (2014).
- Kamer, K. J. & Mootha, V. K. The molecular era of the mitochondrial calcium uniporter. *Nat. Rev. Mol. Cell Biol.* **16**, 545–553 (2015).
- Song, J., Liu, X., Zhai, P., Huang, J. & Lu, L. A putative mitochondrial calcium uniporter in *A. fumigatus* contributes to mitochondrial Ca2+ homeostasis and stress responses. *Fungal Genet. Biol.* **94**, 15–22 (2016).
- Carafoli, E. & Lehninger, A. L. A survey of the interaction of calcium ions with mitochondria from different tissues and species. *Biochem. J.* **122**, 681–690 (1971).
- Gonçalves, A. P. et al. Involvement of mitochondrial proteins in calcium signaling and cell death induced by staurosporine in *Neurospora crassa*. *Biochim. Biophys. Acta* **1847**, 1064–1074 (2015).
- Roger, A. J., Muñoz-Gómez, S. A. & Kamikawa, R. The origin and diversification of mitochondria. *Curr. Biol.* **27**, R1177–R1192 (2017).
- Gabaldón, T. & Koonin, E. V. Functional and evolutionary implications of gene orthology. *Nat. Rev. Genet.* **14**, 360–366 (2013).
- Huang, G. & Docampo, R. The mitochondrial Ca2+ uniporter complex (MCUC) of *Trypanosoma brucei* is a hetero-oligomer that contains novel subunits essential for Ca2+ uptake. *MBio* **9**, e01700–e01718 (2018).
- Chirillo, M. A. et al. Different roles of mitochondrial calcium uniporter complex subunits in growth and infectivity of *Trypanosoma cruzi*. *MBio* **8**, e00574–17 (2017).
- TorrueLLa, G. et al. Phylogenetic relationships within the Opisthokonta based on phylogenomic analyses of conserved single-copy protein domains. *Mol. Biol. Evol.* **29**, 531–544 (2012).
- Tsai, M.-F. et al. Dual functions of a small regulatory subunit in the mitochondrial calcium uniporter complex. *Elife* **5**, e15545 (2016).
- Eddy, S. R. Accelerated profile HMM searches. *PLoS Comput. Biol.* **7**, e1002195 (2011).
- Katoh, K. & Standley, D. M. MAFFT multiple sequence alignment software version 7: improvements in performance and usability. *Mol. Biol. Evol.* **30**, 772–780 (2013).
- Capella-Gutierrez, S., Silla-Martinez, J. M. & Gabaldón, T. trimAl: a tool for automated alignment trimming in large-scale phylogenetic analyses. *Bioinformatics* **25**, 1972–1973 (2009).
- Nguyen, L.-T., Schmidt, H. A., von Haeseler, A. & Minh, B. Q. IQ-TREE: a fast and effective stochastic algorithm for estimating maximum-likelihood phylogenies. *Mol. Biol. Evol.* **32**, 268–274 (2015).
- Huerta-Cepas, J., Serra, F. & Bork, P. ETE 3: reconstruction, analysis, and visualization of phylogenomic data. *Mol. Biol. Evol.* **33**, 1635–1638 (2016).
- Waterhouse, A. M., Procter, J. B., Martin, D. M. A., Clamp, M. & Barton, G. J. Jalview Version 2—a multiple sequence alignment editor and analysis workbench. *Bioinformatics* **25**, 1189–1191 (2009).
- Brandt, B. W., Feenstra, K. A. & Heringa, J. Multi-harmony: detecting functional specificity from sequence alignment. *Nucleic Acids Res.* **38**, W35–W40 (2010).
- Jinek, M. et al. A programmable dual-RNA-guided DNA endonuclease in adaptive bacterial immunity. *Science* **337**, 816–821 (2012).
- Ran, F. A. et al. Double nicking by RNA-guided CRISPR cas9 for enhanced genome editing specificity. *Cell* **154**, 1380–1389 (2013).

46. Bonora, M. et al. Subcellular calcium measurements in mammalian cells using jellyfish photoprotein aequorin-based probes. *Nat. Protoc.* **8**, 2105–2118 (2013).

Acknowledgements

T.G. group acknowledges support from the Spanish Ministry of Economy, Industry, and Competitiveness (MEIC) for the EMBL partnership, and grants “Centro de Excelencia Severo Ochoa 2013–2017” SEV-2012-0208 and BFU2015-67107 co-funded by European Regional Development Fund (ERDF); from the CERCA Programme/Generalitat de Catalunya; from the Catalan Research Agency (AGAUR) SGR857; and grants from the European Union’s Horizon 2020 research and innovation programme under the grant agreement ERC-2016-724173. T.G. also receives support from an INB Grant (PT17/0009/0023–ISCIII-SGEFI/ERDF). F.P. group was supported by the Munich Center for Systems Neurology (SyNergy EXC 2145/ID 390857198) and ExNet-0041-Phase2-3 (“SyNergy-HMGU”) through the Initiative and Network Fund of the Helmholtz Association to F.P.; The Bert L & N Kuggie Vallee Foundation (to F.P. and J.W.); the Juniorverbund in der Systemmedizin “mitOmics” (FKZ 01ZX1405B to V.G.). A.A.P. was supported by a postdoctoral research fellowship from EMBO (118-2017) while writing this article. A.C.S. was partially supported by the Aging and Metabolic Programming project (AMPro).

Author contributions

A.A.P., T.G., and F.P. conceived the project, designed the experiments, and wrote the manuscript. V.G. performed most of the experiments with help from J.W. and A.C.-S. A.A.P. performed computational analysis. T.G. and F.P. supervised work and acquired funding.

Competing interests

The authors declare no competing interests

Additional information

Supplementary information is available for this paper at <https://doi.org/10.1038/s41467-020-17705-4>.

Correspondence and requests for materials should be addressed to F.P. or T.Gón.

Peer review information *Nature Communications* thanks Rosario Rizzuto, and the other, anonymous, reviewers for their contribution to the peer review of this work. Peer reviewer reports are available.

Reprints and permission information is available at <http://www.nature.com/reprints>

Publisher’s note Springer Nature remains neutral with regard to jurisdictional claims in published maps and institutional affiliations.



Open Access This article is licensed under a Creative Commons Attribution 4.0 International License, which permits use, sharing, adaptation, distribution and reproduction in any medium or format, as long as you give appropriate credit to the original author(s) and the source, provide a link to the Creative Commons license, and indicate if changes were made. The images or other third party material in this article are included in the article’s Creative Commons license, unless indicated otherwise in a credit line to the material. If material is not included in the article’s Creative Commons license and your intended use is not permitted by statutory regulation or exceeds the permitted use, you will need to obtain permission directly from the copyright holder. To view a copy of this license, visit <http://creativecommons.org/licenses/by/4.0/>.

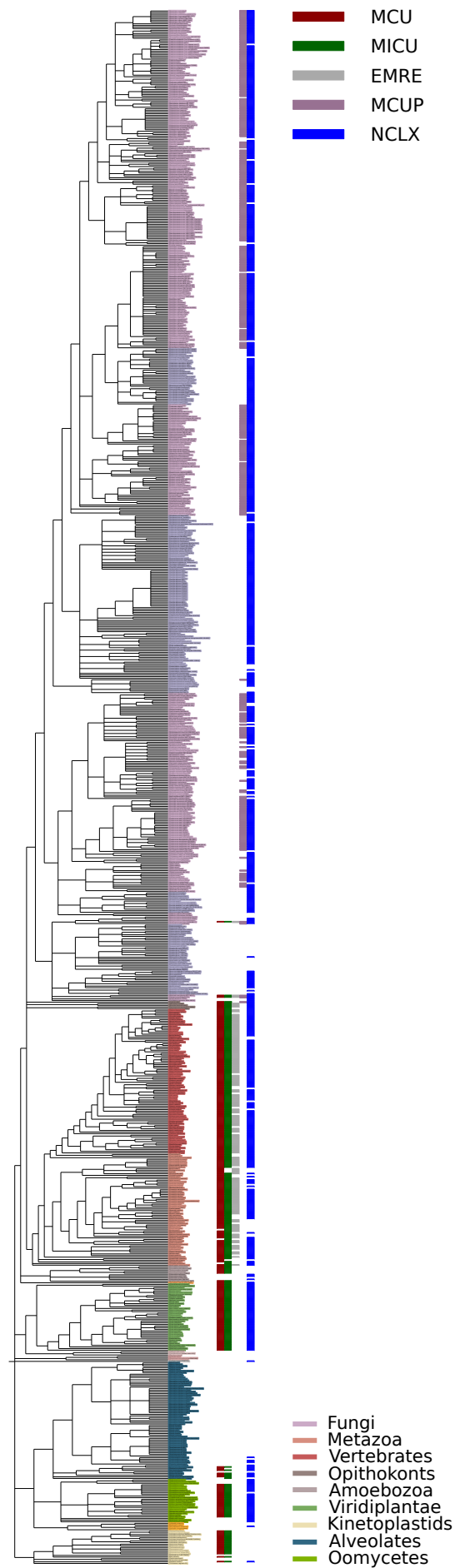
© The Author(s) 2020

Supplementary Information

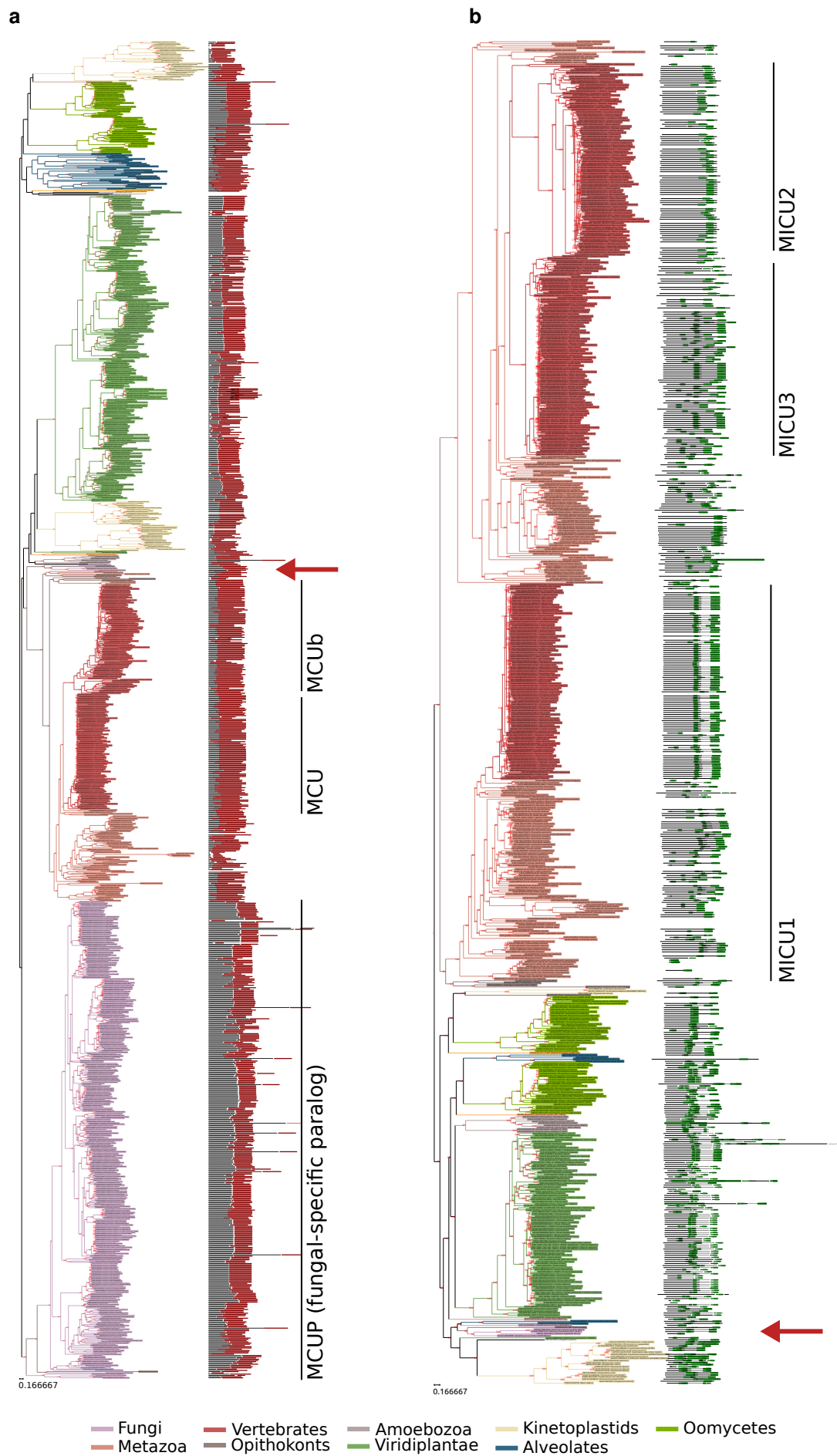
Discovery of EMRE in fungi resolves the true evolutionary history of the
mitochondrial calcium uniporter

Pittis et al.

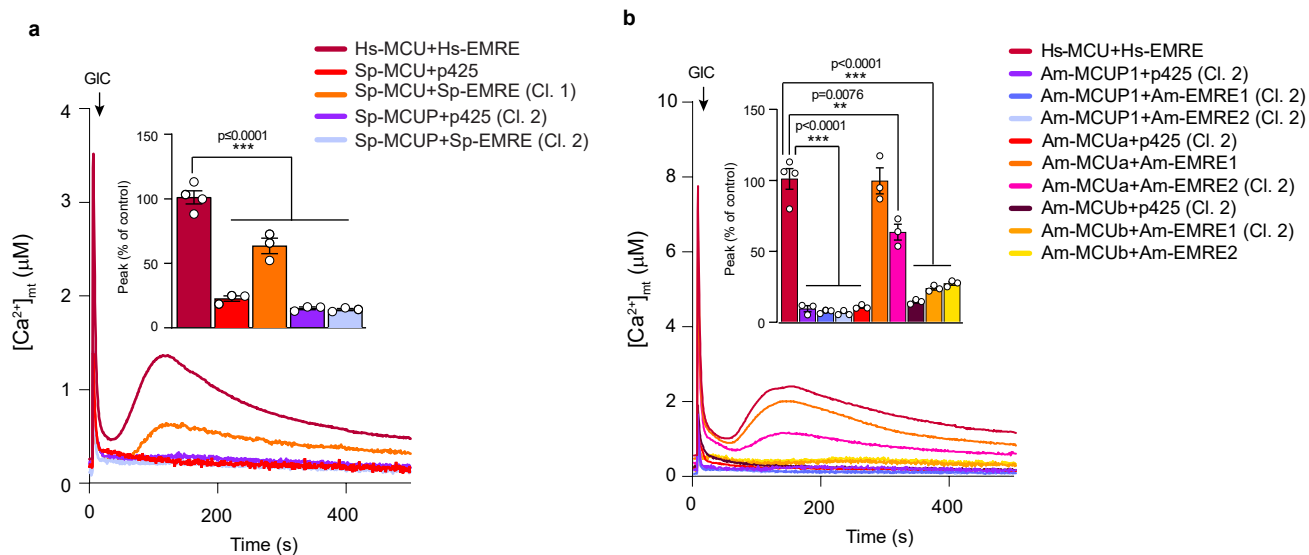
Supplementary Figures 1-12
Supplementary Tables 1-2



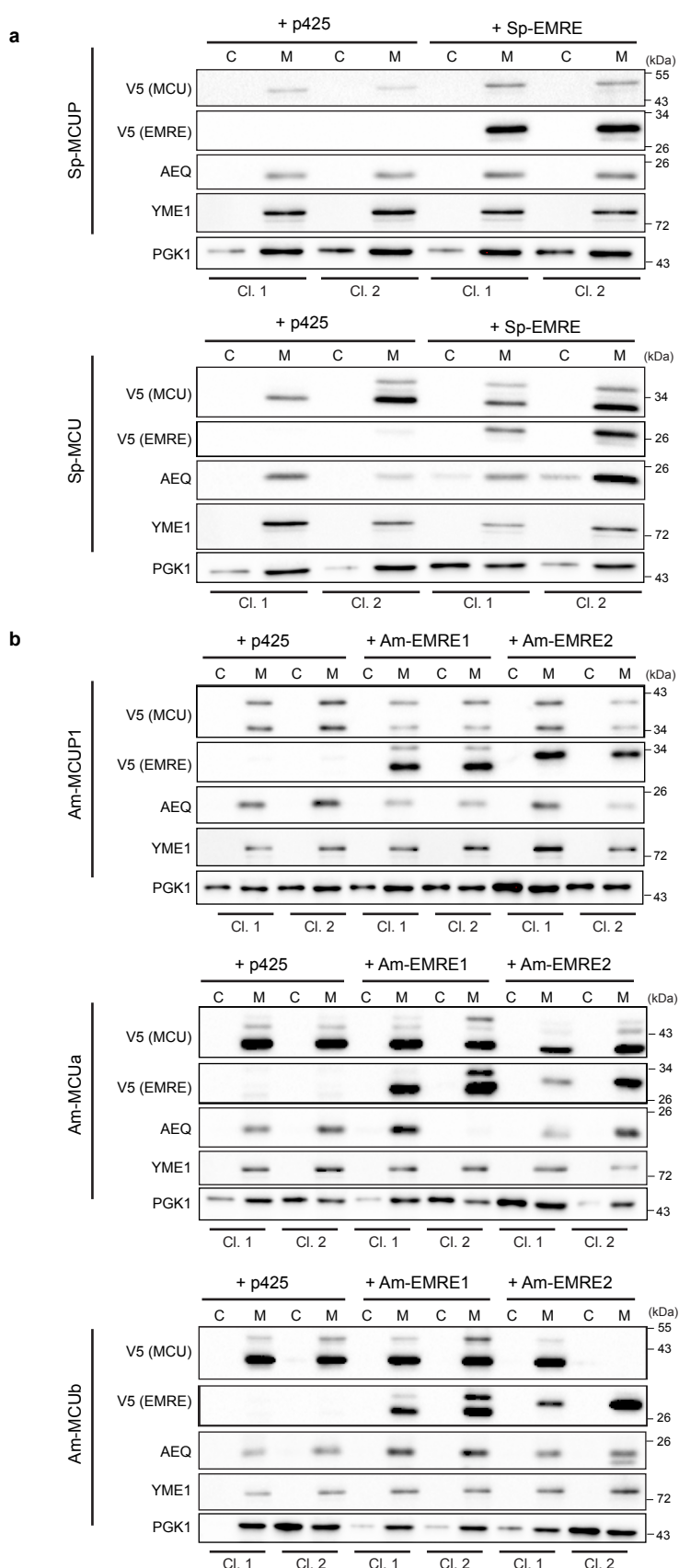
Supplementary Fig. 1. Phylogenetic distribution of the mitochondrial calcium transporter complex protein families. The tree is collapsed to the species level, resulting in 969 species. Extended version of Figure 1, including also the distribution of NCLX, which appears to be largely uncoupled to that of the MCU complex members.



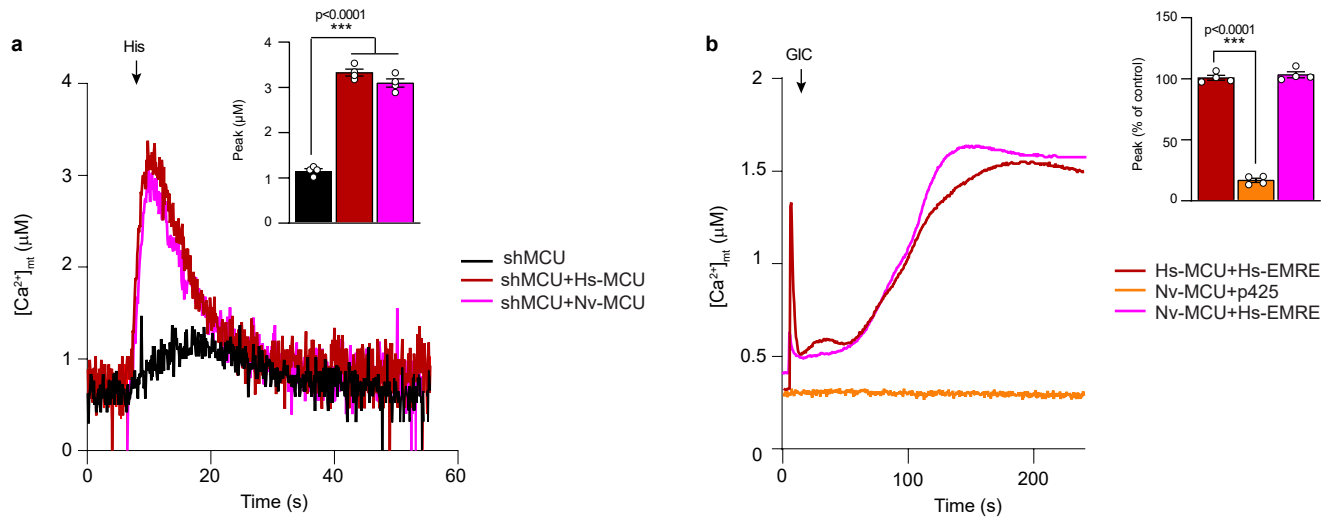
Supplementary Fig. 2. Maximum likelihood (ML) phylogenetic trees of MCU and MICU families. Phylogenies of the 1,064 MCU sequences (a) and the 651 MICU sequences (b). Full version with sequences ids of Fig. 2a,b. The UFBoot (Ultrafast Bootstrap Approximation) support values, as implemented in IQ-TREE 1.6.8, are indicated in red. The main subfamilies are shown, based on the human representatives. The basic domain architecture according to Pfam is plotted on the right. The MCU family is characterized by the presence of one “MCU” domain (in red), while the typical MICU sequence consists of two “EF-hand” domains (in green). In both (a) and (b) position of the animal related MCU and MICU sequences from fungi and *F.alba* are indicated with a red arrow. See also Methods.



Supplementary Fig. 3. Reconstitution of mt- Ca^{2+} uptake in yeast cells expressing *S. punctatus* or *A. macrogynus* MCU and EMRE homologs. a,b. Representative traces and quantification of mt- Ca^{2+} transients in yeast cells expressing human MCU (Hs-MCU) (n=4) or MCU orthologs from *S. punctatus* (Sp-MCU, Sp-MCUP) (n=3) (a) and *A. macrogynus* (Am-MCUa, Am-MCUB, Am-MCUP1) (n=3) (b) with either their respective EMRE orthologs (Hs-EMRE, Sp-EMRE, Am-EMRE1, Am-EMRE2) or an empty vector (p425) upon glucose-induced calcium (GIC) stimulation in presence of 1 mM $CaCl_2$. All data represent mean \pm SEM. *P* values are indicated in the different panels (a-b: ****p* < 0.001, one-way ANOVA with Dunnett's Multiple Comparisons Test). Source data are provided as a Source Data file.



Supplementary Fig. 4. Heterologous expression of *S. punctatus* and *A. macrogynus* MCU and EMRE homologs in yeast. a,b Immunoblot analysis of cytosolic (C) and mitochondrial (M) fractions isolated from yeast clones (Cl.) expressing mt-AEQ together with either (a) *S. punctatus* MCU (Sp-MCUP, Sp-MCU) and EMRE (Sp-EMRE) homologs or (b) *A. macrogynus* MCU (Am-MCUP1, Am-MCUpA, Am-MCUpB) and EMRE (Am-EMRE1, Am-EMRE2) homologs fused to a C-terminal V5-tag, using the following antibodies: α -V5 (Life Technologies, R96025), α -AEQ (Merck/Millipore, MAB4405), α -YME1, PGK1 (Life Technologies, 459250). YME1 was used as control for yeast mitochondrial targeted protein and PGK1 was used as control for cytosolic protein. Source data are provided as a Source Data file.



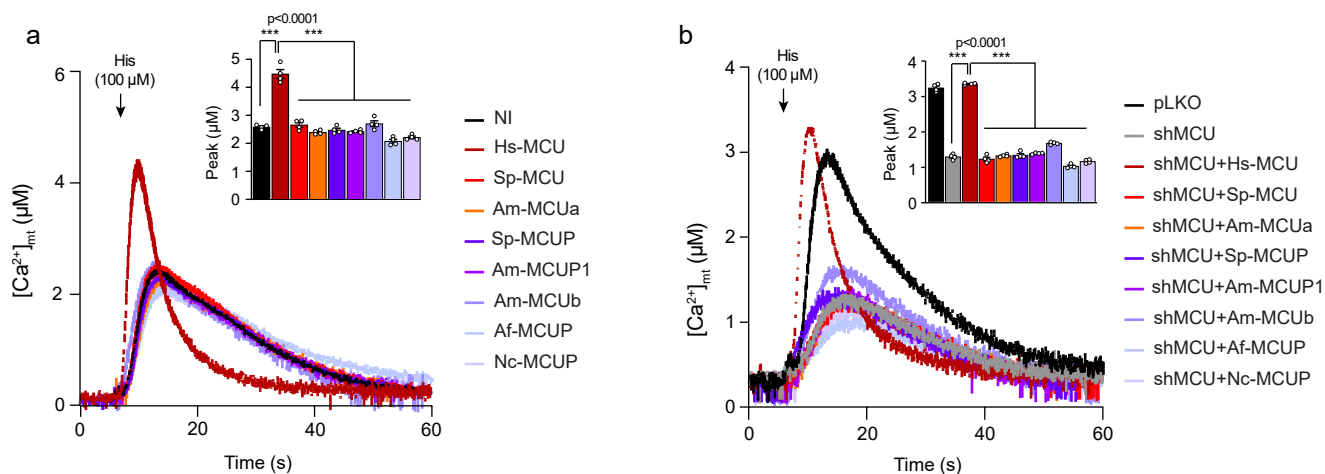
Supplementary Fig. 5. Reconstitution of mt- Ca^{2+} uptake in HeLa and yeast cells expressing *N. vectensis* MCU. **a**, Representative traces and quantification of mt- Ca^{2+} transients in MCU knockdown (shMCU) HeLa cells expressing human (Hs-MCU) and *N. vectensis* MCU (Nv-MCU) upon histamine (His) stimulation ($n=4$). **b**, Representative traces and quantification of mt- Ca^{2+} transients in yeast cells expressing Nv-MCU with either empty vector (p425) or human EMRE (Hs-EMRE) upon glucose-induced calcium (GIC) stimulation in presence of 1 mM $CaCl_2$ ($n=4$). All data represent mean \pm SEM. P values are indicated in the different panels (**a-b**: *** $p < 0.0001$, one-way ANOVA with Dunnett's Multiple Comparisons Test). Source data are provided as a Source Data file.

[illegible]

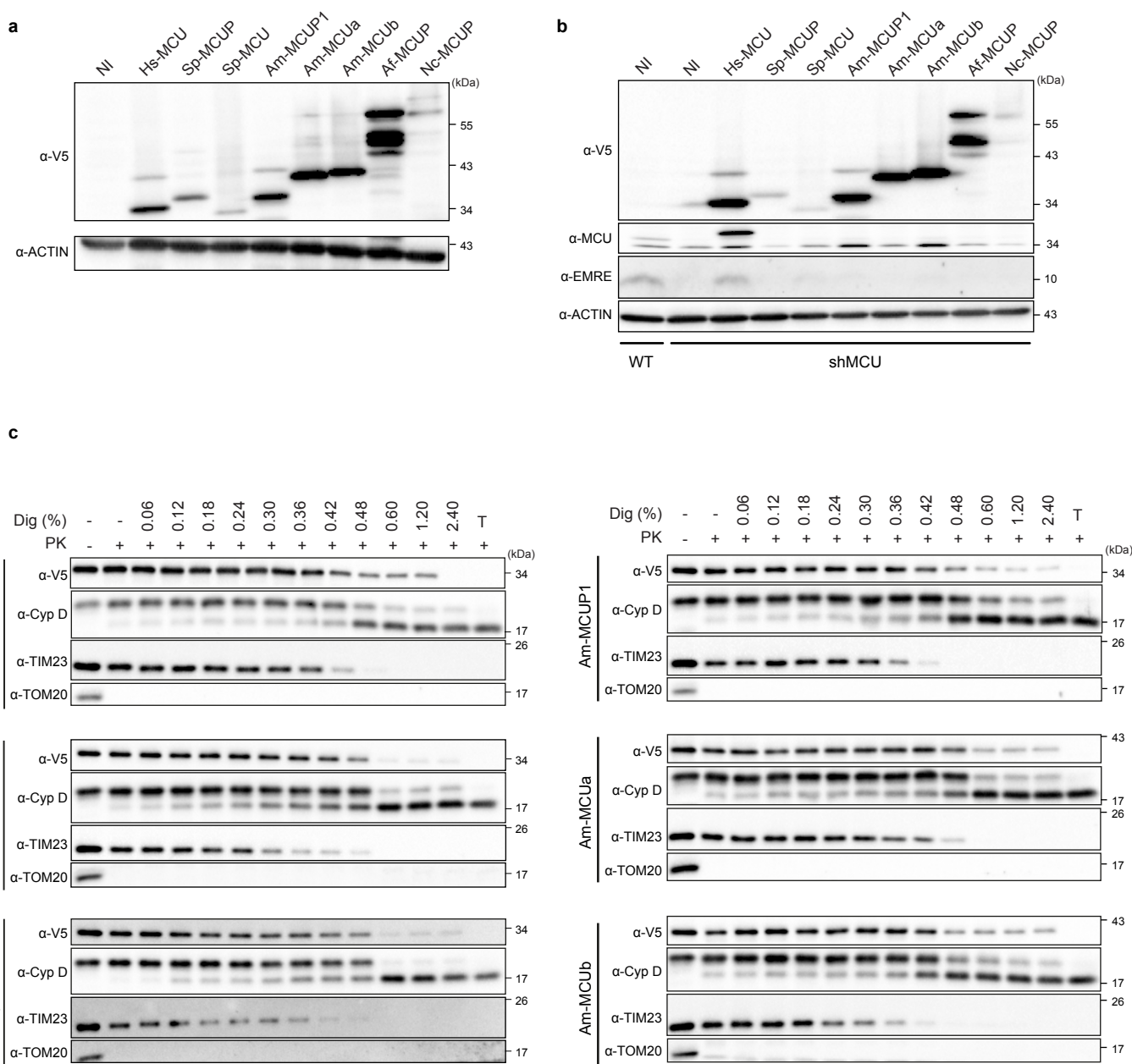
10 20 30 40 50 60 70 80 90 100
Cateneria_anguillulae FL171.0R234531-158
Cateneria_anguillulae FL171.0R234531-305
Allomyces macrocynus ATCC 38327.KNE632291-269
Allomyces macrocynus ATCC 38327.KNE622461-275
Allomyces punctatus DAOM_BRL117.KNE10019381-227
Capsosira covecreeki ATCC 30864.KNE363471-81
Monosiga brevicollis MX1.ED0915791-163
Salpingoeca rosetta EGD908491-89
Amphibia *Ureaster* *ludensis* Asp212-84
Homo_sapiens ENSG000004850291-107



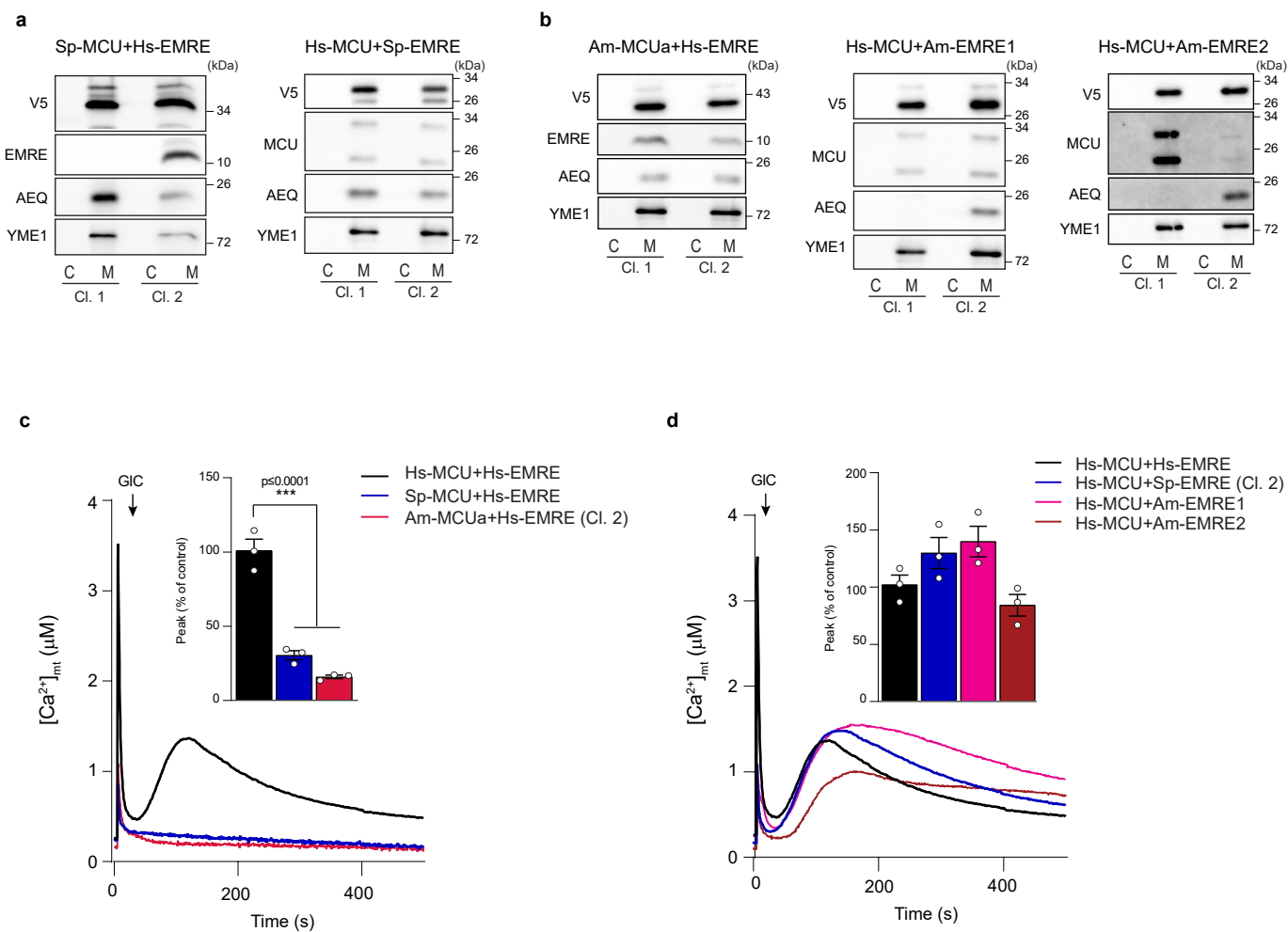
Supplementary Fig. 6. a,b, Multiple sequence alignments of opisthokont members of MCU (a) and EMRE (b) families. In (a) MCU regions poorly aligned or specific to non-opisthokont species have been removed, whereas in (b) the full EMRE sequences are shown, for all the species in (a) where EMRE was detected.



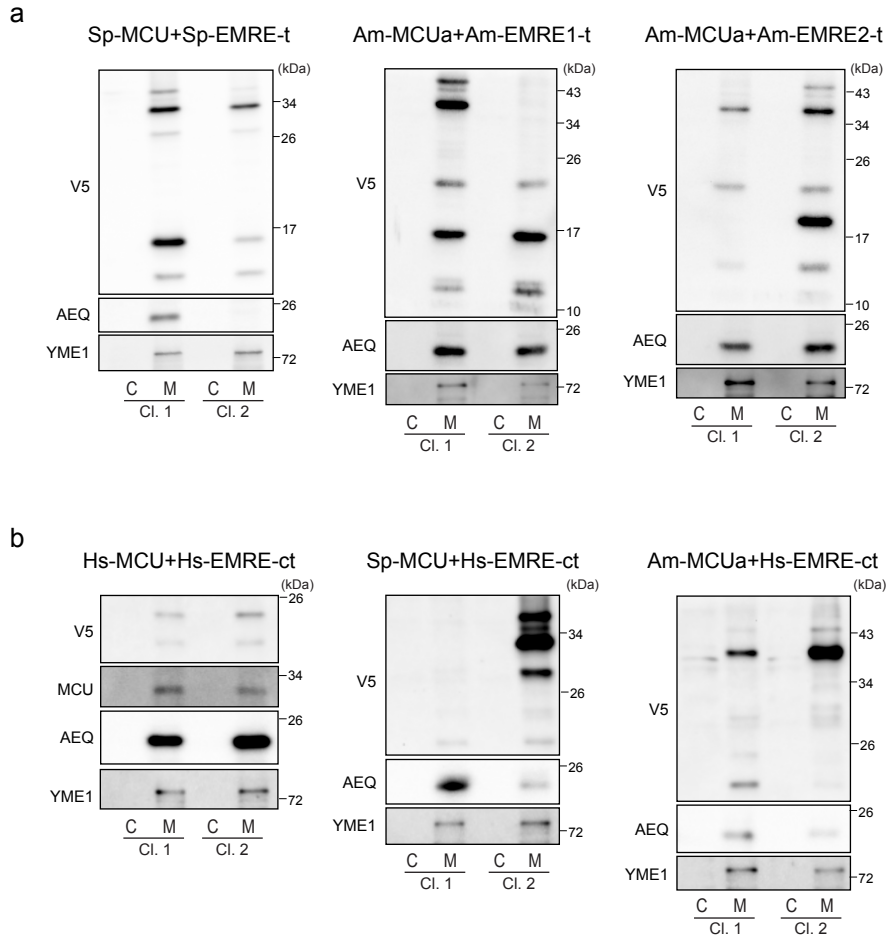
Supplementary Fig. 7. Reconstitution of mt-Ca²⁺ uptake in HeLa cells expressing fungal MCU homologs. a, b. Quantification of mt-Ca²⁺ transients in either wild-type (a) or wild-type (pLKO) and MCU knockdown (shMCU) (b) HeLa cells expressing human (Hs-MCU) or different fungal MCU homologs from *S. punctatus* (Sp-MCU, Sp-MCUP), *A. macrogynus* (Am-MCUa, Am-MCUp, Am-MCUP1), *A. fumigatus* (Af-MCUP) and *N. crassa* (Nc-MCUP) upon histamine (His) stimulation (n=4). NI, not infected. All data represent mean \pm SEM. *P* values are indicated in the different panels (a-b: ****p* < 0.0001, one-way ANOVA with Dunnett's Multiple Comparisons Test). Source data are provided as a Source Data file.



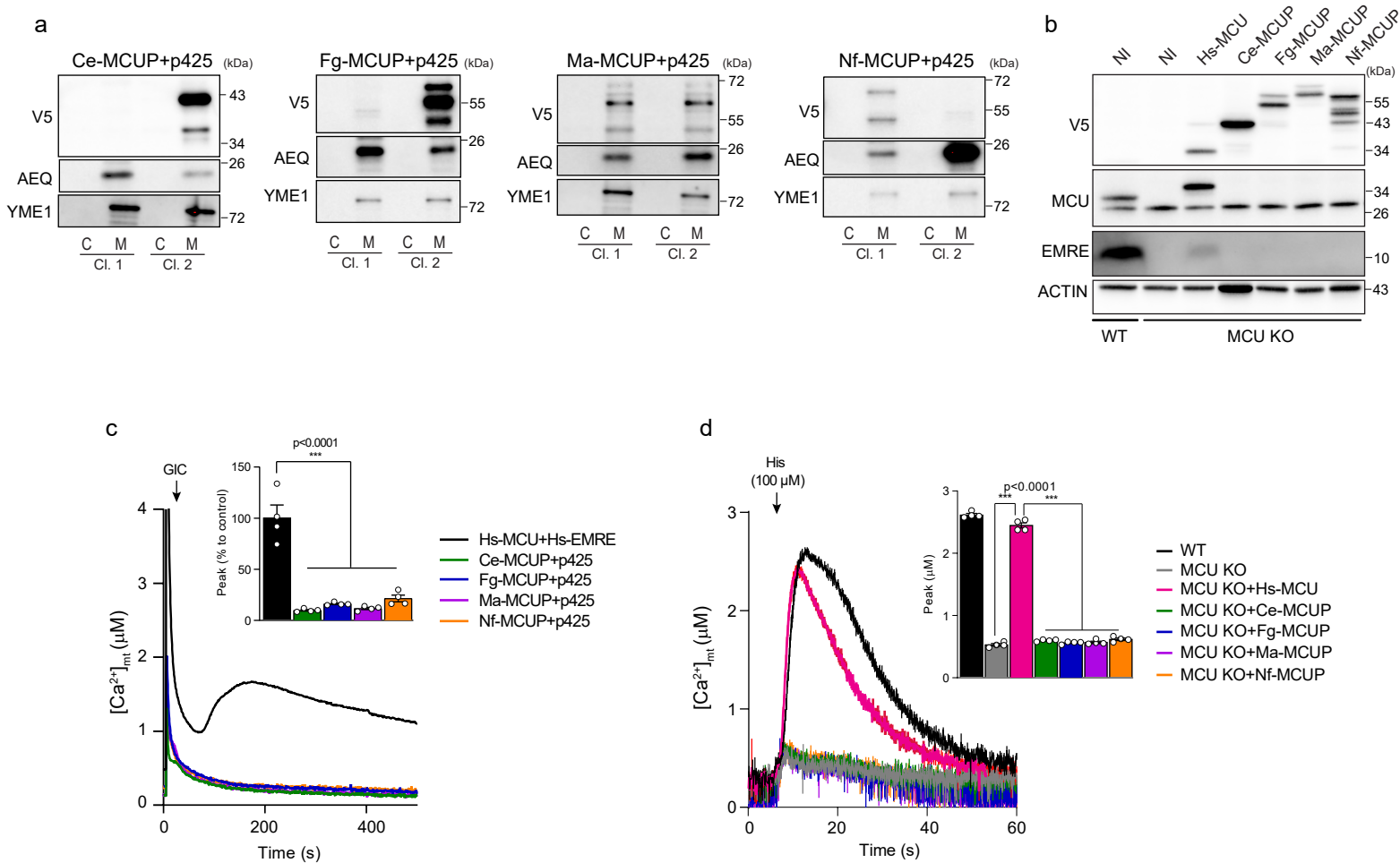
Supplementary Fig. 8. Expression and localization of fungal MCU homologs in HeLa cells. Immunoblot analysis of whole cell lysates from wild-type (WT) (a) and MCU knock-down (shMCU) (b) HeLa mt-AEQ cells stably expressing human or fungal MCU proteins fused to a C-terminal V5 tag using the following antibodies: α -MCU (Sigma Aldrich, HPA01648), α -V5 (Life Technologies, R96025), α -EMRE (Santa Cruz Biotechnology, sc- 86337), α -ACTIN (Sigma-Aldrich, A2228). NI, not infected. c, Analysis of protein topology by proteinase K (PK) treatment of mitochondria isolated from sh-MCU HeLa mt-AEQ cells expressing human and fungal MCU homologs, using the following antibodies: α -V5 (Life Technologies, R96025), α -TIM23 (BD Bioscience, 611222), α -TOM20 (Abcam, ab56783), and α -Cyclophilin D (Cyp D) (Abcam, ab110324). TOM20, TIM23, and Cyp D were used as controls for integral mitochondrial outer membrane, inner membrane and soluble matrix targeted proteins, respectively. T, triton (1%); Dig., digitonin. Source data are provided as a Source Data file.



Supplementary Fig. 9. Reconstitution of mt- Ca^{2+} uptake in yeast cells expressing human MCU and EMRE with either fungal EMRE or MCU orthologs from *S. punctatus* and *A. macrogynus* respectively. **a,b**, Immunoblot analysis of cytosolic (C) and mitochondrial (M) fractions isolated from yeast clones (Cl.) expressing mt-AEQ together with human and either (a) *S. punctatus* or (b) *A. macrogynus* MCU and EMRE orthologs fused to a C-terminal V5-tag using the following antibodies: α -V5 (Life Technologies, R96025), α -MCU (Sigma Aldrich, HPA01648), α -EMRE (Santa Cruz Biotechnology, sc-86337), α -AEQ (Merck/Millipore, MAB4405), α -YME1. YME1 was used as control for yeast mitochondrial targeted protein. **c,d**, Representative traces and quantification of mt- Ca^{2+} transients in yeast cells expressing either MCU (c) or EMRE (d) orthologs from *S. punctatus* and *A. macrogynus* with human EMRE (Hs-EMRE) or MCU (Hs-MCU) respectively upon glucose-induced calcium (GIC) stimulation in presence of 1 mM CaCl_2 ($n=3$). All data represent mean \pm SEM. P values are indicated in the different panels (c: *** $p < 0.001$, one-way ANOVA with Dunnett's Multiple Comparisons Test; d: * $p = 0.036$, one-way ANOVA with Dunnett's Multiple Comparisons Test). Source data are provided as Source Data file.



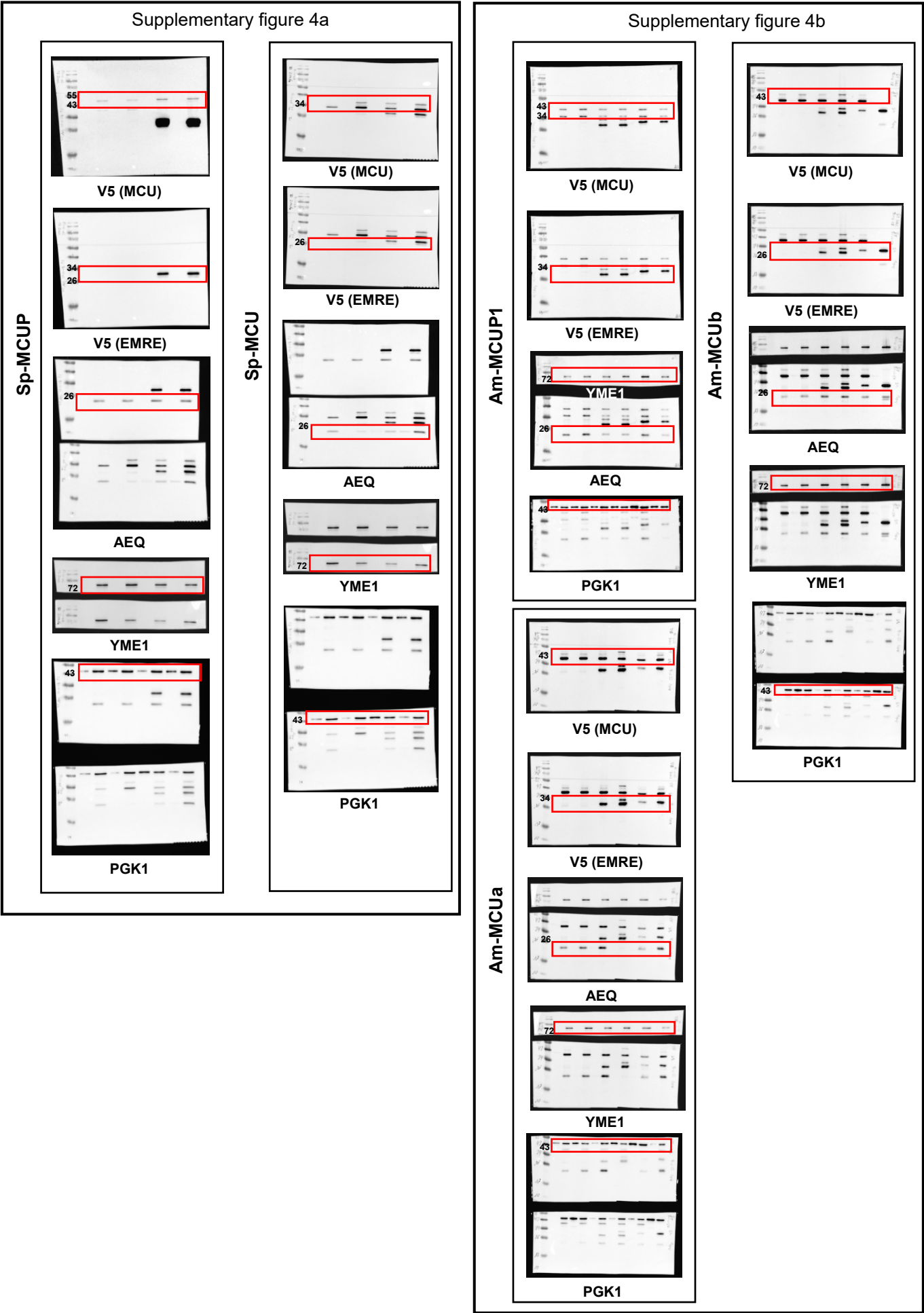
Supplementary Fig. 10. Heterologous expression of *S. punctatus* and *A. macrogynus* MCU and EMRE orthologs in yeast. a,b, Immunoblot analysis of cytosolic (C) and mitochondrial (M) fractions isolated from yeast clones (Cl.) expressing mt-AEQ together with either (a) *S. punctatus* (Sp-MCU) and *A. macrogynus* (Am-MCUa) MCU and their respective truncated EMRE (Sp-EMRE-t, Am-EMRE1-t, Am-EMRE2-t) or (b) Human, *S. punctatus* (Sp-MCU) and *A. macrogynus* (Am-MCUa) MCU and human EMRE with an added fungal extra C-terminal domain (Hs-EMRE-ct), fused to a C-terminal V5-tag, using the following antibodies: α -V5 (Life Technologies, R96025), α -AEQ (Merck/Millipore, MAB4405), α -YME1. YME1 was used as control for yeast mitochondrial targeted protein. Source data are provided as a Source Data file.

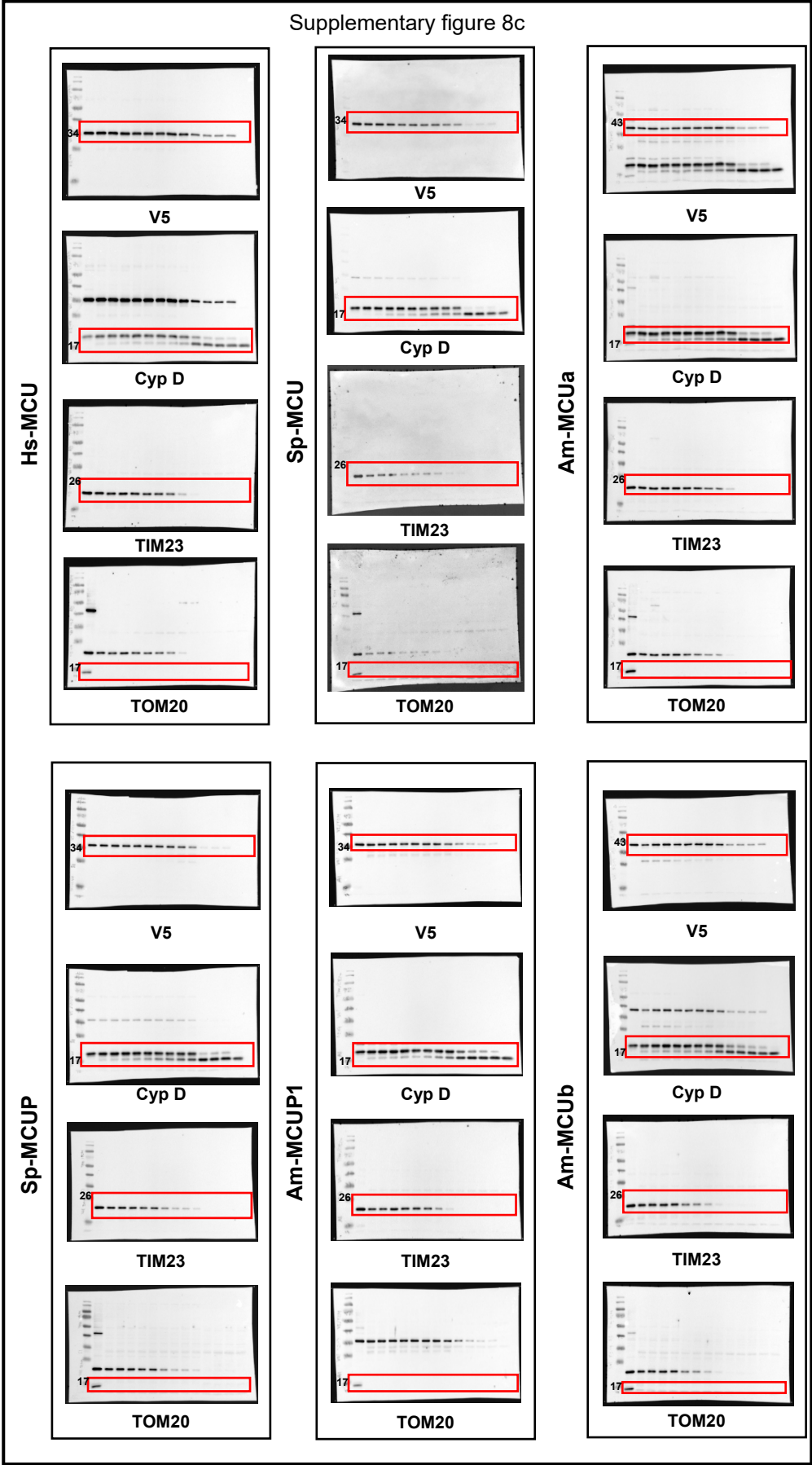
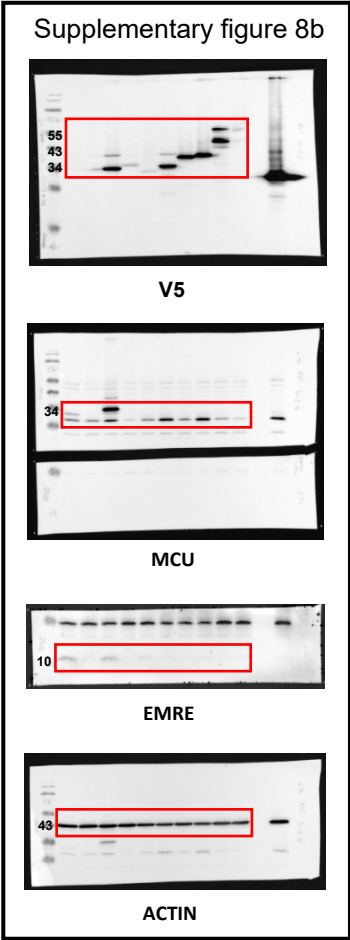
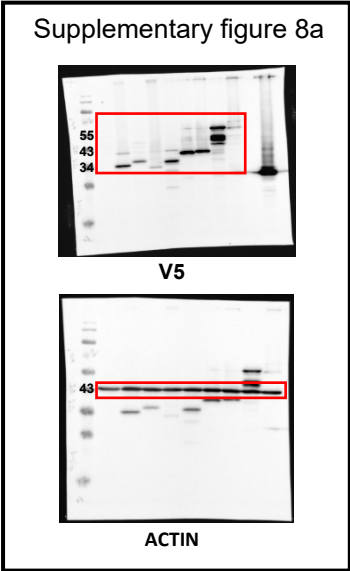


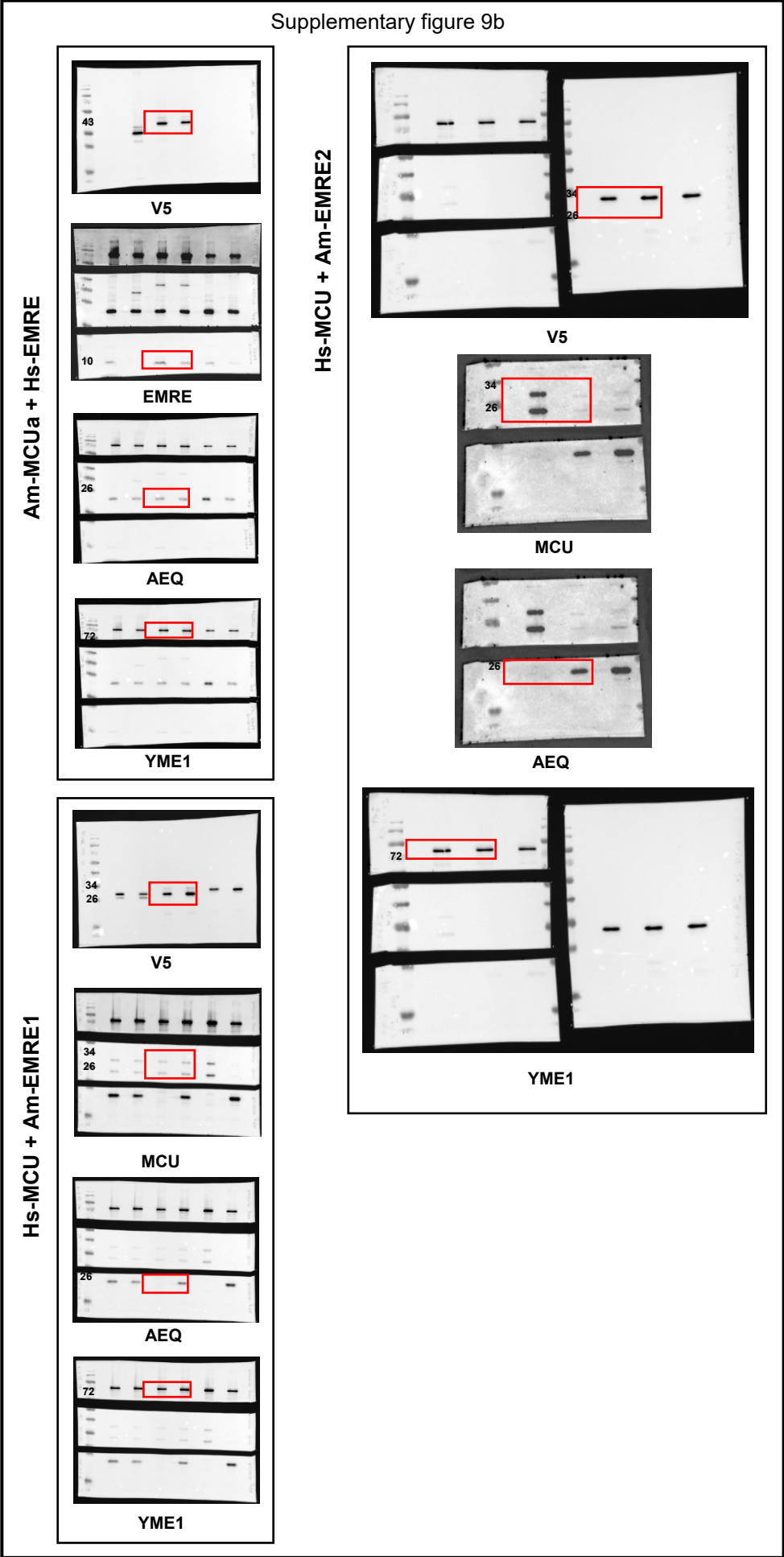
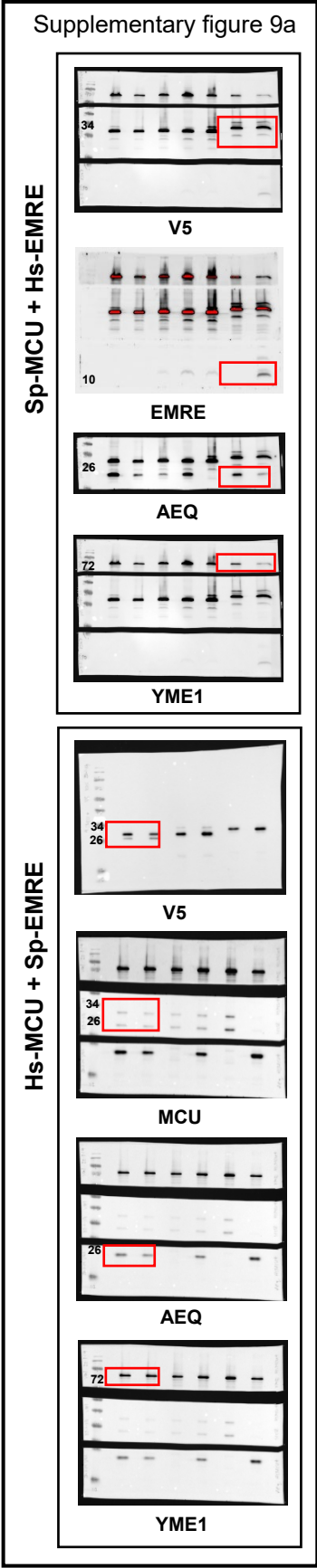
Supplementary Fig. 11. Reconstitution of mt-Ca²⁺ uptake in yeast and HeLa cells expressing fungal MCU paralogs. **a**, Immunoblot analysis of cytosolic (C) and mitochondrial (M) fractions isolated from yeast clones (Cl.) expressing mt-AEQ together with *C. europaea* (Ce-MCUP), *F. graminearum* (Fg-MCUP), *M. acridum* (Ma-MCUP) or *N. fischeri* (Nf-MCUP) MCU paralogs fused to a C-terminal V5-tag and an empty vector (p425) using the following antibodies: α-V5 (Life Technologies, R96025), α-AEQ (Merck/Millipore, MAB4405), α-YME1. YME1 was used as control for yeast mitochondrial targeted protein. **b**, Immunoblot analysis of whole cell lysates from wild-type (WT) or MCU knock-out (MCU KO) HeLa mt-AEQ cells stably expressing human or fungal MCU homolog proteins fused to a C-terminal V5 tag using the following antibodies: α-MCU (Sigma Aldrich, HPA01648), α-V5 (Life Technologies, R96025), α-EMRE (Santa Cruz Biotechnology, sc- 86337), α-ACTIN (Sigma-Aldrich, A2228). NI, not infected. **c**, Representative traces and quantification of mt-Ca²⁺ transients in yeast cells expressing either human MCU (Hs-MCU) and EMRE (Hs-EMRE) or fungal MCU paralogs (Ce-MCUP, Fg-MCUP, Ma-MCUP or Nf-MCUP) and an empty vector (p425) upon glucose-induced calcium (GIC) stimulation in presence of 1 mM CaCl₂ (n=4). **d**, Quantification of mt-Ca²⁺ transients in WT or MCU KO HeLa mt-AEQ cells expressing different fungal MCU paralogs (Ce-MCUP, Fg-MCUP, Ma-MCUP or Nf-MCUP) upon histamine (His) stimulation (n=4). All data represent mean ± SEM. P values are indicated in the different panels (**c-d**: ***p < 0.0001, one-way ANOVA with Dunnett's Multiple Comparisons Test). Source data are provided as Source Data file.

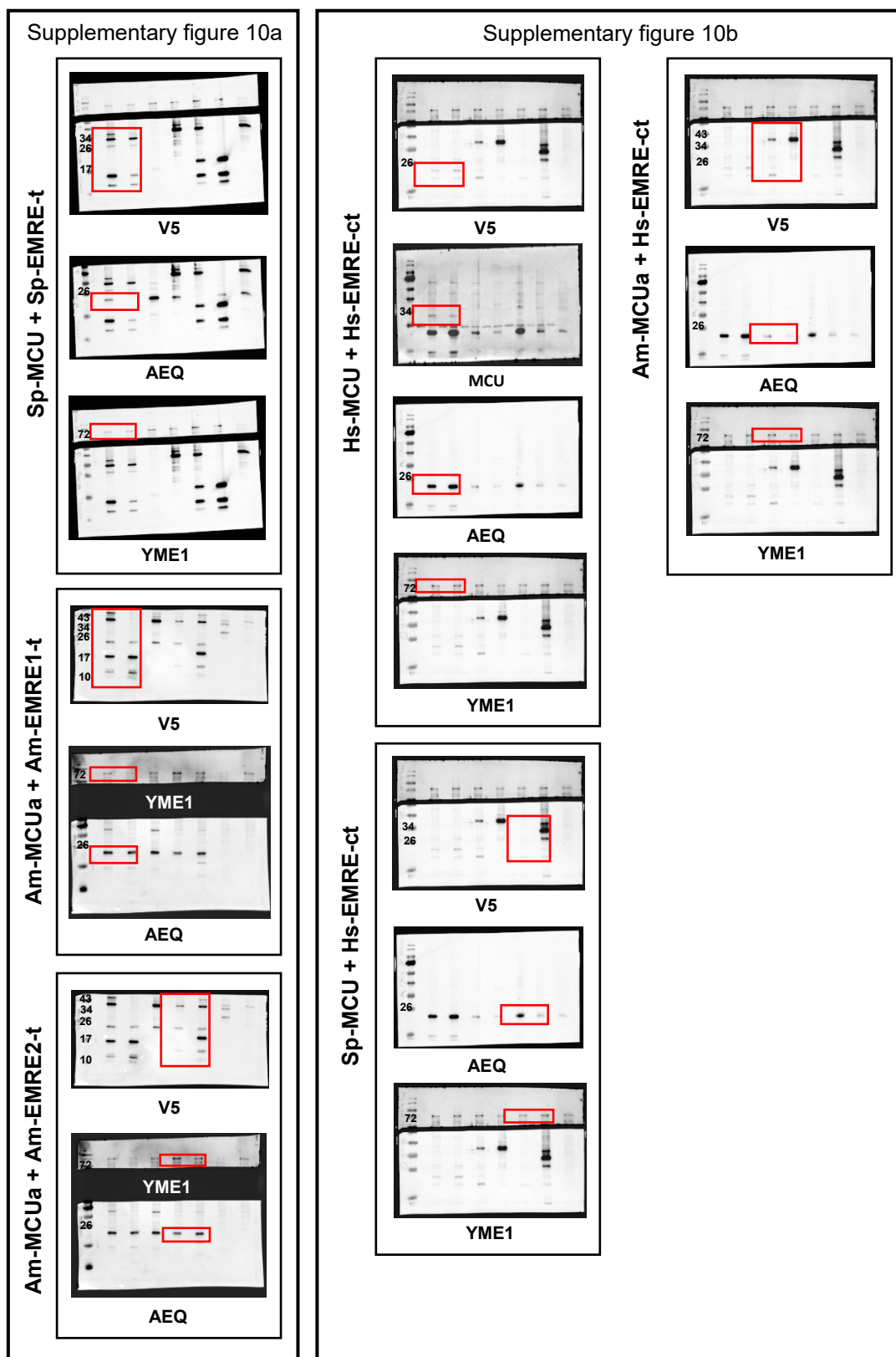
Supplementary Figure 12 Uncropped Original Scans

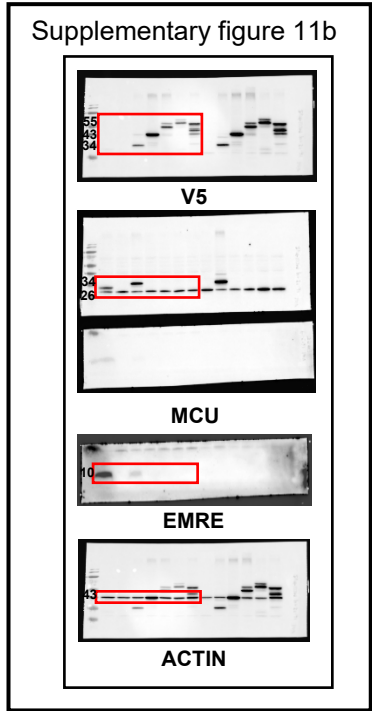
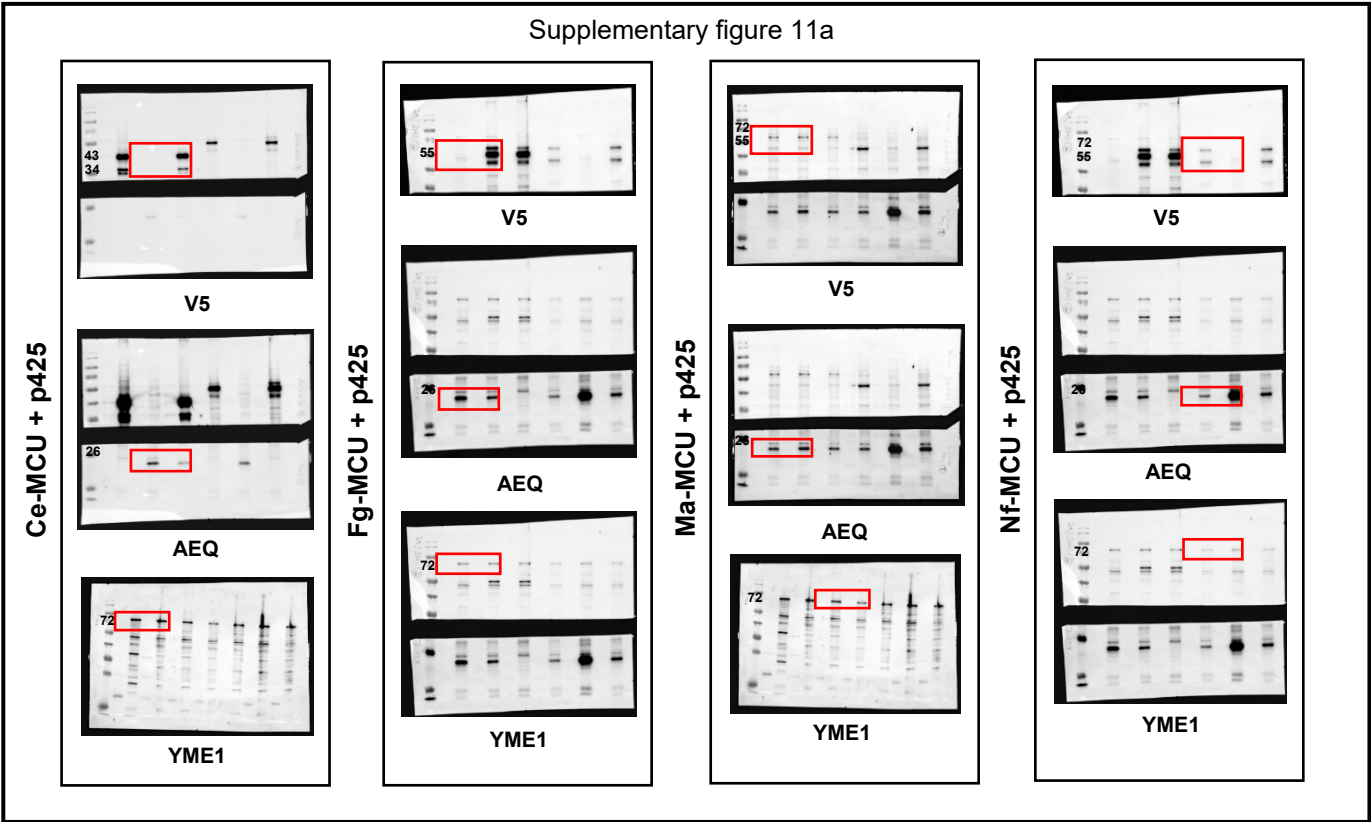
Uncropped immunoblots from Supplementary Figure 4











Supplementary Table 1. List of PCR primers used to amplify cDNA from PuC57 vector and perform Gateway cloning into pLX304 destination vector.

Species	cDNA	Direction	Primer sequence
<i>Spizellomyces punctatus</i>	Sp-MCU	Forward	5'-GGG GAC AAG TTT GTA CAA AAA AGC AGG CTT AGC CAC CAT GCG AAT CCC CTT CCA CCA CGG C-3'
		Reverse	5'-GGG GAC CAC TTT GTA CAA GAA AGC TGG GTT TGT TGC CTC CAC CCT GAC CC-3'
	Sp-MCUP	Forward	5'-GGG GAC AAG TTT GTA CAA AAA AGC AGG CTT AGC CAC CAT GGT GAG CCT GAT TCC AGT GGG GG-3'
		Reverse	5'-GGG GAC CAC TTT GTA CAA GAA AGC TGG GTT AAT CAG TCT GCC CAT TCG TCC AGC-3'
	Sp-EMRE	Forward	5'-GGG GAC AAG TTT GTA CAA AAA AGC AGG CTT AGC CAC CAT GTC CCG CAT TCT GAC ACG ATT CCC A-3'
		Reverse	5'-GGG GAC CAC TTT GTA CAA GAA AGC TGG GTT CCA GAA CTT CAG CCA GCC CCA-3'
	Sp-EMRE-t	Forward	5'-GGG GAC AAG TTT GTA CAA AAA AGC AGG CTT AGC CAC CAT GTC CCG CAT TCT GAC ACG ATT C-3'
		Reverse	5'-GGG GAC CAC TTT GTA CAA GAA AGC TGG GTT CAC CAC CTT CTC ATC GTC ATC CTT GT-3'
<i>Allomyces macrogynus</i>	Am-MCUa	Forward	5'-GGG GAC AAG TTT GTA CAA AAA AGC AGG CTT AGC CAC CAT GCT GTC AAG GGC TCT GCA GGT CG-3'
		Reverse	5'-GGG GAC CAC TTT GTA CAA GAA AGC TGG GTT CCC CTG CTT GCC CTC GCT TGT-3'
	Am-MCUb	Forward	5'-GGG GAC AAG TTT GTA CAA AAA AGC AGG CTT AGC CAC CAT GCT GAT TTC TTG TCG CCT GCT GGC T-3'
		Reverse	5'-GGG GAC CAC TTT GTA CAA GAA AGC TGG GTT TGA CTG CTG CTT TCC TGC GG-3'
	Am-MCUP1	Forward	5'-GGG GAC AAG TTT GTA CAA AAA AGC AGG CTT AGC CAC CAT GTT CGC ACA GTC CCG CCC ATT T-3'
		Reverse	5'-GGG GAC CAC TTT GTA CAA GAA AGC TGG GTT TTT GCC GCC CAG AAT CTC GTG-3'
	Am-EMRE1	Forward	5'-GGG GAC AAG TTT GTA CAA AAA AGC AGG CTT AGC CAC CAT GCC TCA GCT GCA TTT CTC ATC ATC TTT CG-3'
		Reverse	5'-GGG GAC CAC TTT GTA CAA GAA AGC TGG GTT CCA CCA TCG CAG GCT ATT TGA CCC-3'
	Am-EMRE2	Forward	5'-GGG GAC AAG TTT GTA CAA AAA AGC AGG CTT AGC CAC CAT GCC CCC TCT GCA CCA CGC C-3'
		Reverse	5'-GGG GAC CAC TTT GTA CAA GAA AGC TGG GTT CCA CCA CCT CCA ATG GCT TTT CC-3'
	Am-EMRE1-t	Forward	5'-GGG GAC AAG TTT GTA CAA AAA AGC AGG CTT AGC CAC CAT GCC TCA GCT GCA TTT CTC ATC ATC-3'
		Reverse	5'-GGG GAC CAC TTT GTA CAA GAA AGC TGG GTT CAC TCC TGC GTC ATC GTC ATC GT-3'
	Am-EMRE2-t	Forward	5'-GGG GAC AAG TTT GTA CAA AAA AGC AGG CTT AGC CAC CAT GCC CCC TCT GCA CCA CG-3'

		Reverse	5'-GGG GAC CAC TTT GTA CAA GAA AGC TGG GTT CAC TCC TGC GTC CTC ATC GTC A-3'
<i>Homo sapiens</i>	Hs-EMRE-ct	Forward	5'-GGG GAC AAG TTT GTA CAA AAA AGC AGG CTT AGC CAC CAT GGC GTC CGG AGC GGC-3'
		Reverse	5'-GGG GAC CAC TTT GTA CAA GAA AGC TGG GTT CCA GAA CTT CAG CCA GCC CC-3'
<i>Cyphellophora europaea</i>	Ce-MCUP	Forward	5'-GGG GAC AAG TTT GTA CAA AAA AGC AGG CTT AGC CAC CAT GAC TAA AGG CAA GCT GTT GAC GAC-3'
		Reverse	5'-GGG GAC CAC TTT GTA CAA GAA AGC TGG GTT TCT TGG TTC CGT TGT TGT TCT TTC GC-3'
<i>Fusarium graminearum</i>	Fg-MCUP	Forward	5'-GGG GAC AAG TTT GTA CAA AAA AGC AGG CTT AGC CAC CAT GAA CCA CGC TCT AAG GCG C-3'
		Reverse	5'-GGG GAC CAC TTT GTA CAA GAA AGC TGG GTT CGG CCA GGG CCG CAA-3'
<i>Metarhizium acridum</i>	Ma-MCUP	Forward	5'-GGG GAC AAG TTT GTA CAA AAA AGC AGG CTT AGC CAC CAT GGG CCA TGT CTT GGG TGG-3'
		Reverse	5'-GGG GAC CAC TTT GTA CAA GAA AGC TGG GTT GGT CCC AGC CCA TAT CGG TGT-3'
<i>Neosartorya fischeri</i>	Nf-MCUP	Forward	5'-GGG GAC AAG TTT GTA CAA AAA AGC AGG CTT AGC CAC CAT GCG GGC GCT TGT TAG CC-3'
		Reverse	5'-GGG GAC CAC TTT GTA CAA GAA AGC TGG GTT GCG CGT CAC ACT CAT GCT TGA-3'

Supplementary Table 2. List of PCR primers used to amplify cDNAs from pLX304 vector to perform cloning into yeast expression vectors.

Species	cDNA	Direction	Primer sequence
<i>Spizellomyces punctatus</i>	Sp-MCU	Forward	5'- GGG GGA TCC ATG CGA ATC CCC TTC CA-3'
	Sp-MCUP	Forward	5'- GGG GGA TCC ATG GTG AGC CTG ATT CCA G-3'
	Sp-EMRE	Forward	5'- GGG GGA TCC ATG TCC CGC ATT CTG ACA -3'
<i>Allomyces macrogynus</i>	Am-MCUa	Forward	5'- GGG GGA TCC ATG CTG TCA AGG GCT CTG-3'
	Am-MCUB	Forward	5'- GGG GGA TCC ATG CTG ATT TCT TGT CGC C-3'
	Am-MCUP1	Forward	5'- GGG GGA TCC ATG TTC GCA CAG TCC CG-3'
	Am-EMRE1	Forward	5'- GGG GGA TCC ATG CCT CAG CTG CAT TTC T-3'
	Am-EMRE2	Forward	5'- GGG GGA TCC ATG CCC CCT CTG CAC-3'
<i>Cyphellophora europaea</i>	Ce-MCUP	Forward	5'-GGG GGA TCC ATG ACC AAG GGC AAG CT-3'
<i>Fusarium graminearum</i>	Fg-MCUP	Forward	5'-GGG GGA TCC ATG AAC CAC GCC CTG AG-3'
<i>Metarhizium acridum</i>	Ma-MCUP	Forward	5'-GGG GGA TCC ATG GGA CAC GTG CTG G-3'
<i>Neosartorya fischeri</i>	Nf-MCUP	Forward	5'-GGG GGA TCC ATG AGA GCC CTG GTG TCT-3'
<i>Homo sapiens</i>	Hs-EMRE	Forward	5'-GGG CCC GGG ATG GCG TCC GGA GC-3'
	V5	Reverse	5'-GGG CTC GAG CTA CGT AGA ATC GAG ACC GAG-3'

Discussion

4.1 The functional interaction between MCU and MICU1

The results presented in this thesis demonstrate the power of combining comparative genomics analyses with yeast genetics and physiology for dissecting the functional and mechanistic role of each component of the mammalian uniporter. Numerous findings have recently highlighted the physiological importance of obtaining great plasticity and selectivity in mt-Ca²⁺ uptake activity (Mammucari *et al.*, 2017). The tight control between limiting mt-Ca²⁺ influx at cellular rest and ensuring rapid mt-Ca²⁺ uptake upon a cyt-Ca²⁺ signal is essential to regulate the transmission of intracellular Ca²⁺ dynamics into the mitochondria, while preventing excessive mt-Ca²⁺ loading (Duchen, 2000; Hajnóczky *et al.*, 1999). To achieve this, the activation and selectivity of the mitochondrial uniporter has to be tightly regulated. Previously, the selective permeability of Ca²⁺ through the uniporter has been shown to be contributed by the high-affinity ion binding DXXE motif of the MCU pore (Arduino *et al.*, 2017; Baughman *et al.*, 2011; Cao *et al.*, 2017; Chaudhuri *et al.*, 2013; Oxenoid *et al.*, 2016), whose activation and pore opening are modulated by its gating and cooperativity regulators MICU1 and MICU2 or MICU3 (Csordás *et al.*, 2013; Kamer *et al.*, 2017; Mallilankaraman *et al.*, 2012; Patron *et al.*, 2014, 2019). Precise functional roles and physiological implications of the interactions among these subunits of the MCUC on the uniporter activity have only been investigated in mammalian systems thus far. However, the differences observed in the level of gene silencing (Csordás *et al.*, 2013; Mallilankaraman *et al.*, 2012), tissue-specific composition (Murgia and Rizzuto, 2015; Vecellio Reane *et al.*, 2016), stoichiometry and compensatory remodelling (Liu *et al.*, 2016; Paillard *et al.*, 2017) have hampered the interpretations of previous results.

An important goal of the studies presented in this thesis was to establish a testbed for dissecting the functional contribution of each component of the human uniporter. Those studies have been successfully published in Cell Reports (Wettmarshausen, Goh *et al.* 2018). *S. cerevisiae* was chosen as the model system due to the complete absence of any detectable MCU homolog (Bick *et al.*, 2012; Cheng and Perocchi, 2015) and endogenous mt-Ca²⁺ uptake activity in yeast (Arduino *et al.*, 2017; Carafoli and Lehninger, 1971; Kovačs-Bogdán *et al.*, 2014; Yamamoto *et al.*, 2016). In addition, yeast is easily amenable by the expression of human MCUC proteins, such as MCU and EMRE, allowing the reconstitution of mt-Ca²⁺ uptake *in vitro* into the matrix of isolated yeast mitochondria (Arduino *et al.*, 2017; Kovačs-Bogdán *et al.*, 2014; Yamamoto *et al.*, 2016). A yeast-based heterologous system was engineered to investigate the functional interconnection between the highly co-evolved

uniporter subunits, MCU and MICU1, *in vivo*. Consistent to previous studies (Arduino *et al.*, 2017; Kovačs-Bogdán *et al.*, 2014; Yamamoto *et al.*, 2016), both MCU and EMRE were found to be the minimal subunits to trigger mt-Ca²⁺ entry into the matrix of isolated mitochondria. Influx of mt-Ca²⁺ was also reconstituted *in vivo* in yeast upon a physiological stimulus and found to be augmented by the expression of MICU1, in a Ca²⁺-dependent manner, similarly to mammalian cells (Kamer and Mootha, 2014; Perocchi *et al.*, 2010).

Different biological growth conditions were used to understand the cellular advantage provided by the interaction of MCU and MICU1. Among all the conditions tested, Mn²⁺ treatment was identified to be lethal to yeast cells expressing MCU and EMRE, possibly due to the permeability of the uniporter to Mn²⁺ as reported previously (Cao *et al.*, 2017; Csordás and Hajnóczy, 2003; Mela and Chance, 1968; N-EI, 2012; Romslo and Flatmark, 1973; Vinogradov and Scarpa, 1973). Indeed, an independent study had also supported the conductance of Mn²⁺ through the uniporter by demonstrating the high affinity binding of Mn²⁺ to the DXE domain of MCU (Cao *et al.*, 2017). Instead, the co-expression of MICU1, independent of functional EF-hand domains, protected yeast cells from the susceptibility to Mn²⁺ treatment, indicating that Mn²⁺ influx is inhibited by the presence of MICU1. The latter would act as a selectivity lid, only allowing the entry of ions through the uniporter upon the specific binding of Ca²⁺ to its EF-hand domains. Furthermore, these findings indicated that MICU1 is self-sufficient, without MICU2 or MICU3, in gating the activity of the uniporter, supporting the role of MICU1 as the main docking site for MICU2 or MICU3 to carry out their functions in fine tuning the uniporter activity (Patron *et al.*, 2019). These findings were reiterated in mammalian HEK293 cells, whereby the uptake of Mn²⁺ into the mitochondria of cells with a genetic knockout of MICU1 was prevented by the re-expression of MICU1 or by inhibiting MCU with RuRed. As Mn²⁺, unlike Ca²⁺, was unable to bind to the EF-hand domains (Senguen and Grabarek, 2012; Shirran and Barran, 2009), it was therefore insufficient to activate any change in MICU1 conformation to open the MCU channel, similarly shown by Kamer *et al.* (2018).

Finally, the susceptibility of MICU1-KO cells to the MCU-dependent Mn²⁺-induced cell death was shown to be a consequence of an increase in oxidative stress, possibly due to the inhibition of both Na⁺-dependent and Na⁺-independent Ca²⁺ efflux pathways by toxic levels of mitochondrial Mn²⁺ (Gavin *et al.*, 1990), causing an overload of mt-Ca²⁺, increasing oxidative stress and an eventual cell death (Smith *et al.*, 2017). In turn, this Mn²⁺-induced cell death was prevented by a thiol antioxidant, NAC, treatment that has been previously shown to decrease mitochondrial ROS and Mn²⁺-induced oxidative stress (Barreiro *et al.*, 2005; Nagata *et al.*, 2007; Stephenson *et al.*, 2013). As NAC exhibits either a direct antioxidant effect via its free

thiol group or indirectly as a glutathione precursor, the inability of glutathione in preventing Mn^{2+} -induced cell death suggested a direct antioxidant action of NAC in reducing Mn^{2+} -induced protein thiol oxidation (Marreilha dos Santos *et al.*, 2008). Altogether, these findings may prove instrumental to patients with loss-of-function mutations in MICU1, who display high basal mt- Ca^{2+} levels and clinical phenotypes, such as muscle fatigue, under-development and ataxia, that are similarly observed in MICU1-KO mouse models (Antony *et al.*, 2016; Lewis-Smith *et al.*, 2016; Liu *et al.*, 2016; Logan *et al.*, 2014; Musa *et al.*, 2019), possibly attributable to the increase in mitochondrial Mn^{2+} . These findings also suggest that the uniporter is a possible target for neurological diseases that are caused by environmental intoxication of Mn^{2+} , such as Mn^{2+} -rich food, Mn^{2+} aerosols and dusts in mines and smelters, and air pollution from the combustion of gasoline containing methylcyclopentadienyl Mn^{2+} tricarbonyl (O'Neal and Zheng, 2015). Although current therapeutic strategy against Mn^{2+} toxicity aims to either remove patients from the source of Mn^{2+} exposure or alleviate life-threatening Mn^{2+} intoxication by chelation therapies, clinical symptoms have not been improved (Jiang *et al.*, 2006; Walter *et al.*, 2015). While the cellular and molecular mechanism of Mn^{2+} toxicity is still not well understood, the current finding of Mn^{2+} -induced oxidative stress could be targeted to improve clinical symptoms. As NAC, which prevented the MCU-dependent Mn^{2+} -induced cell death, is used clinically, it could constitute an ideal preventive treatment for both MICU1- and Mn^{2+} -related disorders. Future studies will be required to determine the contributions of the uniporter-mediated mitochondrial accumulation of Mn^{2+} in the pathology of MICU1- and Mn^{2+} -related diseases.

Overall, the reconstitution of a regulated uniporter in yeast has provided a clean system for the investigation of an inter-functional interactions between MICU1 and MCU, compared to mammalian systems, whereby those have been obscured by the contributions from other uniporter subunits such as MICU2 (Kamer and Mootha, 2014; Patron *et al.*, 2014; Plovanich *et al.*, 2013). Importantly, unravelling the role of MICU1 as a Ca^{2+} selectivity filter for the uniporter, apart from its gatekeeper's function, may provide insights and implications in preventing MCU-dependent mitochondrial Mn^{2+} -induced cytotoxicity in MICU1-deficient patients (Figure 4.1).

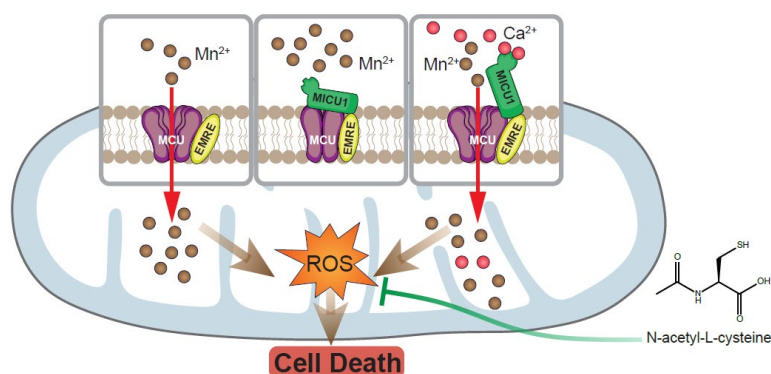


Figure 4.1. Schematic model of MICU1 regulation on the uniporter. In the absence of MICU1, the uniporter is an open pore that allows the entry of cytosolic Mn²⁺ into the mitochondria, resulting in an increase in reactive oxygen species (ROS) production and eventual cell death. The presence of MICU1 prevents Mn²⁺-induced cell death due to the selectivity of the MICU1 for Ca²⁺, maintaining the pore in a closed conformation. However, a rise in cyt-Ca²⁺ during cellular signalling binds to the MICU1 EF-hands, causing a conformational change that opens the uniporter pore, allowing the transport of Ca²⁺ and Mn²⁺ into the mitochondria. An antioxidant treatment with N-acetyl-L-cysteine is able to counteract this Mn²⁺-induced cell death. Red and brown circles indicate Ca²⁺ ions and Mn²⁺, respectively. From Wettmarshausen *et al.* (2018).

4.2 The uniporter evolutionary history

The phylogenetic analysis presented in the first part of this thesis, together with a previous study (Bick *et al.*, 2012), have emphasized the widespread co-evolutionary distribution of MCU and MICU1 across all major eukaryotic groups, with an exception in fungi. Several species in the Basidiomycota and Ascomycota fungal clades (e.g., *N. crassa* and *A. fumigatus*) contain MCU homologs without any detectable MICU1. It is thus foreseeable that mt-Ca²⁺ uptake can take place in those species through the uniporter in a MICU1-independent mechanism. However, fungal MCU homologs from *N. crassa* and *A. fumigatus* were not only unable to complement the loss of mt-Ca²⁺ uptake activity in mammalian MCU knockdown HeLa cells, but were also unable to reconstitute *in vivo* mt-Ca²⁺ uptake in yeast, despite their proper expression, localization and assembly. These findings were in agreement with previous studies that have demonstrated limited Ca²⁺ uptake, in the range of hours, into the mitochondria of *N. crassa* (Carafoli and Lehninger, 1971; Gonçalves *et al.*, 2015), which is independent of mitochondrial membrane potential and is only partially sensitive to Ru360. Although mt-Ca²⁺ uptake activity was previously observed in *A. fumigatus*, the deletion of the MCU homolog from *A. fumigates* only led to a partial decrease in mt-Ca²⁺ influx (Song *et al.*, 2016), indicating that these fungal MCU homologs were not functioning similarly to that of the Ca²⁺-specific mammalian uniporter. Several Ascomycota MCU homologs structures have

been recently determined to understand the mechanism of the uniporter function, without any direct evidence of mt-Ca²⁺ uptake in these respective species (Baradaran *et al.*, 2018; Fan *et al.*, 2018; Nguyen *et al.*, 2018; Yoo *et al.*, 2018). However, Baradaran *et al.* (2018) has reported that fungal MCU homologs are incapable of reconstituting mt-Ca²⁺ uptake when expressed in yeast or mammalian cells. Hence, fungal MCU homologs could be functioning as a non-Ca²⁺ uniporter or could possess a different Ca²⁺ transport mechanism. Further experiments will be necessary to unveil the function of these MCU-like proteins in Fungi.

While evolutionary analyses predicted mt-Ca²⁺ uptake to originate from an ancient eukaryote (Bick *et al.*, 2012), the discovery of EMRE as a metazoan-specific protein, yet essential MCU subunit (Sancak *et al.*, 2013), would contradict this initial hypothesis. The existence of fungal species, such as Ascomycota, whereby MCU homologs exist without MICU1 and EMRE, implies a diversified uniporter composition and regulation in different phylogenetic lineages. In the second part of this thesis (those studies have been successfully published in Nature Communications (Pittis, Goh *et al.* 2020), the evolutionary patterns and distributions of MCU, MICU and EMRE were analyzed to reconcile an apparent paradox of having uniporter homologs in organisms without any detectable mt-Ca²⁺ uptake activity. Through a comprehensive phylogenomic analysis of uniporter subunits across thousands of eukaryotes, two distinct subfamilies of MCUs (animal-like MCU and fungal-specific MCU paralog (MCUP)) were identified to originate from an early duplication event. Most fungal species were found to loss their animal-like MCU, while retaining their paralogous MCUP that were previously found to be unable to conduct mt-Ca²⁺ transport (Carafoli and Lehninger, 1971; Gonçalves *et al.*, 2015; Song *et al.*, 2016). Several MCUPs have been recently assumed to function similarly to Hs-MCU and have been used to study the uniporter structure and regulation (Baradaran *et al.*, 2018; Fan *et al.*, 2018; Nguyen *et al.*, 2018; Yoo *et al.*, 2018). However, these MCUPs have been demonstrated to be incapable of reconstituting *in vivo* mt-Ca²⁺ uptake in yeast or rescuing the loss of mt-Ca²⁺ uptake activity in HeLa cells that lack MCU, suggesting that MCUPs do not function similarly to mammalian MCUs. Moreover, differences in the structure and sequences between fungal and animal-like MCUs have been confirmed by a recent structural analyses (Wang *et al.*, 2019). For example, the linker helix domain in human MCU, which is absent in fungal MCU homologs, has been shown to rotate and maintain an open pore conformation for mt-Ca²⁺ uptake (Wang *et al.*, 2019), suggesting that MCUP may function as a non-classical uniporter that can be explored in future experiments.

Consistent with the phylogenetic analysis presented in the first part of the thesis, the tight co-evolutionary pattern of MCU and MICU orthologs observed across eukaryotes indicated a strong functional inter-dependence between both proteins. Indeed, MICU1 plays an essential

role in the ion-selectivity, gating and cooperative activation of MCU (Csordás *et al.*, 2013; Wettmarshausen *et al.*, 2018), suggesting the reliance of the uniporter on MICU1 for mt-Ca²⁺ homeostasis and cellular physiology. While MICU was predicted to be encoded in species with a functional MCU complex, twelve species were found to contain either one of the two subunits that could be a result of assembly or annotation errors. Interestingly, all species in Onchocercidae, a family of parasitic nematodes (*Brugia malayi*, *Onchocerca volvulus* and *Loa loa*) that cause severe skin infections, blindness or lymphatic swellings in human host (Mathison *et al.*, 2019), have MCU without any MICU1 homologs, possibly due to an undetected or an apparent loss of MICU1 that requires further experimental confirmation. As these parasites possess the minimum components, MCU and EMRE homologs, for uniporter activity, they would be interesting targets to further understand the physiological significance of MICU1 that could provide direct therapeutic strategies against these parasites, which are still unfound to date.

A major finding from the second part of this thesis was the discovery of non-metazoan EMRE sequences and an animal-like uniporter complex, consisting of an animal-like MCU, MICU1 and EMRE homologs, in three chytrid fungal species, including *Allomyces macrogynus* and *Spizellomyces punctatus*, indicating that mt-Ca²⁺ uptake originates from an opisthokont ancestry. Animal-like MCUs from *A. macrogynus* and *S. punctatus*, but not their MCUPs that were found to lack conserved residues, were able to mediate mt-Ca²⁺ uptake in the presence of their respective EMRE orthologs. While chytrid EMREs were able to activate mt-Ca²⁺ uptake activity through their respective animal-like MCUs and human MCU, human EMRE was only able to activate mt-Ca²⁺ uptake through human MCU. Owing to the vast differences between the EMRE sequences of metazoan and fungi, EMRE may have been efficiently developed in metazoan that became incompatible for the interaction with the animal-like MCU from chytrid fungi. Hence, these findings revealed a tight co-evolution of MCU and EMRE and provided valuable information for structural and functional studies to target conserved residues and regions among animal-like MCUs, but not MCUPs, to understand the functional interaction between MCU and EMRE in the regulation of the uniporter activity that is crucial for cellular Ca²⁺ homeostasis.

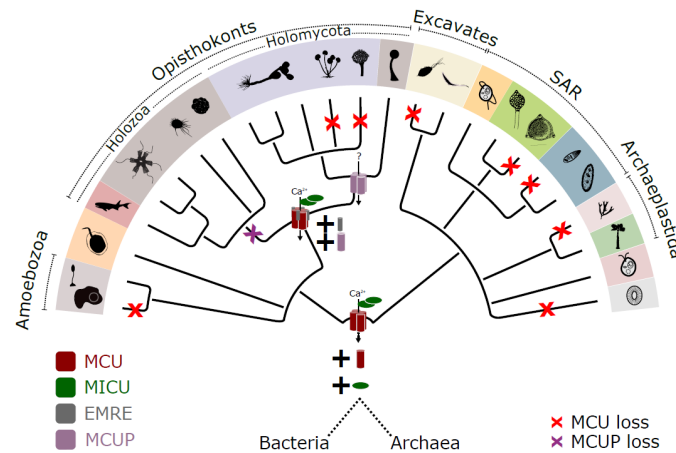


Figure 4.2. Schematic representation of the evolution of the uniporter complex in Eukaryotes. MCU-MICU complex emerges at the origin of eukaryotes, followed by EMRE in opisthokonts. MCUP is only found in Holomycota. Losses of MCU in the various eukaryotic lineages and the loss of MCUP in Holozoa are indicated in red and purple respectively. From Pittis *et al.* (2020).

Overall, a comprehensive phylogenomic analyses has not only resolved the evolutionary paradox of the inconsistent uniporter phylogenetic distribution among eukaryotes, but also discovered non-animal EMRE sequences, which was previously characterised as a metazoan innovation (Sancak *et al.*, 2013), re-setting the origin of mt-Ca²⁺ homeostasis to an ancient opisthokont (Figure 4.2). Altogether, both studies emphasize that the shared evolutionary history of the uniporter subunits reveals additional role of its regulatory subunit and uncovers closely-related orthologs to better understand the regulation of the uniporter and provide insights for diseases with mt-Ca²⁺ dysfunction.

References

- Alam, M.R., Groschner, L.N., Parichatikanond, W., Kuo, L., Bondarenko, A.I., Rost, R., Waldeck-Weiermair, M., Malli, R., and Graier, W.F. (2012). Mitochondrial Ca^{2+} uptake 1 (MICU1) and mitochondrial ca^{2+} uniporter (MCU) contribute to metabolism-secretion coupling in clonal pancreatic β -cells. *J. Biol. Chem.* 287, 34445–34454 (41).
- Anderson, A.J., Jackson, T.D., Stroud, D.A., and Stojanovski, D. (2019). Mitochondria—hubs for regulating cellular biochemistry: Emerging concepts and networks. *Open Biol.* 9 (8).
- Anderson, S., Bankier, A.T., Barrell, B.G., De Bruijn, M.H.L., Coulson, A.R., Drouin, J., Eperon, I.C., Nierlich, D.P., Roe, B.A., Sanger, F., *et al.* (1981). Sequence and organization of the human mitochondrial genome. *Nature* 290, 457–465 (5806).
- Antony, A.N., Paillard, M., Moffat, C., Juskeviciute, E., Correnti, J., Bolon, B., Rubin, E., Csordás, G., Seifert, E.L., Hoek, J.B., *et al.* (2016). MICU1 regulation of mitochondrial Ca^{2+} uptake dictates survival and tissue regeneration. *Nat. Commun.* 7 (10955).
- Arduino, D.M., Wettmarshausen, J., Vais, H., Navas-Navarro, P., Cheng, Y., Leimpek, A., Ma, Z., Delrio-Lorenzo, A., Giordano, A., Garcia-Perez, C., *et al.* (2017). Systematic Identification of MCU Modulators by Orthogonal Interspecies Chemical Screening. *Mol. Cell* 67, 711-723.e7 (4).
- Bagur, R., and Hajnóczky, G. (2017). Intracellular Ca^{2+} Sensing: Its Role in Calcium Homeostasis and Signaling. *Mol. Cell* 66, 780–788 (6).
- Baradaran, R., Wang, C., Siliciano, A.F., and Long, S.B. (2018). Cryo-EM structures of fungal and metazoan mitochondrial calcium uniporters. *Nature* 559, 580–584 (7715).
- Barreiro, E., Sánchez, D., Gáldiz, J.B., Hussain, S.N.A., and Gea, J. (2005). N-acetylcysteine increases manganese superoxide dismutase activity in septic rat diaphragms. *Eur. Respir. J.* 26, 1032–1039 (6).
- Baughman, J.M., Perocchi, F., Girgis, H.S., Plovanich, M., Belcher-Timme, C.A., Sancak, Y., Bao, X.R., Strittmatter, L., Goldberger, O., Bogorad, R.L., *et al.* (2011). Integrative genomics identifies MCU as an essential component of the mitochondrial calcium uniporter. *Nature* 476, 341–345 (7360).
- Bernardi, P. (1999). Mitochondrial transport of cations: Channels, exchangers, and permeability transition. *Physiol. Rev.* 79, 1127–1155 (4).

- Berridge, M.J., and Galione, A. (1988). Cytosolic calcium oscillators. *FASEB J. Off. Publ. Fed. Am. Soc. Exp. Biol.* 2, 3074–3082 (15).
- Berridge, M., Lipp, P., and Bootman, M. (1999). Calcium signalling. *Curr. Biol.* 9 (5).
- Berridge, M.J., Lipp, P., and Bootman, M.D. (2000). The versatility and universality of calcium signalling. *Nat. Rev. Mol. Cell Biol.* 1, 11–21 (1).
- Berridge, M.J., Bootman, M.D., and Roderick, H.L. (2003). Calcium signalling: Dynamics, homeostasis and remodelling. *Nat. Rev. Mol. Cell Biol.* 4, 517–529 (7).
- Bick, A.G., Calvo, S.E., and Mootha, V.K. (2012). Evolutionary diversity of the mitochondrial calcium uniporter. *Science.* 336, 886 (6083).
- Bick, A.G., Wakimoto, H., Kamer, K.J., Sancak, Y., Goldberger, O., Axelsson, A., DeLaughter, D.M., Gorham, J.M., Mootha, V.K., Seidman, J.G., *et al.* (2017). Cardiovascular homeostasis dependence on MICU2, a regulatory subunit of the mitochondrial calcium uniporter. *Proc. Natl. Acad. Sci. U. S. A.* 114, E9096–E9104 (43).
- Bonora, M., and Pinton, P. (2014). The mitochondrial permeability transition pore and cancer: Molecular mechanisms involved in cell death. *Front. Oncol.* 4, 302 (NOV).
- Boulware, M.J., and Marchant, J.S. (2008). Timing in Cellular Ca²⁺ Signaling. *Curr. Biol.* 18, R769–R776 (17).
- Cai, X., and Clapham, D.E. (2012). Ancestral Ca²⁺ signaling machinery in early animal and fungal evolution. *Mol. Biol. Evol.* 29, 91–100 (1).
- Cao, C., Wang, S., Cui, T., Su, X.C., and Chou, J.J. (2017). Ion and inhibitor binding of the double-ring ion selectivity filter of the mitochondrial calcium uniporter. *Proc. Natl. Acad. Sci. U. S. A.* 114, E2846–E2851 (14).
- Carafoli, E., and Crompton, M. (1978). The regulation of intracellular calcium by mitochondria. *Ann. N. Y. Acad. Sci.* 307, 269–284 (1).
- Carafoli, E., and Lehninger, A.L. (1971). A survey of the interaction of calcium ions with mitochondria from different tissues and species. *Biochem. J.* 122, 681–690 (5).
- Carafoli, E., Tiozzo, R., Lugli, G., Crovetti, F., and Kratzing, C. (1974). The release of calcium from heart mitochondria by sodium. *J. Mol. Cell. Cardiol.* 6, 361–371 (4).
- Cárdenas, C., Miller, R.A., Smith, I., Bui, T., Molgó, J., Müller, M., Vais, H., Cheung, K.H., Yang, J., Parker, I., *et al.* (2010). Essential Regulation of Cell Bioenergetics by Constitutive InsP3 Receptor Ca²⁺ Transfer to Mitochondria. *Cell* 142, 270–283 (2).

- Chaudhuri, D., Sancak, Y., Mootha, V.K., and Clapham, D.E. (2013). MCU encodes the pore conducting mitochondrial calcium currents. *Elife* 2013 (2).
- Cheng, Y., and Perocchi, F. (2015). ProtPhylo: identification of protein-phenotype and protein-protein functional associations via phylogenetic profiling. *Nucleic Acids Res.* 43, W160-8 (W1).
- Clapham, D.E. (2007). Calcium Signaling. *Cell* 131, 1047–1058 (6).
- Crompton, M., Capano, M., and Carafoli, E. (1976). The Sodium-Induced Efflux of Calcium from Heart Mitochondria. A Possible Mechanism for the Regulation of Mitochondrial Calcium. *Eur. J. Biochem.* 69, 453–462 (2).
- Csordás, G., and Hajnóczky, G. (2003). Plasticity of mitochondrial calcium signaling. *J. Biol. Chem.* 278, 42273–42282 (43).
- Csordás, G., Thomas, A.P., and Hajnóczky, G. (1999). Quasi-synaptic calcium signal transmission between endoplasmic reticulum and mitochondria. *EMBO J.* 18, 96–108 (1).
- Csordás, G., Golenár, T., Seifert, E.L., Kamer, K.J., Sancak, Y., Perocchi, F., Moffat, C., Weaver, D., De la Fuente, S., Bogorad, R., *et al.* (2013). MICU1 controls both the threshold and cooperative activation of the mitochondrial Ca²⁺ uniporter. *Cell Metab.* 17, 976–987 (6).
- Davies, A.M., Hershman, S., Stabley, G.J., Hoek, J.B., Peterson, J., and Cahill, A. (2003). A Ca²⁺-induced mitochondrial permeability transition causes complete release of rat liver endonuclease G activity from its exclusive location within the mitochondrial intermembrane space. Identification of a novel endo-exonuclease activity residing within. *Nucleic Acids Res.* 31, 1364–1373 (4).
- Debattisti, V., Horn, A., Singh, R., Seifert, E.L., Hogarth, M.W., Mazala, D.A., Huang, K.T., Horvath, R., Jaiswal, J.K., and Hajnóczky, G. (2019). Dysregulation of Mitochondrial Ca²⁺ Uptake and Sarcolemma Repair Underlie Muscle Weakness and Wasting in Patients and Mice Lacking MICU1. *Cell Rep.* 29, 1274-1286.e6 (5).
- Deluca, H.F., and Engstrom, G.W. (1961). Calcium uptake by rat kidney mitochondria. *Proc. Natl. Acad. Sci. U. S. A.* 47, 1744–1750 (11).
- Denton, R.M., and McCormack, J.G. (1980). The role of calcium in the regulation of mitochondrial metabolism. *Biochem. Soc. Trans.* 8, 266–268 (3).
- Denton, R.M., and McCormack, J.G. (1985). Ca²⁺ transport by mammalian mitochondria and its role in hormone action. *Am. J. Physiol. - Endocrinol. Metab.* 12 (6).

- Denton, R.M., and McCormack, J.G. (1990). Ca^{2+} as a second messenger within mitochondria of the heart and other tissues. *Annu. Rev. Physiol.* 52, 451–466.
- Doonan, P.J., Chandramoorthy, H.C., Hoffman, N.E., Zhang, X., Cárdenas, C., Shanmughapriya, S., Rajan, S., Vallem, S., Chen, X., Foskett, J.K., *et al.* (2014). LETM1-dependent mitochondrial Ca^{2+} flux modulates cellular bioenergetics and proliferation. *FASEB J.* 28, 4936–4949 (11).
- Drago, I., De Stefani, D., Rizzuto, R., and Pozzan, T. (2012). Mitochondrial Ca^{2+} uptake contributes to buffering cytoplasmic Ca^{2+} peaks in cardiomyocytes. *Proc. Natl. Acad. Sci. U. S. A.* 109, 12986–12991 (32).
- Drahota, Z., Carafoli, E., Rossi, C.S., Gamble, R.L., and Lehninger, A.L. (1965). The steady state maintenance of accumulated Ca^{++} in rat liver mitochondria. *J. Biol. Chem.* 240, 2712–2720.
- Duchen, M.R. (2000). Mitochondria and calcium: From cell signalling to cell death. *J. Physiol.* 529, 57–68 (1).
- Fan, C., Fan, M., Orlando, B.J., Fastman, N.M., Zhang, J., Xu, Y., Chambers, M.G., Xu, X., Perry, K., Liao, M., *et al.* (2018). X-ray and cryo-EM structures of the mitochondrial calcium uniporter. *Nature* 559, 575–579 (7715).
- Frieden, M., Arnaudeau, S., Castelbou, C., and Demaurex, N. (2005). Subplasmalemmal mitochondria modulate the activity of plasma membrane Ca^{2+} -ATPases. *J. Biol. Chem.* 280, 43198–43208 (52).
- Gavin, C.E., Gunter, K.K., and Gunter, T.E. (1990). Manganese and calcium efflux kinetics in brain mitochondria. Relevance to manganese toxicity. *Biochem. J.* 266, 329–334 (2).
- Giorgi, C., Marchi, S., and Pinton, P. (2018). The machineries, regulation and cellular functions of mitochondrial calcium. *Nat. Rev. Mol. Cell Biol.* 19, 713–730 (11).
- Glitsch, M.D., Bakowski, D., and Parekh, A.B. (2002). Store-operated Ca^{2+} entry depends on mitochondrial Ca^{2+} uptake. *EMBO J.* 21, 6744–6754 (24).
- Gonçalves, A.P., Cordeiro, J.M., Monteiro, J., Lucchi, C., Correia-De-Sá, P., and Videira, A. (2015). Involvement of mitochondrial proteins in calcium signaling and cell death induced by staurosporine in *Neurospora crassa*. *Biochim. Biophys. Acta - Bioenerg.* 1847, 1064–1074 (10).
- Hajnóczky, G., and Csordás, G. (2010). Calcium signalling: Fishing out molecules of mitochondrial calcium transport. *Curr. Biol.* 20, R888 (20).

- Hajnóczky, G., Robb-Gaspers, L.D., Seitz, M.B., and Thomas, A.P. (1995). Decoding of cytosolic calcium oscillations in the mitochondria. *Cell* 82, 415–424 (3).
- Hajnóczky, G., Hager, R., and Thomas, A.P. (1999). Mitochondria suppress local feedback activation of inositol 1,4,5- trisphosphate receptors by Ca^{2+} . *J. Biol. Chem.* 274, 14157–14162 (20).
- Holmström, K.M., Pan, X., Liu, J.C., Menazza, S., Liu, J., Nguyen, T.T., Pan, H., Parks, R.J., Anderson, S., Noguchi, A., *et al.* (2015). Assessment of cardiac function in mice lacking the mitochondrial calcium uniporter. *J. Mol. Cell. Cardiol.* 85, 178–182.
- Jiang, D., Zhao, L., and Clapham, D.E. (2009). Genome-wide RNAi screen identifies Letm1 as a mitochondrial $\text{Ca}^{2+}/\text{H}^{+}$ antiporter. *Science*. 326, 144–147 (5949).
- Jiang, Y.-M., Mo, X.-A., Du, F.-Q., Fu, X., Zhu, X.-Y., Gao, H.-Y., Xie, J.-L., Liao, F.-L., Pira, E., and Zheng, W. (2006). Effective treatment of manganese-induced occupational Parkinsonism with p-aminosalicylic acid: a case of 17-year follow-up study. *J. Occup. Environ. Med.* 48, 644–649 (6).
- Kamer, K.J., and Mootha, V.K. (2014). MICU1 and MICU2 play nonredundant roles in the regulation of the mitochondrial calcium uniporter. *EMBO Rep.* 15, 299–307 (3).
- Kamer, K.J., Grabarek, Z., and Mootha, V.K. (2017). High-affinity cooperative Ca^{2+} binding by MICU 1– MICU 2 serves as an on–off switch for the uniporter . *EMBO Rep.* 18, 1397–1411 (8).
- Kamer, K.J., Sancak, Y., Fomina, Y., Meisel, J.D., Chaudhuri, D., Grabarek, Z., and Mootha, V.K. (2018). MICU1 imparts the mitochondrial uniporter with the ability to discriminate between Ca^{2+} and Mn^{2+} . *Proc. Natl. Acad. Sci. U. S. A.* 115, E7960–E7969 (34).
- Kantrow, S.P., and Piantadosi, C.A. (1997). Release of cytochrome C from liver mitochondria during permeability transition. *Biochem. Biophys. Res. Commun.* 232, 669–671 (3).
- Kennedy, E.D., Rizzuto, R., Theler, J.M., Pralong, W.F., Bastianutto, C., Pozzan, T., and Wollheim, C.B. (1996). Glucose-stimulated insulin secretion correlates with changes in mitochondrial and cytosolic Ca^{2+} in aequorin-expressing INS-1 cells. *J. Clin. Invest.* 98, 2524–2538 (11).
- Kirichok, Y., Krapivinsky, G., and Clapham, D.E. (2004). The mitochondrial calcium uniporter is a highly selective ion channel. *Nature* 427, 360–364 (6972).
- Kohlhaas, M., Nickel, A.G., and Maack, C. (2017). Mitochondrial energetics and calcium coupling in the heart. *J. Physiol.* 595, 3753–3763 (12).

- Kovács-Bogdán, E., Sancak, Y., Kamer, K.J., Plovanich, M., Jambhekar, A., Huber, R.J., Myre, M.A., Blower, M.D., and Mootha, V.K. (2014). Reconstitution of the mitochondrial calcium uniporter in yeast. *Proc. Natl. Acad. Sci. U. S. A.* *111*, 8985–8990 (24).
- Kruman, I.I., and Mattson, M.P. (1999). Pivotal role of mitochondrial calcium uptake in neural cell apoptosis and necrosis. *J. Neurochem.* *72*, 529–540 (2).
- Kudla, J., Batistič, O., and Hashimoto, K. (2010). Calcium signals: The Lead Currency of plant information processing. *Plant Cell* *22*, 541–563 (3).
- Kwong, J.Q., Lu, X., Correll, R.N., Schwanekamp, J.A., Vagnozzi, R.J., Sargent, M.A., York, A.J., Zhang, J., Bers, D.M., and Molkentin, J.D. (2015). The Mitochondrial Calcium Uniporter Selectively Matches Metabolic Output to Acute Contractile Stress in the Heart. *Cell Rep.* *12*, 15–22 (1).
- Lasorsa, F.M., Pinton, P., Palmieri, L., Fiermonte, G., Rizzuto, R., and Palmieri, F. (2003). Recombinant expression of the Ca²⁺-sensitive aspartate/ glutamate carrier increases mitochondrial ATP production in agonist-stimulated Chinese hamster ovary cells. *J. Biol. Chem.* *278*, 38686–38692 (40).
- Lewis-Smith, D., Kamer, K.J., Griffin, H., Childs, A.M., Pysden, K., Titov, D., Duff, J., Pyle, A., Taylor, R.W., Yu-Wai-Man, P., *et al.* (2016). Homozygous deletion in MICU1 presenting with fatigue and lethargy in childhood. *Neurol. Genet.* *2* (2).
- Liu, T., and Rourke, B.O. (2008). Enhancing mitochondrial Ca²⁺ uptake in myocytes from failing hearts restores energy supply and demand matching. *Circ. Res.* *103*, 279–288 (3).
- Liu, X., and Hajnóczky, G. (2009). Ca²⁺-dependent regulation of mitochondrial dynamics by the Miro-Milton complex. *Int. J. Biochem. Cell Biol.* *41*, 1972–1976 (10).
- Liu, J.C., Liu, J., Holmström, K.M., Menazza, S., Parks, R.J., Fergusson, M.M., Yu, Z.X., Springer, D.A., Halsey, C., Liu, C., *et al.* (2016). MICU1 Serves as a Molecular Gatekeeper to Prevent In Vivo Mitochondrial Calcium Overload. *Cell Rep.* *16*, 1561–1573 (6).
- Logan, C. V., Szabadkai, G., Sharpe, J.A., Parry, D.A., Torelli, S., Childs, A.M., Kriek, M., Phadke, R., Johnson, C.A., Roberts, N.Y., *et al.* (2014). Loss-of-function mutations in MICU1 cause a brain and muscle disorder linked to primary alterations in mitochondrial calcium signaling. *Nat. Genet.* *46*, 188–193 (2).
- Lopez, M.F., Kristal, B.S., Chernokalskaya, E., Lazarev, A., Shestopalov, A.I., Bogdanova, A., and Robinson, M. (2000). High-throughput profiling of the mitochondrial proteome using affinity fractionation and automation. *Electrophoresis* *21*, 3427–3440 (16).

- Luongo, T.S., Lambert, J.P., Yuan, A., Zhang, X., Gross, P., Song, J., Shanmughapriya, S., Gao, E., Jain, M., Houser, S.R., *et al.* (2015). The Mitochondrial Calcium Uniporter Matches Energetic Supply with Cardiac Workload during Stress and Modulates Permeability Transition. *Cell Rep.* 12, 23–34 (1).
- Mallilankaraman, K., Doonan, P., Cárdenas, C., Chandramoorthy, H.C., Müller, M., Miller, R., Hoffman, N.E., Gandhirajan, R.K., Molgó, J., Birnbaum, M.J., *et al.* (2012). MICU1 is an essential gatekeeper for mcu-mediated mitochondrial Ca²⁺ uptake that regulates cell survival. *Cell* 151, 630–644 (3).
- Mammucari, C., Gherardi, G., Zamparo, I., Raffaello, A., Boncompagni, S., Chemello, F., Cagnin, S., Braga, A., Zanin, S., Pallafacchina, G., *et al.* (2015). The Mitochondrial Calcium Uniporter Controls Skeletal Muscle Trophism InVivo. *Cell Rep.* 10, 1269–1279 (8).
- Mammucari, C., Raffaello, A., Vecellio Reane, D., and Rizzuto, R. (2016). Molecular structure and pathophysiological roles of the Mitochondrial Calcium Uniporter. *Biochim. Biophys. Acta - Mol. Cell Res.* 1863, 2457–2464 (10).
- Mammucari, C., Gherardi, G., and Rizzuto, R. (2017). Structure, activity regulation, and role of the mitochondrial calcium uniporter in health and disease. *Front. Oncol.* 7 (139).
- Mammucari, C., Raffaello, A., Vecellio Reane, D., Gherardi, G., De Mario, A., and Rizzuto, R. (2018). Mitochondrial calcium uptake in organ physiology: from molecular mechanism to animal models. *Pflugers Arch. Eur. J. Physiol.* 470, 1165–1179 (8).
- Mannella, C.A., Buttle, K., Rath, B.K., and Marko, M. (1998). Electron microscopic tomography of rat-liver mitochondria and their interactions with the endoplasmic reticulum. *BioFactors* 8, 225–228 (3–4).
- Marreilha dos Santos, A.P., Santos, D., Au, C., Milatovic, D., Aschner, M., and Batoréu, M.C.C. (2008). Antioxidants prevent the cytotoxicity of manganese in RBE4 cells. *Brain Res.* 1236, 200–205.
- Mathison, B.A., Couturier, M.R., and Pritt, B.S. (2019). Diagnostic Identification and Differentiation of Microfilariae. *J. Clin. Microbiol.* 57 (10).
- Matlib, M.A., Zhou, Z., Knight, S., Ahmed, S., Choi, K.M., Krause-Bauer, J., Phillips, R., Altschuld, R., Katsube, Y., Sperelakis, N., *et al.* (1998). Oxygen-bridged dinuclear ruthenium amine complex specifically inhibits Ca²⁺ uptake into mitochondria in vitro and in situ in single cardiac myocytes. *J. Biol. Chem.* 273, 10223–10231 (17).

- McCormack, J.G., Halestrap, A.P., and Denton, R.M. (1990). Role of calcium ions in regulation of mammalian intramitochondrial metabolism. *Physiol. Rev.* **70**, 391–425 (2).
- Mela, L., and Chance, B. (1968). Spectrophotometric Measurements of the Kinetics of Ca^{2+} and Mn^{2+} Accumulation in Mitochondria. *Biochemistry* **7**, 4059–4063 (11).
- Morgenstern, M., Stiller, S.B., Lübbert, P., Peikert, C.D., Dannenmaier, S., Drepper, F., Weill, U., Höß, P., Feuerstein, R., Gebert, M., *et al.* (2017). Definition of a High-Confidence Mitochondrial Proteome at Quantitative Scale. *Cell Rep.* **19**, 2836–2852 (13).
- Murgia, M., and Rizzuto, R. (2015). Molecular diversity and pleiotropic role of the mitochondrial calcium uniporter. *Cell Calcium* **58**, 11–17 (1).
- Murgia, M., Giorgi, C., Pinton, P., and Rizzuto, R. (2009). Controlling metabolism and cell death: At the heart of mitochondrial calcium signalling. *J. Mol. Cell. Cardiol.* **46**, 781–788 (6).
- Murphy, E., Pan, X., Nguyen, T., Liu, J., Holmström, K.M., and Finkel, T. (2014). Unresolved questions from the analysis of mice lacking MCU expression. *Biochem. Biophys. Res. Commun.* **449**, 384–385 (4).
- Musa, S., Eyaid, W., Kamer, K., Ali, R., Al-Mureikhi, M., Shahbeck, N., Al Mesaifri, F., Makhseed, N., Mohamed, Z., Alshehhi, W.A., *et al.* (2019). A middle eastern founder mutation expands the genotypic and phenotypic spectrum of mitochondrial MICU1 deficiency: A report of 13 patients. In *JIMD Reports*, (Springer), pp. 79–83.
- N-EI, S. (2012). Mitochondrial Uptake of Ca^{2+} and Other Bivalent Cations. *Biochem. Anal. Biochem.* **01** (05).
- Nagata, K., Iwasaki, Y., Yamada, T., Yuba, T., Kono, K., Hosogi, S., Ohsugi, S., Kuwahara, H., and Marunaka, Y. (2007). Overexpression of manganese superoxide dismutase by N-acetylcysteine in hyperoxic lung injury. *Respir. Med.* **101**, 800–807 (4).
- Nakagawa, T., Shimizu, S., Watanabe, T., Yamaguchi, O., Otsu, K., Yamagata, H., Inohara, H., Kubo, T., and Tsujimoto, Y. (2005). Cyclophilin D-dependent mitochondrial permeability transition regulates some necrotic but not apoptotic cell death. *Nature* **434**, 652–658 (7033).
- Nguyen, N.X., Armache, J.P., Lee, C., Yang, Y., Zeng, W., Mootha, V.K., Cheng, Y., Bai, X. chen, and Jiang, Y. (2018). Cryo-EM structure of a fungal mitochondrial calcium uniporter. *Nature* **559**, 570–574 (7715).
- Norris, V., Grant, S., Freestone, P., Canvin, J., Sheikh, F.N., Toth, I., Trinei, M., Modha, K., and Norman, R.I. (1996). Calcium signalling in bacteria. *J. Bacteriol.* **178**, 3677–3682 (13).

- Nowikovsky, K., Froschauer, E.M., Zsurka, G., Samaj, J., Reipert, S., Kolisek, M., Wiesenberger, G., and Schweyen, R.J. (2004). The LETM1/YOL027 gene family encodes a factor of the mitochondrial K⁺ homeostasis with a potential role in the Wolf-Hirschhorn syndrome. *J. Biol. Chem.* 279, 30307–30315 (29).
- O’Neal, S.L., and Zheng, W. (2015). Manganese Toxicity Upon Overexposure: a Decade in Review. *Curr. Environ. Heal. Reports* 2, 315–328 (3).
- Oxenoid, K., Dong, Y., Cao, C., Cui, T., Sancak, Y., Markhard, A.L., Grabarek, Z., Kong, L., Liu, Z., Ouyang, B., *et al.* (2016). Architecture of the mitochondrial calcium uniporter. *Nature* 533, 269–273 (7602).
- Pacher, P., Csordás, G., Schneider, T.G., and Hajnóczy, G. (2000). Quantification of calcium signal transmission from sarco-endoplasmic reticulum to the mitochondria. *J. Physiol.* 529, 553–564 (3).
- Pagliarini, D.J., Calvo, S.E., Chang, B., Sheth, S.A., Vafai, S.B., Ong, S.E., Walford, G.A., Sugiana, C., Boneh, A., Chen, W.K., *et al.* (2008). A Mitochondrial Protein Compendium Elucidates Complex I Disease Biology. *Cell* 134, 112–123 (1).
- Paillard, M., Csordás, G., Szanda, G., Golenár, T., Debattisti, V., Bartok, A., Wang, N., Moffat, C., Seifert, E.L., Spät, A., *et al.* (2017). Tissue-Specific Mitochondrial Decoding of Cytoplasmic Ca²⁺ Signals Is Controlled by the Stoichiometry of MICU1/2 and MCU. *Cell Rep.* 18, 2291–2300 (10).
- Palmer, A.E., Jin, C., Reed, J.C., and Tsien, R.Y. (2004). Bcl-2-mediated alterations in endoplasmic reticulum Ca²⁺ analyzed with an improved genetically encoded fluorescent sensor. *Proc. Natl. Acad. Sci. U. S. A.* 101, 17404–17409 (50).
- Palty, R., Ohana, E., Hershfinkel, M., Volokita, M., Elgazar, V., Beharier, O., Silverman, W.F., Argaman, M., and Sekler, I. (2004). Lithium-calcium exchange is mediated by a distinct potassium-independent sodium-calcium exchanger. *J. Biol. Chem.* 279, 25234–25240 (24).
- Palty, R., Silverman, W.F., Hershfinkel, M., Caporale, T., Sensi, S.L., Parnis, J., Nolte, C., Fishman, D., Shoshan-Barmatz, V., Herrmann, S., *et al.* (2010). NCLX is an essential component of mitochondrial Na⁺/Ca²⁺ exchange. *Proc. Natl. Acad. Sci. U. S. A.* 107, 436–441 (1).
- Pan, X., Liu, J., Nguyen, T., Liu, C., Sun, J., Teng, Y., Fergusson, M.M., Rovira, I.I., Allen, M., Springer, D.A., *et al.* (2013). The Physiological Role of Mitochondrial Calcium Revealed by Mice Lacking the Mitochondrial Calcium Uniporter. *Nat. Cell Biol.* 15, 1464–1472 (12).

- Patron, M., Checchetto, V., Raffaello, A., Teardo, E., VecellioReane, D., Mantoan, M., Granatiero, V., Szabò, I., DeStefani, D., and Rizzuto, R. (2014). MICU1 and MICU2 finely tune the mitochondrial Ca^{2+} uniporter by exerting opposite effects on MCU activity. *Mol. Cell* 53, 726–737 (5).
- Patron, M., Granatiero, V., Espino, J., Rizzuto, R., and De Stefani, D. (2019). MICU3 is a tissue-specific enhancer of mitochondrial calcium uptake. *Cell Death Differ.* 26, 179–195 (1).
- Perocchi, F., Gohil, V.M., Girgis, H.S., Bao, X.R., McCombs, J.E., Palmer, A.E., and Mootha, V.K. (2010). MICU1 encodes a mitochondrial EF hand protein required for Ca^{2+} uptake. *Nature* 467, 291–296 (7313).
- Pfanner, N., Warscheid, B., and Wiedemann, N. (2019). Mitochondrial proteins: from biogenesis to functional networks. *Nat. Rev. Mol. Cell Biol.* 20, 267–284 (5).
- Pinton, P., Ferrari, D., Magalhaes, P., Schulze-Osthoff, K., Di Virgilio, F., Pozzan, T., and Rizzuto, R. (2000). Reduced loading of intracellular Ca^{2+} stores and downregulation of capacitative Ca^{2+} influx in Bcl-2-overexpressing cells. *J. Cell Biol.* 148, 857–862 (5).
- Pinton, P., Ferrari, D., Rapizzi, E., Di Virgilio, F., Pozzan, T., and Rizzuto, R. (2001). The Ca^{2+} concentration of the endoplasmic reticulum is a key determinant of ceramide-induced apoptosis: significance for the molecular mechanism of Bcl-2 action. *EMBO J.* 20, 2690–2701 (11).
- Pittis, A.A., Goh, V., Cebrian-Serrano, A., Wettmarshausen, J., Perocchi, F., and Gabaldón, T. (2020). Discovery of EMRE in fungi resolves the true evolutionary history of the mitochondrial calcium uniporter. *Nat. Commun.* 11, 4031 (1).
- Plovanich, M., Bogorad, R.L., Sancak, Y., Kamer, K.J., Strittmatter, L., Li, A.A., Girgis, H.S., Kuchimanchi, S., De Groot, J., Speciner, L., *et al.* (2013). MICU2, a Paralog of MICU1, Resides within the Mitochondrial Uniporter Complex to Regulate Calcium Handling. *PLoS One* 8, e55785 (2).
- Pozzan, T., Rizzuto, R., Volpe, P., and Meldolesi, J. (1994). Molecular and cellular physiology of intracellular calcium stores. *Physiol. Rev.* 74, 595–636 (3).
- Putney, J.W., and Thomas, A.P. (2006). Calcium Signaling: Double Duty for Calcium at the Mitochondrial Uniporter. *Curr. Biol.* 16 (18).
- Raffaello, A., De Stefani, D., Sabbadin, D., Teardo, E., Merli, G., Picard, A., Checchetto, V., Moro, S., Szabò, I., and Rizzuto, R. (2013). The mitochondrial calcium uniporter is a multimer that can include a dominant-negative pore-forming subunit. *EMBO J.* 32, 2362–2376 (17).

- Ringer, S. (1883). A further Contribution regarding the influence of the different Constituents of the Blood on the Contraction of the Heart. *J. Physiol.* 4, 29-42 (1).
- Rizzuto, R., and Pozzan, T. (2006). Microdomains of intracellular Ca^{2+} : Molecular determinants and functional consequences. *Physiol. Rev.* 86, 369–408 (1).
- Rizzuto, R., Pinton, P., Carrington, W., Fay, F.S., Fogarty, K.E., Lifshitz, L.M., Tuft, R.A., and Pozzan, T. (1998). Close contacts with the endoplasmic reticulum as determinants of mitochondrial Ca^{2+} responses. *Science*. 280, 1763–1766 (5370).
- Robb-Gaspers, L.D., Burnett, P., Rutter, G.A., Denton, R.M., Rizzuto, R., and Thomas, A.P. (1998). Integrating cytosolic calcium signals into mitochondrial metabolic responses. *EMBO J.* 17, 4987–5000 (17).
- Romslo, I., and Flatmark, T. (1973). Energy-dependent accumulation of iron by isolated rat liver mitochondria. II. Relationship to the active transport of Ca^{2+} . *BBA - Bioenerg.* 325, 38–46 (1).
- Rottenberg, H., and Scarpa, A. (1974). Calcium uptake and membrane potential in mitochondria. *Biochemistry* 13, 4811–4817 (23).
- Sancak, Y., Markhard, A.L., Kitami, T., Kovács-Bogdán, E., Kamer, K.J., Udeshi, N.D., Carr, S.A., Chaudhuri, D., Clapham, D.E., Li, A.A., *et al.* (2013). EMRE is an essential component of the mitochondrial calcium uniporter complex. *Science*. 342, 1379–1382 (6164).
- Schinzel, A.C., Takeuchi, O., Huang, Z., Fisher, J.K., Zhou, Z., Rubens, J., Hetz, C., Danial, N.N., Moskowitz, M.A., and Korsmeyer, S.J. (2005). Cyclophilin D is a component of mitochondrial permeability transition and mediates neuronal cell death after focal cerebral ischemia. *Proc. Natl. Acad. Sci. U. S. A.* 102, 12005–12010 (34).
- Schuit, F.C., In 't Veld, P.A., and Pipeleers, D.G. (1988). Glucose stimulates proinsulin biosynthesis by a dose-dependent recruitment of pancreatic beta cells. *Proc. Natl. Acad. Sci. U. S. A.* 85, 3865–3869 (11).
- Senguen, F.T., and Grabarek, Z. (2012). X-ray structures of magnesium and manganese complexes with the N-terminal domain of calmodulin: Insights into the mechanism and specificity of metal ion binding to an EF-hand. *Biochemistry* 51, 6182–6194 (31).
- Shamseldin, H.E., Alasmari, A., Salih, M.A., Samman, M.M., Mian, S.A., Alshidi, T., Ibrahim, N., Hashem, M., Fageih, E., Al-Mohanna, F., *et al.* (2017). A null mutation in MICU2 causes abnormal mitochondrial calcium homeostasis and a severe neurodevelopmental disorder. *Brain* 140, 2806–2813 (11).

- Shao, J., Fu, Z., Ji, Y., Guan, X., Guo, S., Ding, Z., Yang, X., Cong, Y., and Shen, Y. (2016). Leucine zipper-EF-hand containing transmembrane protein 1 (LETM1) forms a $\text{Ca}^{2+}/\text{H}^{+}$ antiporter. *Sci. Rep.* 6, 1–9 (1).
- Shirran, S.L., and Barran, P.E. (2009). The Use of ESI-MS to Probe the Binding of Divalent Cations to Calmodulin. *J. Am. Soc. Mass Spectrom.* 20, 1159–1171 (6).
- Smith, M.R., Fernandes, J., Go, Y.M., and Jones, D.P. (2017). Redox dynamics of manganese as a mitochondrial life-death switch. *Biochem. Biophys. Res. Commun.* 482, 388–398 (3).
- Song, J., Liu, X., Zhai, P., Huang, J., and Lu, L. (2016). A putative mitochondrial calcium uniporter in *A. fumigatus* contributes to mitochondrial Ca^{2+} homeostasis and stress responses. *Fungal Genet. Biol.* 94, 15–22.
- Spät, A., Szanda, G., Csordás, G., and Hajnóczy, G. (2008). High- and low-calcium-dependent mechanisms of mitochondrial calcium signalling. *Cell Calcium* 44, 51–63 (1).
- Spinelli, J.B., and Haigis, M.C. (2018). The multifaceted contributions of mitochondria to cellular metabolism. *Nat. Cell Biol.* 20, 745–754 (7).
- De Stefani, D., Raffaello, A., Teardo, E., Szabó, I., and Rizzuto, R. (2011). A forty-kilodalton protein of the inner membrane is the mitochondrial calcium uniporter. *Nature* 476, 336–340 (7360).
- Stephenson, A.P., Schneider, J.A., Nelson, B.C., Atha, D.H., Jain, A., Soliman, K.F.A., Aschner, M., Mazzio, E., and Renee Reams, R. (2013). Manganese-induced oxidative DNA damage in neuronal SH-SY5Y cells: Attenuation of thymine base lesions by glutathione and N-acetylcysteine. *Toxicol. Lett.* 218, 299–307 (3).
- Stimers, J.R., and Byerly, L. (1982). Slowing of sodium current inactivation by ruthenium red in snail neurons. *J. Gen. Physiol.* 80, 485–497 (4).
- Suomalainen, A., and Battersby, B.J. (2018). Mitochondrial diseases: The contribution of organelle stress responses to pathology. *Nat. Rev. Mol. Cell Biol.* 19, 77–92 (2).
- Szabadkai, G., and Duchen, M.R. (2008). Mitochondria: The hub of cellular Ca^{2+} signaling. *Physiology* 23, 84–94 (2).
- Tsai, M.-F., Phillips, C.B., Ranaghan, M., Tsai, C.-W., Wu, Y., Williams, C., and Miller, C. (2016). Dual functions of a small regulatory subunit in the mitochondrial calcium uniporter complex. *Elife* 5, e15545.

- Tsai, M.F., Jiang, D., Zhao, L., Clapham, D., and Miller, C. (2014). Functional reconstitution of the mitochondrial $\text{Ca}^{2+}/\text{H}^{+}$ antiporter letm1. *J. Gen. Physiol.* **143**, 67–73 (1).
- Vasington, F.D., Gazzotti, P., Tiozzo, R., and Carafoli, E. (1972). The effect of ruthenium red on Ca^{2+} transport and respiration in rat liver mitochondria. *BBA - Bioenerg.* **256**, 43–54 (1).
- Vasington, F.D., and Murphy, J. V (1962). Ca ion uptake by rat kidney mitochondria and its dependence on respiration and phosphorylation. *J. Biol. Chem.* **237**, 2670–2677.
- Vecellio Reane, D., Vallese, F., Checchetto, V., Acquasaliente, L., Butera, G., De Filippis, V., Szabò, I., Zanotti, G., Rizzuto, R., and Raffaello, A. (2016). A MICU1 Splice Variant Confers High Sensitivity to the Mitochondrial Ca^{2+} Uptake Machinery of Skeletal Muscle. *Mol. Cell* **64**, 760–773 (4).
- Vinogradov, A., and Scarpa, A. (1973). The initial velocities of calcium uptake by rat liver mitochondria. *J. Biol. Chem.* **248**, 5527–5531 (15).
- Walter, E., Alsaffar, S., Livingstone, C., and Ashley, S.L. (2015). Manganese toxicity in critical care: Case report, literature review and recommendations for practice. *J. Intensive Care Soc.* **17**, 252–257 (3).
- Wang, F., Yuan, R.Y., Li, L., Meng, T.G., Fan, L.H., Jing, Y., Zhang, R.R., Li, Y.Y., Liang, Q.X., Dong, F., *et al.* (2018). Mitochondrial regulation of $[\text{Ca}^{2+}]_i$ oscillations during cell cycle resumption of the second meiosis of oocyte. *Cell Cycle* **17**, 1471–1486 (12).
- Wang, Y., Nguyen, N.X., She, J., Zeng, W., Yang, Y., Bai, X. chen, and Jiang, Y. (2019). Structural Mechanism of EMRE-Dependent Gating of the Human Mitochondrial Calcium Uniporter. *Cell* **177**, 1252-1261.e13 (5).
- Westermann, B. (2015). The mitochondria-plasma membrane contact site. *Curr. Opin. Cell Biol.* **35**, 1–6.
- Wettmarshausen, J., Goh, V., Huang, K.T., Arduino, D.M., Tripathi, U., Leimpek, A., Cheng, Y., Pittis, A.A., Gabaldón, T., Mokranjac, D., *et al.* (2018). MICU1 Confers Protection from MCU-Dependent Manganese Toxicity. *Cell Rep.* **25**, 1425-1435.e7 (6).
- Wiederkehr, A., Szanda, G., Akhmedov, D., Matak, C., Heizmann, C.W., Schoonjans, K., Pozzan, T., Spät, A., and Wollheim, C.B. (2011). Mitochondrial matrix calcium is an activating signal for hormone secretion. *Cell Metab.* **13**, 601–611 (5).
- Wu, Y., Rasmussen, T.P., Koval, O.M., Joiner, M.L.A., Hall, D.D., Chen, B., Luczak, E.D., Wang, Q., Rokita, A.G., Wehrens, X.H.T., *et al.* (2015). The mitochondrial uniporter controls fight or flight heart rate increases. *Nat. Commun.* **6** (6081).

- Yamamoto, T., Yamagoshi, R., Harada, K., Kawano, M., Minami, N., Ido, Y., Kuwahara, K., Fujita, A., Ozono, M., Watanabe, A., *et al.* (2016). Analysis of the structure and function of EMRE in a yeast expression system. *Biochim. Biophys. Acta - Bioenerg.* *1857*, 831–839 (6).
- Yi, M., Weaver, D., and Hajnóczky, G. (2004). Control of mitochondrial motility and distribution by the calcium signal: A homeostatic circuit. *J. Cell Biol.* *167*, 661–672 (4).
- Ying, W.L., Emerson, J., Clarke, M.J., and Sanadi, D.R. (1991). Inhibition of mitochondrial calcium ion transport by an oxo-bridged dinuclear ruthenium ammine complex. *Biochemistry* *30*, 4949–4952 (20).
- Yoo, J., Wu, M., Yin, Y., Herzik, M.A., Lander, G.C., and Lee, S.Y. (2018). Cryo-EM structure of a mitochondrial calcium uniporter. *Science* (80-.). *361*, 506–511 (6401).
- Zelter, A., Bencina, M., Bowman, B.J., Yarden, O., and Read, N.D. (2004). A comparative genomic analysis of the calcium signaling machinery in *Neurospora crassa*, *Magnaporthe grisea*, and *Saccharomyces cerevisiae*. *Fungal Genet. Biol.* *41*, 827–841 (9).
- Zong, W.X., and Thompson, C.B. (2006). Necrotic death as a cell fate. *Genes Dev.* *20*, 1–15 (1).

Contributions

In Publication I, I had personally performed the experiments of Fig. 3D-F, 4A-B, 4F-H, S3, S4A-B, S4E-F. I had also performed the immunoblot for Fig. 1C. Together with Jennifer Wettmarshausen, we performed the experiment for Fig. 2E.

In Publication II, I had personally performed the experiments of Fig. 3B-C, 4C-F, Supplementary Fig. 3-4, 7-12.

All the experiments and data in the figures as indicated were analyzed and illustrated by myself.

Acknowledgement

I would like to extend my sincere gratitude to my supervisor Dr. Fabiana Perocchi for her invaluable guidance, support and patience throughout these PhD years. I would also like to thank my Thesis Advisory committee, Prof. Dr. Barbara Conradt, Dr. Holger Prokisch and Prof. Dr. Thomas Meitinger, for their support over the years. A big thank you to PD Dr. Dejana Mokranjac and Dr. Sigurd Braun for their help and guidance in my experiments.

To all the former and current members of AG Perocchi, thank you for all your support over the years. I would like to specially thank Jennifer, Anja, Daniela, Li, Cecilia, Matteo and Yi Ming for guiding me both experimentally and intellectually. I would also like to thank Giuseppe, Natalia and Hilda for giving me a hand with my experiments during the last months of my PhD.

I would like to thank my fellow colleagues and friends at the Genzentrum who have been very helpful and kind that made my first three years of PhD there an enjoyable one. I would also like to thank my fellow colleagues from the Institute of Diabetes and Obesity at the Helmholtz Zentrum Munich for their kind assistance, especially during our laboratory move into the institute that allowed me to get started with my experiments in no time during the last year of my PhD. I would like to specially thank Sandrine for always being there to help and support at the institute.

To my dearest family, thank you for all the love and support throughout these years. It has definitely been harder being so far apart, but the mental support has kept me going. I would also like to thank all my dearest friends from all over the world who have been very understanding and encouraging.